# Island effects on marine production and circulation around the island of South Georgia, Southern Ocean

**Dissertation**

zur Erlangung des Akademischen Grades eines

Doktor der Naturwissenschaften

- Dr. rer. Nat. -

Gutachter:
Prof. Dr. Reiner Schlitzer
Prof. Dr. Michal Kucera

vorgelegt dem

Fachbereich 5 - Geowissenschaften

der Universität Bremen

von

**Inès Borrione**

Tag des öffentlichen Kolloquiums: Universität Bremen, 19. Dezember 2013

Dedicated to my parents

Jumana and Enzo

-the sparkles of it all-

for their profound love

encouragement

and support

It was tough, it seemed impossible and endless. Looking back, I realize it was also fun!

# Table of Contents

## Abstract

Regions of the Southern Ocean (SO) where phytoplankton blooms can develop and lead to biomass levels above those of the typically poor high-nutrient low-chlorophyll (HNLC) waters have two important repercussions on the local and global (eco) system. First, intense phytoplankton blooms, which are at the base of the marine trophic web, generate and sustain ecosystem hot-spots; second, blooms regulate local and global ocean biogeochemistry, due to the role of phytoplankton in the cycles of nutrients and carbon (i.e., the biological carbon pump). After the first evidences for iron limitation in HNLC waters and the formulation of the "iron hypothesis", productive regions in the SO were investigated not only for their roles in the (eco)system but also to understand mechanisms for iron enrichment (i.e., iron sources and its chemical cycle) and the effects of iron availability on primary productivity and on the global carbon cycle including the potentials for atmospheric (anthropogenic) $CO_2$ drawdown.

Therefore, the region around South Georgia (37°W, 55°S), a relatively small island in the western Atlantic sector of the SO, is a focal point of Antarctic research as South Georgia phytoplankton blooms are among the largest and most intense of the SO. However, despite increasing scientific effort there is still ample debate on the processes generating the observed high levels of productivity; moreover, no existing study described accurately the long-term spatio-temporal variability of South Georgia blooms, and investigated their causes. This PhD thesis focusses on these three aspects. An interdisciplinary approach was used, combining chemical, biological and physical observations from in situ and satellite-based data archives, as well as from simulations with a biogeochemical model (ROMS_AGRIF-PISCES) including iron limitation. Model results presented in this thesis derive from the first example of a regional biogeochemical model applied to the South Georgia region.

Results show that several environmental controls regulate primary productivity around South Georgia (i.e., temperature, nutrient availability, light and local circulation). Nevertheless, in the 13 years of satellite ocean colour observations, phytoplankton blooms (identified as regions where chlorophyll *a* concentrations were greater than 0.75 mg $m^{-3}$) occurred every year without an evident long term temporal trend. Phytoplankton blooms occupied a well defined geographical region ~ 145 000 $km^2$ to the north of South Georgia, named the typical bloom area. Across this vast area blooms followed an unexpected annual bimodal pattern likely controlled by the availability of surface silicate concentrations, and not by iron availability as one would expect. Simulations with the biogeochemical model were tailored to investigate the relative importance of sedimentary and atmospheric iron sources and describe the main transport pathways of iron in the region, integrating the very limited number of iron observations. Overall, model results agree well with the very few observations, and provide a unique large scale (yet detailed) view of iron distributions. Results clearly show iron enrichment from the island, in particular from its very shallow shelf area. Conversely, in the model dust deposition (mostly originating from South America) plays a small role downstream of South Georgia, with almost no effects on surface chlorophyll *a* concentrations. Iron released to the water column from the island and its shelf region is

dispersed by circulation forming a very large iron and Chlorophyll *a* concentration plume that extends several hundreds of km due northeast of the island.

***

## Zusammenfassung

Regionen des Südozeans (SO), in denen sich Phytoplanktonblüten entwickeln und zu Biomassenproduktion über der typischer HNLC-Gebiete (high-nutrient low-chlorophyll; hohe Nährstoff- und geringe Chlorophyllkonzentrationen) führen, wirken sich in zweierlei Hinsicht auf das lokale sowie das globale (Öko)system aus. Erstens bilden ausgeprägte Planktonblüten, welche die Basis der marinen Nahrungskette darstellen, ökologische Hotspots und erhalten diese aufrecht, und zweitens wird durch die Rolle des Phytoplanktons im Nähr- und Kohlenstoffkreislauf (biologische Pumpe) die lokale und globale Ozeanbiogeochemie reguliert. Nach ersten Hinweisen auf eine Eisenlimitierung von HNLC-Gebieten und der Aufstellung der sogenannten „Eisen-Hypothese“, wurden Produktionsregionen des Südozeans auf ihre Rolle im (Öko)system, auf Mechanismen der Eisenanreicherung (Quellen von Eisen und sein chemischer Kreislauf) und auf die Effekte der Verfügbarkeit von Eisen auf Primärproduktion und den globalen Kohlenstoffkreislauf hin untersucht. Auch wurde das Potential dieser Mechanismen auf eine mögliche Senkung des atmosphärischen (anthropogenen) $CO_2$- Gehaltes erörtert.

Phytoplanktonblüten im Gebiet um Südgeorgien (37°W, 55°S), einer kleinen Insel im Südatlantik, gehören zu den intensivsten und größten Planktonblüten im gesamten SO und rücken dieses Gebiet in den Fokus der antarktischen Forschung. Trotz intensiver wissenschaftlicher Bemühungen ist die Herkunft der enormen Produktivität um Südgeorgien immer noch umstritten. Bislang beschreibt keine Studie die langzeitliche und räumliche Variabilität der südgeorgischen Planktonblüten. Diese Aspekte sollen in der vorliegenden Doktorarbeit geklärt werden. Um dies zu erreichen, wurde ein interdisziplinärer Ansatz unter der Kombination von chemischen, biologischen und physikalischen Beobachtungen und Simulationen mit einem biogeochemischen Modell (ROMS_AGRIF-PISCES; mit Eisenlimitierung) angewendet. Die Modellierungsergebisse dieser Arbeit stellen das erste Beispiel der Anwendung eines biogeochemischen Modelles auf die Region um Südgeorgien dar.

Die Resultate zeigen, dass unterschiedliche Faktoren (Temperatur, Nährstoffgehalt, Licht und lokale Strömungen) die Produktivität um Südgeorgien beeinflussen. Dennoch konnte durch die Untersuchung von jährlich auftretenden Phytoplanktonblüten (Regionen mit einer Konzentration von Chlorophyll *a* höher als 0.75 mg $m^{-3}$) in Satellitenfarbdaten über einen Zeitraum von 13 Jahren kein eindeutiger Langzeittrend ermittelt werden. Phytoplanktonblüten treten nördlich von Südgeorgien in einem klar begrenzten Gebiet von etwa 145.000 $km^2$ auf

und folgen einem unerwarteten bimodalen Muster, welches wahrscheinlich durch die Verfügbarkeit oberflächennahen Silikates und nicht wie erwartet von verfügbarem Eisen bestimmt wird. Alle Simulationen mit dem biogeochemischen Modell waren auf die Untersuchung des Einflusses von sedimentären und atmosphärischen Eisenquellen zugeschnitten und beschreiben die regionalen Transportwege von Eisen unter Einbeziehung einer sehr geringen Anzahl von Eisenmessungen.

Insgesamt steht das Modell in gutem Einklang mit diesen Messungen und ermöglicht somit einen bisher unerreicht großflächigen und detaillierten Einblick in die Verbreitung von Eisen. Die Ergebnisse zeigen eine eindeutige Anreicherung von Eisen durch die Landmasse Südgeorgiens sowie durch ihre flachen Schelfgebiete. Im Gegenzug spielt Staubeintrag (hauptsächlich aus Südamerika) im Modell nur eine untergeordnete Rolle ohne nennenswerte Auswirkungen auf die oberflächennahen Chlorophyll *a* Konzentrationen. Eisen, welches durch die Insel und ihre Schelfregionen in die Wassersäule eingetragen wird, wird durch Strömungen verteilt und bildet eine Wolke mit ausgeprägten Chlorophyll *a* Konzentrationen, die sich über mehrere hundert Kilometer nordöstlich der Insel erstreckt.

# 1 Introduction

## *1.1 The Southern Ocean*

The Southern Ocean (latitudes south of 50°S, Fig. 1.1) is the fourth largest ocean, after the Pacific, Atlantic and Indian Oceans. Despite the Southern Ocean's apparent remoteness, all physical, chemical and biological processes occurring here, including those described in this thesis and their modifications caused by global warming, have repercussions at the global scale and have the potentials to influence global atmospheric $CO_2$ levels (de Baar et al., 1995). Differently from the more familiar Mediterranean Sea or the Atlantic Ocean, the Southern Ocean is an open-boundary ocean, in the sense that it has no side land barriers at its sides and can thus encircle uninterrupted the Antarctic continent linking the Atlantic, Indian and Pacific Oceans. Therefore the Southern Ocean redistributes from one ocean to the other water properties such as temperature or salinity, dissolved gases or macronutrients (Rintoul et al., 2001). The Southern Ocean, in fact, is an important component of the global ocean conveyor belt, a system of surface and deep currents driven by temperature, salinity and winds that connects in approximately 1000 years all the Earth's oceans. The main hydrographic feature of the Southern Ocean is the Antarctic Circumpolar Current (ACC). Without any land barrier to obstruct its 24000 km path around Antarctica, the ACC is the world's strongest current, transporting 120-150 Sverdrups (Sv=$10^6$ $m^3$ $s^{-1}$ ; Olbers et al., 2004; Zhang et al., 2008; Whitworth et al., 1982).

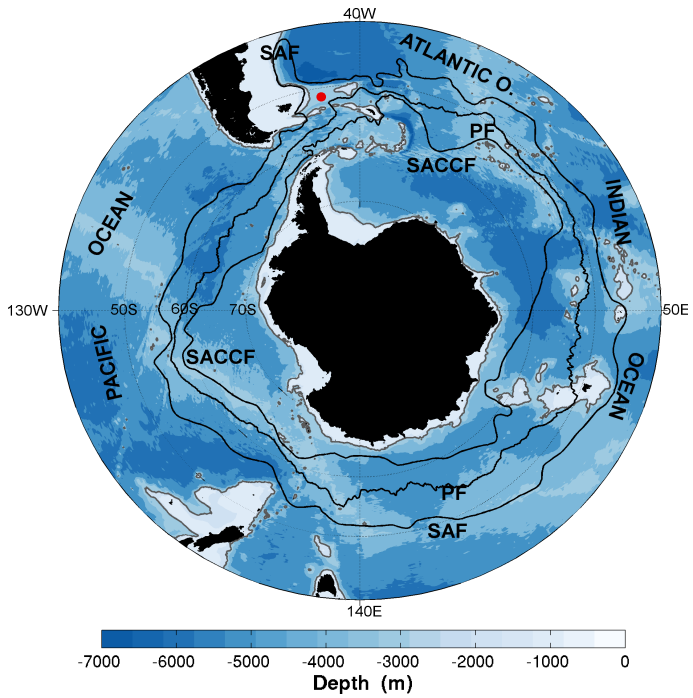


*Fig. 1.1 Bathymetry of the Southern Ocean (latitudes south of 50°S), and the main ACC fronts: the Sub-Antarctic Front (SAF, Orsi et al., 1995), the Polar Front (PF, Moore et al., 1999) and the Southern ACC Front (SACCF, Thorpe et al., 2002). The red dot west of South Georgia points to Shag Rocks Passage.*

Since the early studies, the ACC has been described as a banded structure, with calmer zones of relatively uniform water mass properties, called frontal zones, alternated to narrow

and deep-reaching current cores, named fronts, which are characterized by large surface velocities and pronounced water property gradients in the north-south (i.e., meridional) direction (i.e., Sievers and Nowling, 1984; Orsi et al., 1995; Venables et al., 2012). The main ACC fronts are marked in Fig. 1.1: from north to south these are the sub-Antarctic Front (SAF), the Polar Front (PF) and the Southern ACC Front (SACCF). Traditionally located using in situ hydrographic measurements of temperature and salinity (i.e., Orsi et al., 1995; Boehme et al., 2008), more recently the position of the ACC fronts can also be determined using satellite measurements of sea surface temperature (i.e., Dong et al., 2006; Moore et al., 1999) or sea surface altimetry (i.e., Sokolov and Rintoul, 2009; Venables et al., 2012).

The primary source of momentum for the eastwards flowing ACC are the southern hemisphere westerly winds (Allison et al., 2010; Olbers et al., 2004) blowing at sustained speeds that often rise above 15 m $s^{-1}$ (COADS; Da Silva et al., 1994). The same winds have a second important impact on surface circulation. Due to the Ekman transport theory, for which in the southern hemisphere a strong wind generates a net water movement at 90° to the left of the wind direction, the southern hemisphere westerlies generate a northwards transport of surface waters. This northwards transport allows for heat and fresh-water exchanges between Antarctic waters and those found to their north, but also generates the Antarctic Divergence to the south the ACC, where very deep and nutrient-rich waters upwell to the surface. This upwards vertical transport is responsible for the particularly high concentrations of the main nutrients needed for phytoplankton growth, i.e., macronutrients like phosphate, silicate and nitrate (the latter in Fig. 1.2a). Consequently, ocean waters around Antarctica, and in particular those at the surface where primary productivity occurs (i.e., the sufficiently sunlit euphotic layer), provide environmental conditions that are potentially optimal for the growth of phytoplankton. Nevertheless, as presented in the following chapter, during the main phytoplankton growing season, which in the Southern Ocean corresponds to the months of October through February (Mongin et al., 2008; Moore and Abbott, 2000; Thomalla et al., 2011), only in certain regions primary productivity reaches its potentials and rises well above the typically very low background levels.

## *1.2 High-nutrient low-chlorophyll waters and the role of iron*

At the beginning of the phytoplankton growing season and during austral summer, due to the combined effects of winter convective mixing and the Antarctic Divergence mentioned above, the concentrations of macronutrients across most of the Southern Ocean (in Fig. 1.2a, nitrate is shown as example) are well above the requirements for phytoplankton growth (nitrate > 25 nM; silicate > 35 nM; phosphate > 1.5 nM; Ridgwell et al., 2002). Nevertheless, as clearly evidenced from a comparison of Fig. 1.2a with contemporaneous satellite estimates of surface chlorophyll *a* concentrations (Chl *a*, a proxy for phytoplankton biomass, in Fig. 1.2b) in most of the Southern Ocean primary productivity is low (i.e., Chl $a < 0.5$ mg $m^{-3}$) and at times close to zero ( i.e., in the Pacific and Indian sectors of the Southern Ocean). Low to very low productivity levels during the phytoplankton growth season suggest a limited ability of phytoplankton to optimally utilize all the available macronutrients. Therefore in these regions the biological carbon pump (i.e., Robinson et al., 2010), a mechanism contributing to atmospheric carbon drawdown through the combination of (i) photosynthesis, which converts

dissolved inorganic carbon (including anthropogenic $CO_2$) to organic biomass, and (ii) all processes removing it from the surface to the deep ocean (i.e., sinking of dead cells or faecal material) functions well below its potentials. This condition, particularly valid for the Southern Ocean, has led to the hypothesis that during glacials, when atmospheric $CO_2$ levels were well below modern levels more dust deposition and thus iron input determined a more efficient biological carbon pump (i.e., the "iron-hypotheses", Martin, 1990a).

The observation of very low productivity despite elevated macronutrient concentrations in the Southern Ocean, the initially called "Antarctic Paradox" (Hart, 1934) is known today as the high-nutrient low-chlorophyll (HNLC) paradox and has been reported also in the Subarctic Pacific Ocean (Boyd et al., 2004) and the Equatorial Pacific Ocean (Coale et al., 1996). Of all HNLC regions, however, the Southern Ocean is by far the largest.

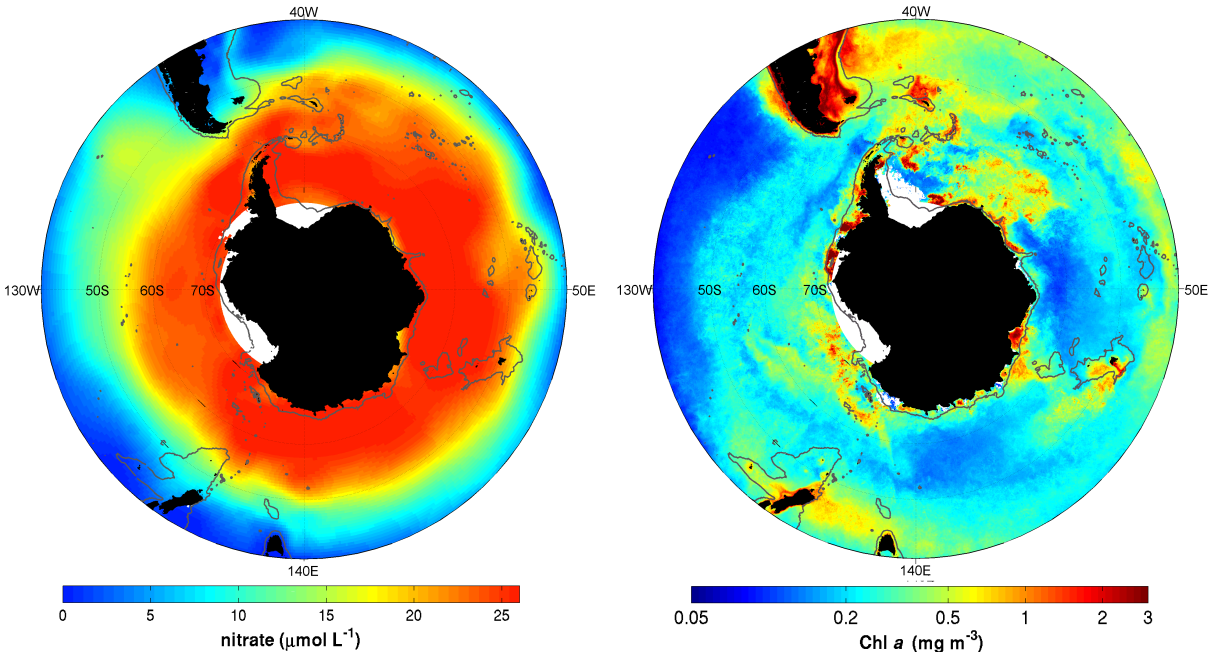


*Fig. 1.2. (A) Surface nitrate concentrations from CARS09 (Ridgway et al., 2002) and (B) Chl a concentrations from SeaWiFS ocean colour measurements during January (i.e., Austral summer) in the Southern Ocean.*

Several environmental conditions, often acting in concert, are believed to determine HNLC conditions by reducing phytoplankton cellular growth or controlling phytoplankton accumulation during the well lit (austral) summer season. For example heavy grazing pressure (a top-down control) exerted by protozoans, mesozooplankton like copepods (Smetacek et al., 2004; Mazzocchi et al., 2009), but also larger zooplankton like krill or salps, which may limit the accumulation of phytoplankton before a bloom is formed (Atkinson et al., 2008; Loeb et al., 2010; Whitehouse et al., 2009, Blain et al., 2001). A mixed layer depth deeper than the critical depth, defined as the depth at which total production in the overlaying water column equals losses by respiration, as would occur after periods of high wind velocities and storms (which are common events in the Southern Ocean throughout the whole year), can also reduce

observed Chl *a* concentrations. This occurs because deep mixed layer depths reduce the total amount of radiation picked up by phytoplankton for photosynthesis, but also "dilute" phytoplankton biomass over a much larger volume (Smetacek and Naqvi, 2008; Venables and Meredith, 2010). Bio-limiting concentrations of one or more trace elements (i.e., micronutrients) like iron, copper, manganese, cobalt, or zinc which are required for several intracellular chemical reactions (Brand et al., 1983) are also considered important bottom-up controls on phytoplankton growth. Among the trace elements mentioned above, several lines of evidence from laboratory and/or in situ experiments have clearly indicated that bio-limitation due to insufficient concentrations of iron, most of all, can determine the widespread HNLC observed in the Southern Ocean (Martin et al., 1990b; Hinz et al., 2012; Breitbarth et al., 2010 and references therein). As presented in the following chapter, it is the characteristic chemical cycle of iron in sea-water that reduces its concentrations below phytoplankton requirements, but also below the detection limit of modern instrumentation (sub-nanomoles; Achterberg et al., 2001; Breitbarth et al., 2010).

## *1.3 Iron in sea-water*

The important biological role of iron in the marine system was initially hypothesised by Hart (1934) to explain what he named the "Antarctic Paradox". His intuitive observations have been extensively investigated with numerous experiments in the laboratory and at sea conducted since the late 80's: in all experiments controlled iron addition was followed by increased phytoplankton growth and a reduction of nutrient concentrations (Martin et al., 1990b; Hinz et al., 2012; Breitbarth et al., 2010 and references therein). Moreover, the nutrient-like vertical profile of iron in the ocean provides an additional indication of its importance for biology. In fact, close to the surface, where biological activity is highest (i.e., the euphotic zone) iron concentrations are generally at their minimum (< 0.1 nM) increasing with depth to concentrations of several nanomoles close to the sea-floor where they typically reach their maxima (Klunder et al., 2011; de Jong et al., 2012; de Baar and de Jong 2001). In fact, all living organisms require iron, as it plays an important role for the storage and transport of energy within the cell. Iron is actively involved in nitrate reduction and $N_2$ fixation, and in phytoplankton it is involved in photosynthesis and adaptation to low light levels (see Venables and Moore 2010; Sunda and Huntsman 1995; Brand et al., 1983).

The very low concentrations of iron in sea-water and high potentials for contamination due to its ubiquity during both sampling and measurements, have strongly limited the number and quality of iron observations (i.e., Bowie et al., 2006; Breitbarth et al., 2010; Achterberg et al., 2001). Thanks to the development of clean and very accurate measurement techniques, the total number of iron measurements has progressively increased, and several chemical reactions in the iron cycle are now known and can be included, even if still in a simplified manner, in biogeochemical models (Jiang et al., 2013; Moore and Braucher, 2008; Aumont, et al., 2006; Parekh et al., 2004; Tagliabue et al., 2009a). Of all, the Southern Ocean is the most poorly sampled ocean, especially far from coastal regions (Breitbarth et al., 2010; Moore and Braucher, 2008). However, thanks to international programs like GEOTRACES (http://www.geotraces.org/), which aims at studying the large-scale distribution and

biogeochemistry of the key trace elements (including iron), these fundamental measurements are progressively increasing, providing additional information on the chemical cycle and speciation of iron, as well as on its seasonality and spatial variability (Breitbarth et al., 2010; Klunder et al., 2011; Thuróczy et al., 2012). Indeed, more information will also help improve the performance of existing biogeochemical models (Aumont and Bopp, 2006; Mahowald et al., 2005; Moore and Braucher, 2008; de Jong et al., 2012; Le Quéré et al., 2005).

It is now known, that several mechanisms (often acting contemporaneously) introduce iron to the oceans (Fig. 1.3). The most important are: (1) run-off and fluvial input from the weathering of rocks and soil (de Baar and de Jong, 2001; Tovar-Sanchez et al., 2006); (2) deposition of aeolian dust, whether directly downwind dry regions like the deserts in South America or Australia, or following ice melt (Johnson et al., 2010; Lin et al., 2011; Mahowald et al., 2005; Tegen and Fung 1995; Cassar et al., 2007; Raiswell et al., 2008); (3) hydrothermal activity (Klunder et al., 2011; Tagliabue et al., 2010); (4) processes occurring at the sediment-water interface along the coast and the sea-floor, like sediment resuspension, diffusion of iron from the sediments, or mixing with iron-rich pore waters (Johnson et al., 1997; Lam et al., 2006; Elrod et al., 2004; Sachs et al., 2009). Close to source regions iron concentrations can rise to several nanomoles (Moore and Braucher, 2008; Klunder et al., 2011; Blain et al., 2001; Nielsdóttir et al., 2012) however iron concentrations ultimately depend on the magnitude and duration of each iron input mechanism (i.e., sporadic or continuous input, point-source or wide-spread source), the horizontal and vertical distances to each source, as well as on the efficiency of iron transport mechanisms (i.e., diffusion vs. later transport by local circulation; Blain et al., 2008; de Jong et al., 2012; Nishioka et al., 2011; Planquette et al., 2007).

Once iron Fe(II) is introduced in seawater (Fig. 1.3), a large part is rapidly oxidixed by oxygen and $H_2O_2$ to its less soluble form Fe(III), or scavenged onto sinking particulate matter (i.e., dead cells). A very small percentage of the newly introduced Fe(II) remains in its dissolved form (dFe), thanks to the large variety and high concentrations of ligands, i.e. organic compounds, that are produced by phytoplankton and bacteria, or that derive from the degradation of organic matter (Gerringa et al., 2008; Hunter and Boyd, 2007; Johnson e al., 1997; Moore and Braucher, 2008). Part of the free-inorganic or ligand-complexed iron is removed by biological activity which is also responsible for the recycling of iron in the water column (Baker and Croot, 2010; Schmidt et al., 2011; Tovar-Sanchez et al., 2007). Physical processes, like lateral and vertical advection as well as diffusion, are responsible for the distribution of iron away from its source regions; of the three mentioned processes previous studies in the Southern Ocean (i.e., de Jong et al., 2012; Planquette et al., 2007) agree that lateral advection is the most important and efficient long-distance supplier of dFe.

Due to the biological importance of iron, and its bio-limiting concentrations in most of the surface ocean, during austral spring and/or austral summer, phytoplankton blooms are observed in regions of the ocean that enter in contact with any of the iron sources mentioned above. These regions, often termed as high-nutrient high-chlorophyll, are addressed in the following chapter.

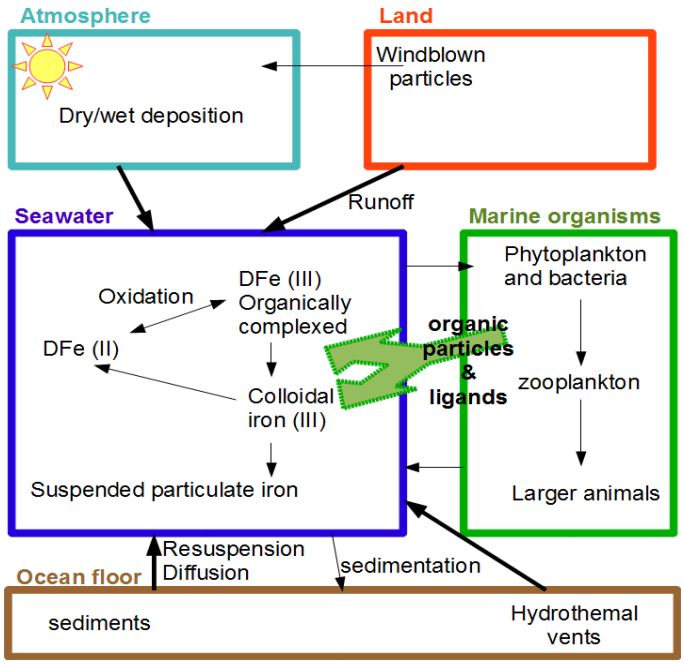


*Fig. 1.3. Schematics of the chemical cycle of iron in sea-water, modified from Achterberg et al., (2001). Minor sources of iron, like those of volcanic origin (i.e., Benitez-Nelson et al., 2003) or due to iceberg or glacial melt (i.e., Lin et al., 2011; Raiswell et al., 2008) are not included in the figure, but may locally play an important role.*

## *1.4 High-nutrient high-chlorophyll regions*

Whereas low Chl *a* concentrations characterize most of the Southern Ocean (HNLC, i.e. Chl *a* < 0.5 mg $m^{-3}$; Moore and Abbott 2000; Comiso et al., 1993, blue to green colors in Fig 1.2b), medium to very high Chl *a* concentrations (i.e., 0.5 – 1 mg $m^{-3}$ and > 1 mg $m^{-3}$, respectively) are observed close to iron sources. For example, surface Chl *a* concentrations ranging 0.5 – 1 mg $m^{-3}$ are observed in irregular and episodic patches and/or filaments in the permanently open ocean zone (POOZ, Tréguer and Jacques 1992) due to the interaction of the flow with shallow topographic features or due to the variability in local hydrography, which may lead to upwelling hot-spots in correspondence to meanders or eddies (Blain et al., 2007; Kahru et al., 2007; Moore and Abbott, 2000; Naveira Garabato et al., 2002; Park et al., 2010; Sokolov and Rintoul, 2007). Moreover, medium pigment biomass concentrations are observed following the deposition of dust from dry continental areas and major deserts as those in South America or Australia (Mahowald et al., 2005; Li et al., 2008; Johnson et al., 2010; Meskhidze et al., 2007). Although recent studies clearly indicate the importance of dust deposition in promoting phytoplankton growth in land remote regions (Cassar et al., 2007; Jickells et al., 2005), the magnitude and timing of its effects are still unclear, due to limitations in our knowledge of dust transport pathways and deposition fluxes, as well as on the complex chemistry of dust in the atmosphere and in the surface ocean (Mahowald et al., 2005; Baker and Croot, 2010).

Very high levels of pigment biomass (>1-3 mg $m^{-3}$) are observed annually along continental margins and coastal areas, in open polynias, and along the ice edge of the marginal ice zone (Arrigo and van Dijken, 2003; Fitch and Moore, 2007; Lutz et al., 2010; Clarke et al., 2008; Lannuzel et al., 2007; Smith et al., 2008). The marginal ice zone is defined as the region influenced by the seasonal retreat and advance of pack-ice (Tréguer and Jacques, 1992). Of particular interest are annual phytoplankton blooms associated to the presence of islands which generate hot-spots of productivity in oligotrophic remote regions,

hence modifying locally the ecosystem but also biogeochemistry (i.e., carbon drawdown and the nutrient cycles). Examples of phytoplankton blooms associated to islands (marked in Fig. 1.4) are those observed around South Georgia (investigated in detail in this thesis), the South Sandwich and Orkney Islands in the Atlantic Southern Ocean, and those associated to the Crozet and Kerguelen archipelagos in the Indian Southern Ocean. The presence of phytoplankton blooms downstream of islands falls in the category of the so called "island mass effects" (see Section 1.5 below).

Following the formulation of the "iron hypothesis" in the early 90's (Martin et al., 1990a) and the idea that human-controlled input of iron could generate "artificial" high-nutrient high-chlorophyll regions, enhancing the biological carbon pump (Buesseler et al., 2004; Smetacek and Naqvi, 2008), a succession of in-situ oceanic iron addition experiments were performed to test the validity of the iron hypothesis. These artificial iron fertilization experiments contributed to the understanding of the role of iron on the food web-structure and ecosystem dynamics (i.e., role of bottom-up versus top-down controls on bloom development and termination), as well as on its effect on the cycles of carbon and those of the major macronutrients; nevertheless they reached very different conclusions regarding the efficiency of iron input on $CO_2$ drawdown, due to differences in the duration of the experiments, initial conditions and time of year (Boyd et al., 2007; Breitbarth et al., 2010; Buessler et al., 2008; Mazzocchi et al., 2009; Smetacek and Klaas et al., 2012; Westberry et al., 2013 and references threin).

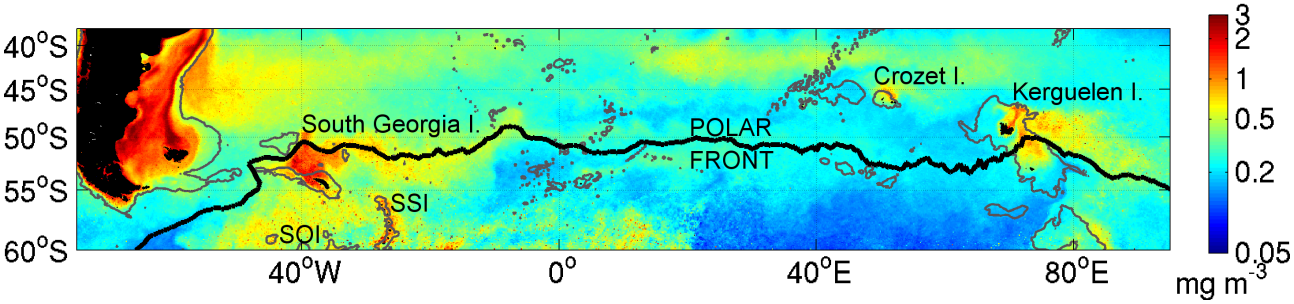


*Fig. 1.4. Austral summer 1997-2010 climatology of Chl a in the Atlantic and Indian sector of the Southern Ocean as from SeaWiFS ocean color imagery. The figure highlights the locations of the main island mass effects in the Southern Ocean. SSI and SOI indicate the South Sandwich and South Orkney islands respectively. 2000 m bathymetry contours are shown with thin lines. The Polar Front from (Moore et al., 1999) is also marked.*

## *1.5 The island mass effect*

It is common knowledge for fishermen and divers that in the middle of almost any oligotrophic sea or ocean, isolated islands and shallow sea mounts are rich in different forms of life, similarly to what one would describe for an oases in the middle of a desert. Enhanced biological productivity around an island of the Hawaiian chain was scientifically documented by Doty and Oguri (1956) who coined the phrase ‘‘island mass effect’’.

Several mechanisms can perturb physical, chemical and biological background conditions (i.e., water temperature, nutrient concentrations or productivity) generating an island mass effect. An island along the path of a current acts as a blockage to the flow (Hasegawa et al., 2004). The current is thus forced to separate before the island, and then converge downstream of the island in order to resume its course. It has been observed that convergence at the lee side (i.e., downstream) of the island, can cause upwelling or shoaling of isopycnals leading to nutrient enrichment and a decrease in surface temperatures (Hasegawa et al., 2004; Blain et al., 2001). Also, flow disturbance by an island may determine formation of eddies (Heywood et al., 1990), or regions of calmer waters which may provide favourable conditions for the accumulation of phytoplankton or prevent larval pools being washed away (Boehlert et al., 1992). Coastal (planktonic) species may "seed" the open-ocean up to several hundreds of km downstream of the island (i.e., Korb et al., 2004). Finally, the island may serve as a source of chemical elements (i.e., macro- or micronutrients, like iron) introduced in the surrounding waters with run-off or shelf processes along the coast.

The latter case of island mass effect, especially, applies to the HNLC Southern Ocean where islands act as local, yet important source of iron perturbing the area around and downstream of the island for several hundreds of km (Korb et al., 2004). In satellite imagery of ocean colour (i.e., Fig. 1.4), in fact, the presence of islands is evident as they are surrounded by Chl a concentrations that are up to two orders of magnitude higher than in the surrounding low-chlorophyll waters (i.e., 10 mg $m^{-3}$ vs. 0.1 mg $m^{-3}$, Blain et al., 2001). The most documented island mass effects in the Southern Ocean are those of the Kerguelen (48.5–49.71S, 68.5–70.51E) and Crozet (45.5–47.01S, 49.0–53.01E) islands in the Indian Ocean (Blain et al., 2001, 2007, 2008; Bakker et al., 2007, Poulton et al., 2007) and the island mass effect observed around South Georgia (Whitehouse et al., 1996; Atkinson et al., 2001; Korb et al., 2008, 2010, 2012). High productivity around these very isolated islands provides an important food resource for both pelagic and benthic ecosystems, and thus also on the large numbers of marine birds and mammals feeding on them and that often migrate to these islands during the breeding season (Atkinson et al., 2001; Bailleul et al., 2007; Hogg et al., 2011). Moreover, phytoplankton blooms associated to these islands enhance carbon uptake (Bakker et al., 2007; Jones et al., 2012; Blain et al.,2007; Jouandet et al., 2008; Boutin et al., 2009; Pollard et al., 2009; Morris et al., 2013), an aspect that in recent years has raised much attention in the scientific community (Charette et al., 2013). It is believed, in fact, that iron enrichment downstream of islands produces a carbon drawdown above any other observed after experiments of artificial iron fertilisation (Pollard et al., 2009; Blain et al., 2007).

## *1.6 Study area – South Georgia*

South Georgia (37°W, 55°S) is a relatively small island of the Atlantic sector of the Southern Ocean (Figs.1.1 and 1.4) located at the northeastern limit of the Scotia Sea, along the North Scotia Ridge. It is a long and narrow mountainous island (~ 190 km long and 35 km wide) with a very rugged coastline, characterized by numerous valleys and bays, and an extended continental shelf (30-100 km, Gordon et al., 2008). Beyond the continental shelf the continental slope drops to the abyssal plain, which surrounds the island at all sides and on average reaches depths greater than 3000 m (Fretwell et al., 2009, see also Fig. 3.2.2 ). Due to

the low average annual temperatures (+2.0 °C) and high precipitations rates, the island is heavily glacierized and almost 50% of its surface is covered with permanent snow and ice (Gordon et al., 2008). During austral winter, however, South Georgia is free from Antarctic pack-ice, as the latter remains at least 300 km south of the island (Whtehouse et al., 2008; Gordon et al., 2008; http://www.iup.uni-bremen.de/seaice/amsr/, from Gordon et al., 2008).

South Georgia is located in the Polar Frontal Zone, between the Polar Front and the Southern ACC Front (Fig. 1.1). The Polar Front crosses the North Scotia Ridge at Shag Rocks Passage and then flows east remaining always due north of the island; the SACCF reaches South Georgia from the southwest, it flows around the southern shelf-break of the island and then veers anticyclonically towards the Georgia Basin before resuming its eastwards course (Orsi et al., 1995; Thorpe et al., 2002). Waters downstream of South Georgia are transported to the north and northwest of the island, where they flow anticyclonically along the borders of the Georgia Basin following contours of rapid depth variations (Fig. 1.5; Korb et al., 2008; Meredith et al., 2003).

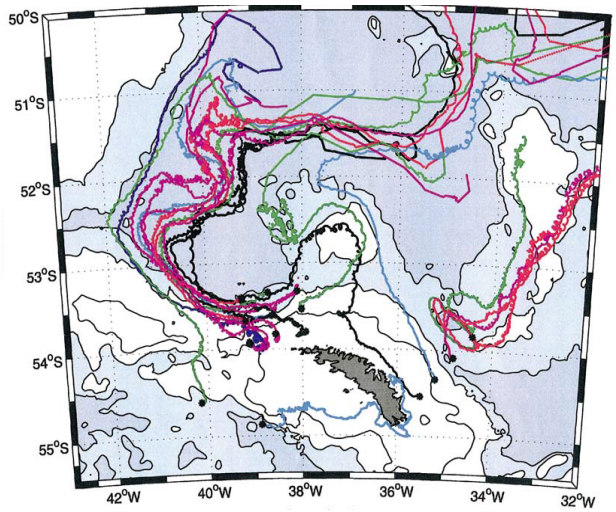


*Fig. 1.5. Surface circulation patterns around South Georgia as from surface drifters deployed over the shelf of South Georgia. The 500, 2500 and 3500m isobaths are indicated by the white, light grey and grey areas, respectively. This plot is reproduced from Meredith et al. (2003).*

The ACC and its fronts control the chemical properties of the waters surrounding the island (Whitehouse et al., 1996; Korb and Whitehouse, 2004). In particular, the Polar Front traces the boundary between the silicate poor waters observed to its north and the silicate rich waters to its south (Coale et al. 2004). Consequently, during austral spring (i.e., the beginning of the phytoplankton growing season) at the surface all macronutrients are well above phytoplankton requirements: nitrates and silicates normally range 20-30 nM, whereas phosphate concentrations are close to 1.3-2 nM (Boyer et al., 2009 for the World Ocean Database 2009). At the end of the growing season, after intense diatom-dominated blooms (Korb et al., 2008, 2010, 2012) of all macronutrients only silicate concentrations may be reduced to very low (at times limiting) levels (Whitehouse et al., 1996; 2008a).

Despite the island's relatively small size (~ 3700 $km^2$), satellite ocean colour imagery from the region around and downstream of the island reveal large and intense phytoplankton blooms with Chl *a* concentrations often greater than 10 mg $m^3$ that can extend, along the

mean path of the Polar Front, for more than 2500 km (Korb et al., 2004, Fig. 1.4). High productivity around South Georgia is known since the early expeditions to the Southern Ocean (late 1700s), which had established sealing and whaling grounds, fortunately banned since the mid 1960s. Today important commercial fisheries exploit South Georgia's krill and finfish stocks. Abundant fish stocks attract large colonies of marine and land based predators migrating to South Georgia during the feeding and breeding seasons (Atkinson et al., 2001; Trathan et al., 2008).

Initially driven by commercial interests (whaling and sealing), the marine ecosystem around South Georgia was frequently surveyed during the *Discovery Investigations* between the 1920s and 1930s. Since the 1980s South Georgia is a focal area for many of the British Antarctic Survey's marine ecological/scientific studies, which have mostly focussed on the northwestern and northeastern shelf of the island. During the past years, satellite oceanography (Whitehouse et al., 2012; Korb and Whitehouse, 2004; Korb et al., 2004), lagrangian instruments (i.e., argo floats: Venables and Moore, 2010; and surface drifters, Korb et al., 2008; Ward et al., 2005; Meredith et al., 2003), animal borne sensors (Trathan et al., 2008; Boehme et al., 2008), as well as modelling simulations (Young et al., 2011; Thorpe et al., 2002), have strongly improved our knowledge of the environment.

Recent studies aimed at quantifying long-term environmental modifications revealed a substantial warming trend in ocean and air temperatures between 1925 and 2006 (i.e., +1.55°C and +0.5°C, respectively; Whitehouse et al., 2008b), reflected in the progressive retreat of most of the South Georgia glaciers (Gordon et al., 2008). It is believed that the temperature rise at South Georgia will likely have implications on the cold-adapted (and often endemic) benthic species (Hogg et al., 2011) as well as on organisms belonging to the pelagic ecosystem such as krill (Atkinson et al., 2001; Atkinson et al., 2004; Whitehouse et al., 2009). A continued decline in their stocks will certainly have implications on the whole Antarctic food web, considering that krill is a critical resource for many marine birds and mammals (Atkinson et al., 2001; 2008).

## *1.7 Thesis objectives*

As mentioned above, South Georgia has been a focal area of the British Antarctic Survey's scientific investigations since the 1980's. However, mostly due to the remoteness of the region and the limited data coverage, very few are the long term studies, especially those that considered both the coastal and the open ocean waters surrounding South Georgia. Two studies assessed the variability of ocean and air temperature around South Georgia using historic datasets (Whitehouse et al., 2008b; Gordon et al., 2008), while most of the other studies examined primary productivity (or other environmental variables) over a series of few years, generally contemporaneously to oceanographic cruises in the region (i.e., Tarling et al., 2012). Therefore, to date is missing a detailed long term study investigating primary productivity over the whole South Georgia region that includes the coastal and open ocean waters north and downstream of the island. The first aim of this thesis is to fill in this gap, but also understand which environmental factors may determine the observed spatial and

temporal patterns. This information can set a useful reference for future observational and modelling studies, but also help plan ecosystem management (Young et al., 2011).

Section 1.3 has introduced the fundamental role of iron in HNLC waters. Since the early studies around South Georgia (i.e., Whitehouse et al., 1996), iron enrichment was suggested as an important cause for the large and intense blooms observed around and downstream of the island. Nevertheless, due to the difficulties associated to iron sampling (see Sect. 1.3), to date only two studies reported iron measurements (Holeton et al., 2005; Nielsdóttir et al., 2012). Thanks to the potentials of modelling (see Section 2.3) this tool was chosen to investigate further iron enrichment around the island, in particular its potential sources and transport pathways. Both objectives required the implementation and validation of the first coupled hydrodynamic-biogeochemical model applied to the South Georgia region.

Summarizing, the PhD research project presented in this thesis aims at the following objectives:

1. Description of primary productivity patterns around South Georgia, i.e.:
    1. Spatial distribution of phytoplankton blooms in the region
    2. Inter-annual variability of Chl *a* concentrations
    3. Seasonal cycle of Chl *a* concentrations
    4. Identification of the environmental factors leading points 1.1, 1.2, and 1.3.
2. Analysis of processes leading to iron enrichment around South Georgia. Therefore:
    1. Implementation of the coupled hydrodynamic-biogeochemical model ROMS-PISCES to the South Georgia region
    2. Understanding of the relative importance of atmospheric and sedimentary sources of iron
    3. Description of the main iron transport pathways around and downstream of the island.

Datasets and methods utilized to address the objectives listed above are described in section 2. Results obtained from the analysis and interpretation of the collected data are presented and discussed in Section 3 in the form of 4 manuscripts. The thesis concludes with a summary of the major findings of this PhD and presents question and objectives proposed for future research.

In addition to the results strictly related to this PhD project, in the thesis' annex are presented the preliminary results from the Indo-German iron fertilization experiment LOHAFEX, conducted in the Atlantic sector of the Southern Ocean between 7 January 2009 and 19 March 2009. As a participant to the expedition, I contributed to the work on board as member of the “zooplankton group”.

## 2 Data and methods

Albeit the remoteness of the South Georgia region and its often prohibitive sea-state and climate conditions, ecological, scientific and commercial interests have motivated research expeditions to the region since the early 1930s' (i.e., the Discovery Investigations, Deacon 1933, 1937; Hart, 1934). Oceanographic in situ data collected from a variety of instrumentation and made available by the scientific community are collected in the World Ocean Database (WOD, see below for more details on the dataset). Spatial and temporal coverage of WOD09 (i.e., the 2009 version of WOD, Boyer et al., 2009) in the South Georgia region are shown in Figs. 2.1a and 2.2b, respectively, regardless of the sampling technique and type of measurement.

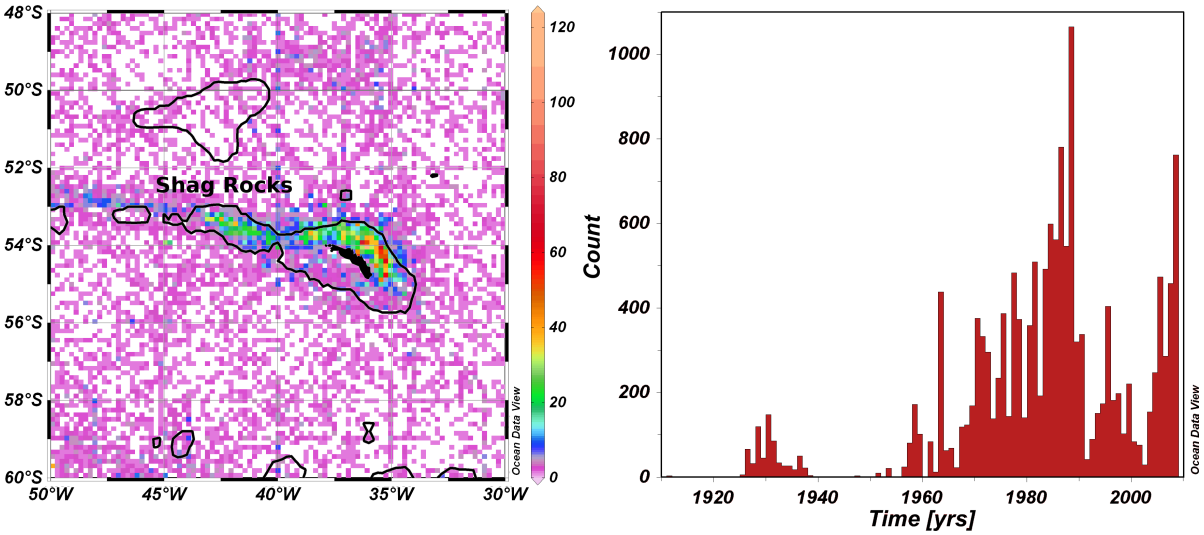


*Fig.2.1 Spatial (A) and temporal (B) coverage of the WOD09 (Boyer et al., 2009) in the South Georgia region. The colourscale in (A) and the y-axis in (B) indicate the total number of available measurements. All panels were created using Ocean Data View (Schlitzer, 2012).*

Fig. 2.1a clearly shows that except for the northeastern and northwestern shelf of the island (regions recurrently sampled by British Antarctic Survey expeditions, Whitehouse et al., 2008b; Meredith et al., 2005) and Shag Rocks (~42°W, 53.5°S) in most of the South Georgia region the total number of available observations is close to or below 10. Therefore, large sectors of the region have been rarely sampled, or not sampled at all (white areas in Fig. 2.1a). Moreover, as shown in Fig. 2.1b, there is a large drop in the number of measurements during austral winter when meteorological and sea-state conditions are prohibitive; therefore, in situ measurements around the island are seasonally biased, allowing for rare year-round time series (Whitehouse et al., 2008b). Consequently, a comprehensive study of the region needs a multidisciplinary approach, but must also rely on several and potentially very different types and sources of data. This challenging approach was adopted during the PhD research study presented in the thesis. Its outcomes, collected in the publications reported in Section 3 highlight the importance of publicly available oceanographic datasets and tools,

without which large part of this study was not possible. Data used for this work can be grouped in three categories: 1) data collected in situ, 2) data collected remotely using satellite sensors, and 3) data produced by model simulations. The publication presented in Section 3.4, for example, results from the combination of all three categories. An introduction of each data category is given below. To avoid redundancy, details on how the data were processed are given in each publication.

## *2.1 In situ measurements*

Oceanographic in situ measurements utilized in this study are available from the World Ocean Database (WOD, http://www.nodc.noaa.gov). There are several WOD editions starting from 1994. The most recent is from 2009 (WOD09; Boyer et al., 2009) and contains (world-wide) approximately 9.1 million measurements, more than twice the number available in WOD94. The WOD consists of a collection of physical (i.e., temperature, salinity), biological (i.e., chlorophyll, phytoplankton and zooplankton groups) and chemical (i.e., macronutrients, oxygen, alkalinity, pH) measurements, for each value, the database keeps record of the location, time and depth of sampling. Measurements were collected using very different platforms, including station data, profiling floats, drifters and more recently also tagged marine mammals. Macronutrient measurements from WOD09 are used in Sections 3.2 and 3.4.

Variables stored in the WOD09 have been averaged in time, gridded and interpolated (using the optimal-interpolation technique) to produce the World Ocean Atlas climatology (WOA, http://www.nodc.noaa.gov), a three-dimensional dataset with a uniform horizontal resolution (1° grid), and 33 vertical levels. The WOA is available as annual, seasonal and monthly-means and is updated approximately every four years following each WOD edition. WOA09, for example, provides a climatology for temperature (Locarnini et al., 2010), salinity (Antonov et al., 2010), oxygen (Garcia et al., 2010a) and nutrients (Garcia et al., 2010b). The WOA version of 2005 (Conkright et al., 2002) is the default dataset used to construct the boundary and initial conditions for the ROMS-PISCES model presented in Section 2.3 below.

The CSIRO Atlas of the Regional Seas (CARS, http://www.marine.csiro.au/~dunn/cars2009/; Ridgway et al., 2002) is another climatological dataset including WOD data. CARS data are available at a resolution of 0.5°. The interpolation technique used to produce CARS maximises resolution in data-rich regions, and adopts an algorithm that takes into account bottom topography and land barriers (Dunn and Ridgway, 2002) so that oceanographic gradients and patterns appear to better reflect ocean circulation. The CARS version of 2009 is used for the validation of model results presented in Section 3.4.

In the same publication are also used in situ measurements of dissolved iron. The latter measurements, however, are not included in any of the publicly available datasets or atlases presented above, and were provided directly by Nielsdóttir et al., 2012.

## 2.2 Satellite observations

The advent of satellite remote sensing determined a great advance in oceanography, complementing the limited number of in situ measurements, especially in the southern hemisphere. Satellite remote sensing can provide a synoptic view of very large ocean surfaces at spatial resolutions that, for some sensors, can reach few hundreds of meters. Satellites on geostationary or polar orbits provide information on the Earth's surface with a time resolution of approximately one day. Indeed, satellite remote sensing is not without limitations. First of all, satellite measurements pertain to the surface of the oceans only (the sub-surface layers are not sampled). Second, depending on the "observing" technique, data coverage can suffer from two important limitations: cloud cover, when measuring ocean colour and sea surface temperature (using infrared radiation) and reduced light levels. The latter affects ocean color measurements during the poorly illuminated seasons (i.e., winter), in particular at the high latitudes.

Several oceanographic variables can be measured using satellite remote sensing. Ocean colour imagery of surface chlorophyll *a* concentrations (a proxy for phytoplankton biomass) and satellite altimetry are used throughout the whole thesis. The former is used to describe the presence and development of phytoplankton blooms, while the latter allows a measure of sea surface height and hence a description of surface circulation. Other satellite derived measurements used in this study (see Section 3.2) are sea surface temperature (SST), photosynthetically available radiation (PAR, a measure of how much solar radiation can be used for photosynthesis) and wind velocities. Table 2.1 summarizes all satellite-derived datasets used for this study.

*Table 2.1 List of all satellite-derived variables utilized in this study.*

| Variable | Sensor / satellite | Data source |
|---|---|---|
| Chl *a* | SeaWiFS | http://oceancolor.gsfc.nasa.gov/ |
| Chl *a* | MODIS | http://oceancolor.gsfc.nasa.gov/ |
| SST | MODIS | http://oceancolor.gsfc.nasa.gov/ |
| Winds | QuikSCAT | http://www.ifremer.fr/opendap/cerdap1/cersat/wind/l4/ |
| PAR | MODIS | http://oceancolor.gsfc.nasa.gov/ |
| Altimetry | Aviso | http://www.aviso.oceanobs.com/duacs |

## 2.3 Hydrodynamic-biogeochemical modelling

It is difficult to resolve the large scale temporal and spatial evolution of processes involving biology and/or biogeochemistry using in situ measurements alone. This is particularly valid for the Southern Ocean where in situ measurements are limited in number,

and suffer from a seasonal bias. Remote sensing contributes positively to the data coverage of selected oceanographic parameters, however also satellite imagery suffers from sampling limitations. In this context, numerical modeling can help fill in some of the remaining gaps. Modeling, in fact, provides the means to test hypothesis and understand processes in a virtual and large scale laboratory, even when little data is available for the validation of results. Simulations can be repeated and modified several times, and all modeled variables are returned at the same spatial and temporal resolution, an aspect that is very difficult to achieve using real data, but that is fundamental to understand links between processes (i.e., circulation and distribution of nutrients).

In this study, two models were used in a coupled configuration. The hydrodynamic model ROMS (Regional Oceanic Modeling System, Shchepetkin and McWilliams 2005) provided the ocean physical setting around the island (i.e., ocean circulation, temperature, salinity), while the biogeochemical model PISCES (Pelagic Interaction Scheme for Carbon and Ecosystem Studies, Aumont and Bopp, 2006) was used to simulate biology and biogeochemistry (i.e., phytoplankton, zooplankton and micro- and macronutrients). The presence in PISCES of an iron cycle and phytoplankton iron-limitation is the key aspect of the model when investigating biogeochemistry in the HNLC Southern Ocean.

ROMS is an open source, community-supported model. The ROMS code and its application-specific options (i.e., activation of processes related to tidal forcing, biogeochemistry and sediment transport) have been downloaded from the web (http://www.romsagrif.org) together with all the pre- and post-processing tools (Penven et al., 2008) necessary for data preparation and model set up (i.e., domain size, horizontal and vertical resolution, initial and boundary conditions). The model's code is written in Fortran, the pre and post-processing tools are written in MATLAB, while all model input and outputs conforms to the NetCDF data format (http://www.unidata.ucar.edu/software/netcdf/). The model was run on 64 IBM parallel computers hosted at the Deutsches Klimarechenzentrum (DKRZ, http://www.dkrz.de/) in Hamburg (Germany).

PISCES (Aumont and Bopp, 2006) is a 24-compartment biogeochemical model (Fig. 2.2). It simulates the biogeochemical cycles of oxygen, carbon and the cycle of the main nutrients controlling phytoplankton growth, like phosphate, nitrate, ammonia and silicate (macronutrients), and iron. The iron cycle in PISCES is described with more detail in Section 3.4 and Fig. 3.4.3; here we summarize the main aspects. In the model the iron cycle is relatively complex: iron is introduced to the ocean from the sediments or dust deposition; once in the water column it interacts with ligands (complexation), organic particles (scavenging) and the biological compartment (uptake, exudation, remineralization). The phytoplankton compartment comprises nanophytoplankton and diatoms; of the two, only the latter requires silicate for growth. Moreover, PISCES includes a grazer compartment (i.e., micro- and meso- zooplankton) as well as a non-living compartment, composed of big and small organic particles as well as dissolved organic matter. In all living compartments the total biomass in carbon is calculated explicitly and the Redfield C/N/P ratios are assumed constant. Additionally, for the phytoplankton compartment PISCES explicitly calculates values for chlorophyll (Chl), iron and, for diatoms only, silicate.

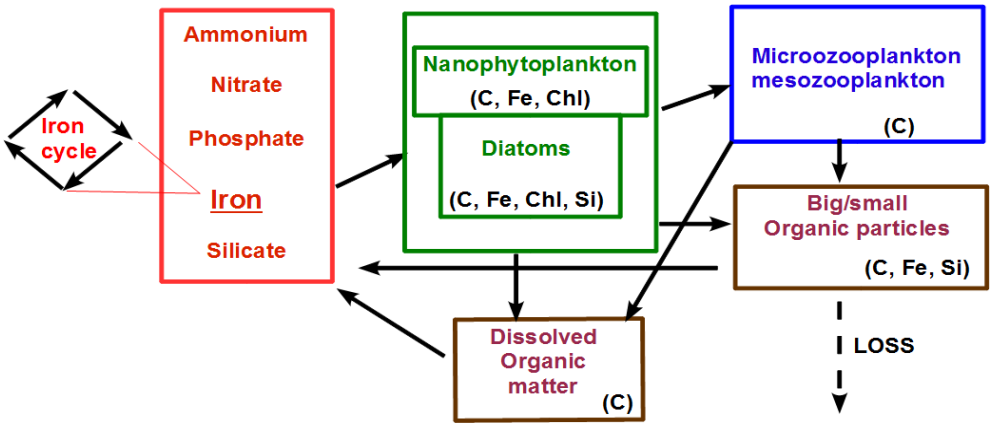


*Fig. 2.2. Schematics of the PISCES modelling structure and compartments (modified from Aumont and Bopp, 2006). Between parenthesis are indicated the prognostic variables for phytoplankton, grazers and the non living compartment. A detailed schematics of the iron cycle is depicted in Section 3.4 (Fig. 3.4.3).*

Thanks to their versatility, the models employed in this study have been used (separately, or coupled to other models) for several different applications (i.e., Karakas et al., 2006; Penven et al., 2006; Aumont and Bopp, 2006; Slemons et al., 2009; Tagliabue et al., 2009a), but never for the South Georgia area. Therefore, before ROMS-PISCES could be used for the scientific purposes of this PhD project, several preliminary simulations were performed to identify the model-setup that best reproduced in situ and satellite observations.

Setting up ROMS-PISCES for the South Georgia region revealed to be particularly problematic and several aspects had to be considered jointly. Table 2.2 reports all the datasets used for testing of the optimal model set-up.

First, bathymetry around South Georgia is very complex (Fretwell et al., 2009), with several regions of rapid depth variations, mounds and basins that are known to influence local circulation (i.e., Meredith et al., 2003; Korb et al., 2008). Therefore, it was important to choose the most representative bathymetric dataset as well as the optimal parameters used to prepare the topography used by the model. Second, South Georgia is located in a very dynamic system (the ACC); the ACC fronts, which flow very close to the island, control the physical and biogeochemical ocean properties around the island. Therefore, it was important that model boundary conditions allowed an acceptable representation of the ACC fronts around the island, as well as the main characteristics of physical and biogeochemical water properties. Third, South Georgia experiences pronounced seasonal variations (solar insulation, temperature changes), therefore, it was necessary to identify the best surface forcing fields, which determine the model's atmosphere-ocean heat and fresh water fluxes. Fourth, South Georgia is located very close to the northern limit of winter pack-ice. Sea-ice influences ocean-atmosphere heat exchanges; its formation and melting modifies ocean temperature and salinity. As the version of ROMS used in this study did not include a component able to model or account for sea-ice formation, it was necessary to carefully trace the southern limit of the modeling domain: the outcome was a compromise allowing sufficient space between the island and the chosen southern boundary but also the maximum distance possible from the same boundary and the winter limit of pack-ice. Finally, several simulations were dedicated to

testing the optimal horizontal resolution of the model. The size of the grid in fact, controls (i) the degree of topographic smoothing, (ii) the scale and details of oceanic processes that can be simulated (i.e., mesoscale features, eddies, vertical upwelling, mixing, Chelton et al., 1998; Young et al., 2011) but also (iii) the computing resources required for each model time-step. In the final model configuration, ROMS-PISCES required 12 hours of computing time to simulate one model year.

*Table 2.2. Dateset names and their references for topography, surface forcing fields and boundary conditions tested during the implementation of ROMS_AGRIF-PISCES to the region surrounding South Georgia. Datasets denoted with an asterisk, are those used in the final model configuration.*

| **Dataset name** | **Main reference** |
|---|---|
| Bathymetry | |
| ETOPO2* | Smith and Sandwell, 1997 |
| GEBCO | http://www.gebco.net/ |
| Ocean boundary conditions | |
| SODA* | Carton and Giese., 2008 |
| WOA* | Conkright et al., 2002 |
| ECCO | Stammer et al., 2002 |
| ORCA* | Aumont and Bopp, 2006 |
| Surface forcing | |
| QuikSCAT* | http://www.ifremer.fr |
| CORE | Griffies et al., 2009 |
| NCEP | Kistler et al., 2001 |
| COADS* | Da Silva et al., 1994 |
| PATHFINDER* | Casey and Cornillon, 1999 |

# 3 Results

Results obtained during this PhD project are presented in four publications, and a manuscript on work in progress. A brief introduction to each contribution is given below.

In Section 3.1. a 10 year long time series of SeaWiFS ocean colour images is analysed to describe the inter-annual variability of Chl a concentrations in the Scotia Sea. Ocean colour climatological maps are used to describe the seasonal evolution of Chl a concentrations in the region. Results highlight two regions with regular patterns, yet characterized by contrasting levels of primary productivity: around South Georgia intense phytoplankton blooms are observed regularly, while upstream the Shackleton Transverse Ridge, in the Southern Drake Passage region, phytoplankton blooms are very rare and Chl a concentrations are regularly very low (< 0.2 mg $m^{-3}$). Environmental conditions behind the observations are presented briefly.

Section 3.2 presents a detailed study of primary productivity patters around the island of South Georgia. Satellite ocean colour and altimetry measurements, available between 1997 and 2010 (13 yrs), as well as in situ measurements of macronutrients were used jointly to investigate the natural variability (in space and time) of South Georgia phytoplankton blooms. We could identify the typical bloom area, a confined region where phytoplankton blooms have occurred most regularly and where, therefore, phytoplankton bloom are expected to be predictable. We suggest iron replete conditions, and indicate that the occurrence of phytoplankton blooms is controlled in space by circulation and regulated in time by surface silicate concentrations, temperature and light.

Section 3.3 combines results from satellite ocean colour imagery and altimetry with results from the preliminary ROMS_AGRIF-PISCES simulations. This contribution provides the first overview of the South Georgia "island mass effect". It is highlighted that surface circulation controls the spatial distribution of phytoplankton blooms around the island. Model simulation are used to show the potential distribution of surface dissolved iron originating from the island. Causes for discrepancies between the model and observations are indicated briefly.

Section 3.4 uses all results presented in the previous sections to validate results from the coupled hydrodynamic-biogeochemical model ROMS_AGRIF-PISCES, implemented to the South Georgia region for the first time. The biogeochemical model accounts for iron-limitation of phytoplankton growth, a key process in HNLC waters. First, simulated iron concentrations were compared to the few available in situ measurements showing good agreement with the data. Second, model results were used to investigate the relative importance of atmospheric and sedimentary iron sources to the region, but also how iron is distributed downstream of South Georgia. Results provide modelling evidence for iron-replete conditions over the typical bloom area, and highlight that shallow sediments around the island are more important sources of dissolved iron than dust deposition.

Section 3.5 presents preliminary results from ROMS_AGRIF-PISCES simulations aimed at understanding if and how increased iron sources around the island can modify iron

availability and hence primary productivity downstream of South Georgia. Model results confirm the important role of circulation in determining the shape and maximum extension of blooms around South Georgia. Moreover results show that even at extremely high (and unrealistic) iron concentrations, modelled Chl a concentrations never reach magnitudes observed in satellite imagery. This possibly occurs because increased iron concentrations increase the importance of processes removing it from the water column.

## *3.1 A 10 year long time series of SeaWiFS data shows spatial and temporal variability of phytoplankton blooms in the Scotia Sea region*

I. Borrione* and R. Schlitzer

Alfred Wegener Institute for Polar and Marine Research, Bremerhaven, Germany
Ines.Borrione@awi.de, Reiner.Schlitzer@awi.de

Published as:
I. Borrione and R. Schlitzer, A 10 year long time series of SeaWiFS data shows spatial and temporal variability of phytoplankton blooms in the Scotia Sea region. Proceedings "Oceans from Space" Venice 2010. V. Barale, J.F.R. Gower, L. Alberotanza (Eds) European Commission, EUR 24324 EN, 266, pp. 41-42, doi:10.2788/8394, 2010.

### Abstract

Monthly averaged satellite imagery of chlorophyll a in the south-western sector of the Atlantic Ocean shows intense and recurrent blooms around the Antarctic Peninsula, the Island of South Georgia and the South Sandwich Islands. Analysis of a 10 year long time series of SeaWiFS ocean color images allows studying seasonal trends and inter-annual variability. Although specific areas show a regular pattern of low or high productivity, certain years appear to be strikingly productive or well below the climatological average. Circulation patterns, continental shelves as well as Antarctic Circumpolar Front are shown to be the major factors controlling extension of highly productive patches.

**Keywords:** Scotia Sea, SeaWiFS, primary productivity.

### 3.1.1 Introduction

The Scotia Sea area, included between the North and South Scotia Ridge (SSR), and between the Drake Passage and the South Sandwich Islands (SSI), has always been recognized as a High Nutrient Low Chlorophyll (HNLC) region which experiences intense summer phytoplankton blooms; it is characterized by an average depth greater than 2000m, where ridges, trenches, plateaus and islands complicate its bathymetry. The main water masses are those included in the Antarctic Circumpolar Current (ACC) which carries a uniquely high nutrient content. While the current flows next to continental shelves waters are naturally fertilized with iron, enhancing primary productivity. Ecosystems around the Antarctic Peninsula and the South Sandwich Islands result more complex by the advance and retreat of sea-ice.

Bands of enhanced chlorophyll a concentration (Chl-a) are strongly localized around island ecosystems and shallower topographic features (i.e. the Antarctic Peninsula continental shelf, the SSR and offshore the island of South Georgia, hereafter SG). Previous works indicate that in this domain in-situ Chl-a may reach values higher than 10 mg/m^3 (Korb et al., 2004; Holm-Hansen et al., 2004). The iron deficiency hypothesis (Blain et al., 2001) together with sea-ice melting (Smith et al., 2008), ocean circulation patterns (i.e. eddies), and the "island mass effect" (Blain et al., 2001) may jointly explain such striking events for a HNLC region.

A synoptic study of such a vast region is possible only via satellite imagery, although winter darkness does not allow measurements between April and July; nevertheless, remote sensing remains for this region the key observational tool where weather and sea-state conditions strongly limit high resolution in-situ measurements.

### 3.1.2 Resolving temporal and spatial dynamics

#### SeaWiFS data

SeaWiFS derived estimates of surface Chl-a were obtained from the Goddard Distributed Active Center. Level-3, monthly composites at 9 km resolution were retrieved for the period between January 1998 and December 2007. As winter conditions limited ocean color coverage of the domain, analysis was restricted to the spring and summer seasons. Each monthly Chl-a image was combined into a climatological average. The Chl-a relative error was calculated as the ratio between the standard deviation and the climatological average and was used to infer its variability. Single monthly images were finally observed to pin-point years which appear to be exceptionally productive or well below average.

#### Seasonal trends

Although data is limited to latitudes greater than 60S, due mostly to sea-ice extent, data coverage is sufficient to show August as the month where Chl-a starts increasing. Most of the domain has concentration values close to zero, except along shallower bathymetries (SSR and north of the South Georgia basin) where they are included between 0.2 and 0.5 mg/m^3. Absolute Chl-a values progressively increase till December when they go beyond 3 mg/m^3. In this month surface areas with Chl-a concentrations greater than 0.5 mg/m^3 reach their maximum extension. After January productivity starts decreasing. In March, concentrations remain below 1 mg/m^3. Fig. 3.1.1 shows three snapshots (September, December and March) of the recurrent bloom north of SG, as an example of the above described seasonal trend.

#### Inter-annual variability

The climatological average of the most productive months (December and January) shows high Chl-a above the Argentine Shelf, and along a band running from the Antarctic Peninsula continental shelf, above the SSR, up to the SSI. A high productive plume is found also north

of SG, spreading eastward. Nevertheless, this pattern is not fully representative: certain years, in fact, may show a significantly lower or higher productivity. In December 2000, for example, the bloom north of SG is strongly reduced, and limited to a narrow band of high productivity extending east of the island, following a meandering path. Regions of greater inter-annual variability appear to be the surroundings of island ecosystems, such as the western Antarctic Peninsula, and the SSI.

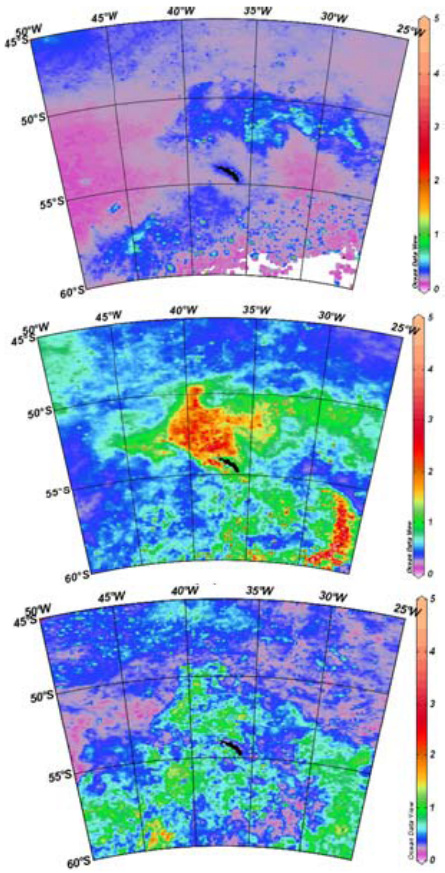


*Fig. 3.1.1. Climatological average of SeaWiFS derived estimates of surface Chl-a, for September (top), December (middle) and March (bottom) of the region surrounding the South Georgia island. The sequence elucidates the seasonal development of the recurrent summer bloom north of the island.*

## The Shackleton Fracture Zone – an example of permanent low productivity

Similarly to the area upstream the Drake Passage, where Chl-a remains below 0.2 mg/m^3 throughout most of austral summer, also the region adjacent the Shackelton Fracture Zone shows constant low productivity values (Fig. 3.1.3-left, violet region delimited by the 0.2 Chl-a contour). The ridge extends across Drake Passage acting as a barrier to the ACC, deflecting the Southern ACC Front westward. The relative error map for the same region (Fig. 3.1.2 - right), confirms that this low productivity region shows no variability (relative error<0.5).

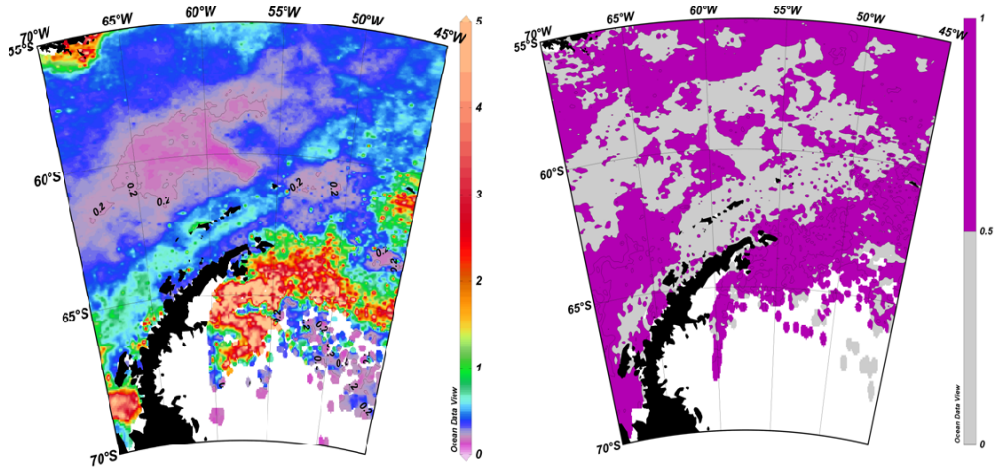


*Fig. 3.1.2. Climatological average of SeaWiFS derived estimates of Chl-a for Dec. (left); relative error (RE) of the measurement calculated as the ratio between the standard deviation and the climatological average of December (right). The map focuses on the region surrounding the Shackelton Ridge (dashed line). Results show this region to be consistently low in productivity (RE <0.5grey, RE>0.5 in magenta).*

## Factors confining phytoplankton blooms

Spatial development of patches with high Chl-a appears to be mostly controlled by circulation patterns, extension of continental shelves and position of the ACC fronts. The highly productive regions of the Argentine Shelf and the western Antarctic Peninsula fall in the first case: the greatest Chl-a gradient, coincides with the 500m depth bathymetry contour. Circulation patterns, as inferred from surface drifter trajectories seem to control the shape of the western border of the bloom north of SG bloom. Finally, the borders north and south of the plume extending east of SG, coincide approximately with the Polar Front and the Southern Antarctic Circumpolar Current Front, respectively. Another factor, localized in the northwestern Weddell Sea, may be the melting of sea-ice which may stabilize surface waters and release trapped particles, possibly rich in bio-available Iron. This effect could occur at the eastern tip of the Antarctic Peninsula: Fig. 3.1.2 (left).

## 3.1.3 Conclusions

A decade of SeaWiFS ocean color images has allowed studying the development and distribution of primary productivity in the Scotia Sea and along the Antarctic Peninsula. Results show seasonal enhanced productivity along shelf areas and the main island ecosystems. Although certain blooms occur regularly every year, their extension and maximum Chl-a concentration can be very variable. Circulation patterns, bathymetry and ACC front are responsible for their location and extension.

## Acknowledgements

This work was funded by the ESSReS (Earth System Science Research School) scholarship.

## *3.2 Distribution and recurrence of phytoplankton blooms around South Georgia, Southern Ocean*

I. Borrione* and R. Schlitzer

Alfred Wegener Institute for Polar and Marine Research, Columbusstrasse, 7568 Bremerhaven, Germany

Correspondence to: I. Borrione (ines.borrione@awi.de)

Published as:

Borrione, I., and Schlitzer, R.: Distribution and recurrence of phytoplankton blooms around South Georgia, Southern Ocean, Biogeosciences, 10, 217-231, doi: 10.5194/bg-10-217-2013, 2013.

### Abstract

South Georgia phytoplankton blooms are amongst the largest of the Southern Ocean and are associated with a rich ecosystem and strong atmospheric carbon drawdown. Both aspects depend on the intensity of blooms, but also on their regularity. Here we use data from 12 yr of SeaWiFS ocean colour imagery and calculate the frequency of bloom occurrence (FBO) to re-examine spatial and temporal bloom distributions. We find that upstream of the island and outside the borders of the Georgia Basin, blooms occurred in less than 4 out of the 12 yr (FBO <4). In contrast, FBO was mostly greater than 8 downstream of the island, i.e., to the north and northwest, and in places equal to 12, indicating that blooms occurred every year. The typical bloom area, defined as the region where blooms occurred in at least 8 out of the 12 yr, covers the entire Georgia Basin and the northern shelf of the island. The time series of surface Chlorophyll a (Chl a) concentrations averaged over the typical bloom area shows that phytoplankton blooms occurred in every year between September 1997 and September 2010, and that Chl a values followed a clear seasonal cycle, with concentration peaks around December followed in many years by a second peak during late austral summer or early autumn, suggesting a bi-modal bloom pattern. The bloom regularity we describe here is in contrast with results of Park et al. (2010) who used a significantly different study area including regions that almost never exhibit bloom conditions.

### 3.2.1 Introduction

Phytoplankton blooms play a key role in pelagic and benthic food webs, on the transfer of organic matter to the sea floor as well as on ocean biogeochemistry (Falkowski et al., 1998). In the presence of sufficient nutrient supply and light levels, phytoplankton can grow and accumulate to bloom levels where loss rates due to mortality (i.e. grazing) and sinking are exceeded. Across most of the Southern Ocean, despite the fhigh macro-nutrient content of surface waters transported by the easterly flowing Antarctic Circumpolar Current (ACC),

Chlorophyll a (Chl a) concentrations generally remain low and do not exceed 0.5 mg $m^{-3}$ (Comiso et al., 1993; Moore and Abbott, 2000). According to the iron hypothesis (Martin et al., 1990), these High Nutrient Low Chlorophyll (HNLC) conditions are due to iron limitation. In fact, when iron-stress was reduced by an exogenous source of iron, as for example during artificial iron fertilization studies (Boyd et al., 2007), phytoplankton blooms were observed. In natural conditions, regular blooms develop close to coastal regions and downstream of islands, where land masses constitute reliable sources of iron; examples are the western Antarctic Peninsula (e.g. Smith et al., 2008) or the sub-Antarctic Kerguelen and Crozet islands (Blain et al., 2008; Pollard et al., 2009; Planquette et al., 2007).

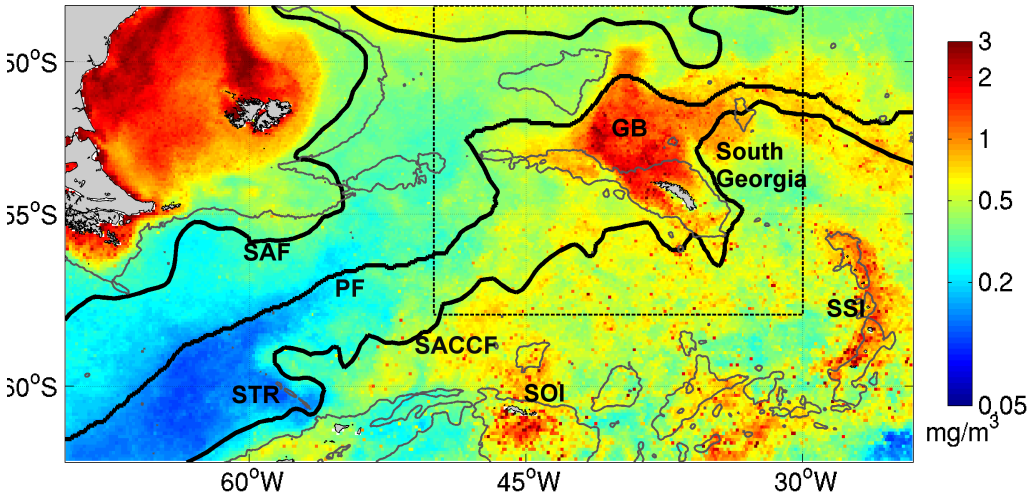


*Fig. 3.2.1. Chlorophyll a climatology derived from SeaWiFS Austral summer (Dec-Feb, from 1997-2010) in the south-western sector of the Atlantic Southern Ocean. Bold lines indicate the Sub-Antarctic Front (SAF, Orsi et al., 1995), the Polar Front (PF, Moore et al., 1999) and the Southern ACC Front (SACCF, Thorpe et al., 2002). Bathymetric contours for the 2000m are indicated with thin lines. The position of the Shackleton Transverse Ridge (STR), that of the South Orkney Islands (SOI), the Georgia Basin (GB) and the South Sandwich Islands (SSI) are also indicated.*

In the Southwestern Atlantic sector of the Southern Ocean (Fig. 3.2.1), strict HNLC conditions are mostly found in the Southern Drake Passage region, especially to the west of the Shackleton Transverse Ridge (STR in Fig. 3.2.1), where the absence of iron sources west of Drake Passage are believed to limit phytoplankton growth (Dulaiova et al., 2009; Hopkinson et al., 2007). East of the Drake Passage, phytoplankton blooms occur in response to diverse iron fertilization processes, including shelf-sediment interactions, i.e. along the shelf and continental regions of the Antarctic Peninsula or over the Southern Patagonian shelf (Ardelan et al., 2010; Hewes et al., 2008; Lutz et al., 2010), atmospheric dust depositions downwind of South America whether directly or following sea-ice melting (Lannuzel et al., 2007; Gassó and Stein, 2007; Smith et al., 2008), mesoscale features such eddies (Kahru et al., 2007) or iceberg melt (Lin et al., 2011). Whereas phytoplankton blooms in the open ocean waters of the Scotia Sea are short-lived and often unpredictable (Whitehouse et al., 2012), east of South America (north of the Sub-Antarctic Front) and downstream of islands they are recorded frequently. Among all island systems of the Scotia Sea (i.e., South Orkney or the South Sandwich Islands, indicated as SOI and SSI in Fig. 3.2.1), phytoplankton blooms of

South Georgia are the largest and most intense, with Chl a concentrations often exceeding 10 mg $m^{-3}$ (e.g., Korb et al., 2004).

The island of South Georgia, located at the north-eastern limit of the Scotia Sea, generates the largest meander in the eastward flowing ACC. As seen in Fig. 3.2.1, just before approaching South Georgia, the Polar Front (PF) veers north, and then resumes its eastward flow north of the island (Moore et al., 1999); to the south of the island, the Southern ACC Front (SACCF), which approaches South Georgia from the southwest, kinks westwards towards the Georgia Basin, before resuming its eastwards course (Orsi et al., 1995; Thorpe et al., 2002; Boehme et al., 2008). In response to this particular hydrography of the region, South Georgia phytoplankton blooms develop to the northwest of the island over the deep waters of the Georgia Basin (3500-4000m, see Fig. 3.2.2 for a map of bathymetry around South Georgia).

The highly productive environment of South Georgia is known to sustain a rich ecosystem, characterized by large stocks of krill, numerous colonies of marine and land based predators (Atkinson et al., 2001), as well as a shelf region reported to have the highest recorded biodiversity in the Southern Ocean (Hogg et al., 2011). Consequently, much attention has been dedicated to the understanding of primary productivity regimes associated to South Georgia, by means of shipboard measurements (e.g. Whitehouse et al., 2008a; Korb and Whitehouse, 2004), as well as from satellite imagery (Korb et al., 2012; Korb et al., 2004; Park et al., 2010). These studies mostly focussed on the region located south of 50°S, in particular on the southern portion of the Georgia Basin and the island's shelf. Results have indicated phytoplankton growing seasons ranging between 3 and 6 months, as well as significant spatial and temporal variability in surface Chl a concentrations. In particular, a recent multi-year study indicated that around South Georgia phytoplankton blooms showed low predictability and no regular seasonality (Park et al., 2010). Considering that the shelf of South Georgia is likely providing a reliable supply of shelf-derived iron, similar to the other major sub-Antarctic islands of the Southern Ocean (i.e., those of the Crozet and Kerguelen plateaus (Blain et al., 2008; Pollard et al., 2009; Chever et al., 2010)) one would expect the presence of regular seasonal blooms; hence, the results of Park et al. (2010) are rather unexpected.

In this study we utilize satellite ocean colour imagery to re-examine the spatial and temporal patterns of primary productivity associated to South Georgia. Following Korb et al. (2008) we define phytoplankton blooms as Chl a values equal or greater than 0.75 mg $m^{-3}$. Our area of study, the South Georgia region (rectangle in Fig. 3.2.1), was chosen in order to include the entire main bloom area revealed by the summer climatology and lies between (50°W, 30°W) and (48°S, 58°S).

### 3.2.2 Data and Methods

#### Ocean colour measurements

The 13 year-long time series of Sea-viewing Wide Field-of-View Sensor (SeaWiFS) data (McClain et al., 1998) was used for this study. Satellite imagery in fact, remains the

preferential tool for a quasi-synoptic view of a region as large as that surrounding South Georgia.

Freely available Standard Mapped Images - Level 3 (SMI-L3) products, for the years between 1997 and 2010, combined to form monthly and eight-day Chl a averages, processed by the Goddard Space Flight Center and projected on a regular spatial grid of 9 km, were retrieved from the distributed Active Archive Center from http://oceancolor.gsfc.nasa.gov/. In our analysis we focus on Austral summer (December to February) as this is the period when Chl a biomass reaches its peak concentrations and coincides with the season when most oceanographic cruises are conducted and cloud cover is reduced. No SeaWiFS data are available for the months of January and February 2008, therefore we excluded the 2007/2008 summer season from the calculation of frequency of bloom occurrences (see below).

Several efforts have been made to validate SeaWiFS measurements with in situ data collected in Antarctic waters. Although results may differ between regions of interest, it is a general agreement that the SeaWiFS global chlorophyll algorithm performs adequately when compared to direct measurements of Chl a (Arrigo et al., 2008; Korb et al., 2004; Holm-Hansen et al., 2004) albeit concentrations above ~0.5 mg $m^{-3}$ are underestimated (Garcia et al., 2005; Szeto et al., 2011).

### Pixel count algorithm and frequency of bloom occurrences

The focus of this study is to investigate the spatial and temporal dynamics of Chl a concentrations that pertain to phytoplankton bloom conditions. Southern Ocean blooms were distinguished by Comiso et al., (1993) as having Chl a values >1 mg $m^{-3}$. However, because of the tendency of SeaWiFS to underestimate mid to higher Chl a, we chose 0.75 mg $m^{-3}$ as a threshold value to define phytoplankton blooms, which has been also used by Korb et al. (2008) and is very close to the 0.8 mg $m^{-3}$ value adopted by Fitch and Moore (2007). Consequently, only Chl a concentrations higher than 0.75 mg $m^{-3}$ were accounted for and grouped in a single bloom category, independent from the bloom magnitude.

For every SeaWiFS data pixel in the South Georgia region (domain indicated in Fig. 3.2.1) we calculate the December-February austral summer average for each of the 12 yr between 1997 and 2010; missing values (i.e., due to cloud cover) were excluded in the calculations. In each of the 12 December-February austral summer averages, nearly all pixels from the main South Georgia bloom region contain Chl a concentration data. Then we calculate for every pixel the number of years (i.e., the number of austral summer averages) during which Chl a concentrations exceeded the bloom threshold value 0.75 mg $m^{-3}$.

Results are displayed as frequency of bloom occurrence (FBO) plots, where the colour scale indicates the number of summer seasons when Chl a concentrations corresponded to bloom conditions. For each pixel in the frequency plot (~60 $km^2$), the obtained FBO give an indication of the recurrence, and hence the predictability level of phytoplankton blooms. Phytoplankton blooms can be considered very recurrent (hence very predictable) in regions where FBO are closest to 12, which is the total number of austral summer seasons included in the analysis. Intermediate FBO (~ 6) indicate that Chl a concentrations fell recurrently both

above and below the threshold (i.e., pronounced variability) in the 12-year period while reduced FBO (FBO <4) indicate less frequent or rare bloom events.

To assess the sensitivity of the results to the chosen threshold, we repeated the calculations with slightly different values (i.e., 0.7 mg $m^{-3}$ or 0.8 mg $m^{-3}$), but found nearly identical patterns in all cases. Further, we checked that the results obtained from the FBO calculated from seasonal averages (i.e., trimesters) is comparable to the FBO calculated by considering each summer month independently (i.e., not combined to form seasonal averages).

### Surface water circulation

Surface circulation patterns in the South Georgia region were obtained from AVISO satellite altimetry (http://www.aviso.oceanobs.com/duacs/). Weekly delayed-time mapped absolute dynamic topography data, re-sampled on a regular 0.25° grid, were extracted for the months of December through February and for the period between 1997 and 2010. The AVISO altimeter product is based on multiple altimeter missions (Jason-1&2, T/P, Envisat, GFO, ERS-1 & 2 and Geosat) and provides a consistent and homogeneous dataset. The altimeter data were averaged to form an austral summer climatology for the 1997 to 2010 period (Fig. 3.2.2). In addition, averages for individual months were used for instantaneous comparisons with monthly ocean colour composites (Fig. 3.2.4).

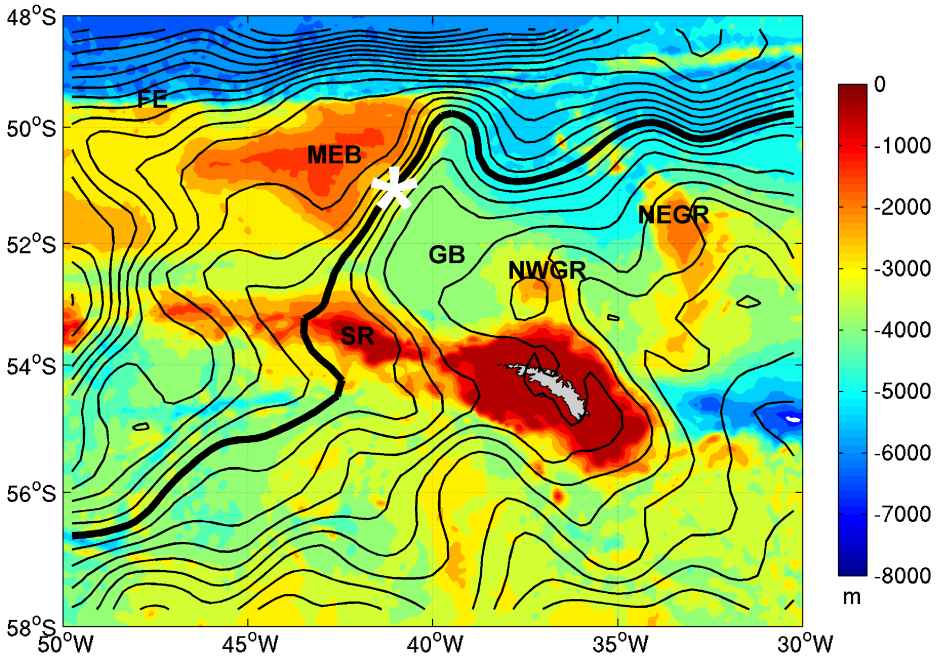


*Fig. 3.2.2. Bathymetry (in colour) and climatological circulation (black lines) in the South Georgia region. Black lines correspond to AVISO dynamic topography isopleths for the summer climatology (Dec-Feb, from 1997-2010). Isopleths are equally spaced every 5dyn cm, and dynamic topography values decrease from north to south; for reference, the -71dyn cm contour line used by Venables et al. (2012) to locate the southern extent of the Polar Front is shown in bold. FE: Falkland Escarpment, MEB: Maurice Ewing Bank, GB: Georgia Basin, SR: Shag Rocks, NWGR: North West Georgia Rise and NEGR: North East Georgia Rise. The position of the MEB-GB margin, referred to in the text, is indicated with a white star.*

Surface dynamic topography contours represent geostrophic streamlines, and indicate pathways and strength of surface circulation; the former are parallel to isopleths, while the latter are stronger when isopleths run closer.

### Macronutrients

In order to characterize the seasonal cycle of macronutrient concentrations in the South Georgia region, we retrieved surface (0-50m) water concentrations of nitrate, phosphate and silicate from the World Ocean Database 2009 (WOD09, Boyer et al., 2009). Data from WOD09 are distributed by the NOAA National Oceanographic Data Center (http://www.nodc.noaa.gov/OC5/WOD09/pr_wod09.html).

### Sea Surface Temperature, Photosynthetically Active Radiation and wind speed

SMI-L3 eight-day Terra-MODIS (Moderate Resolution Imaging Spectroradiometer) averages of Sea Surface Temperatures (SST), processed by the Goddard Space Flight Center and projected on a regular spatial grid of 9 km, were retrieved for the South Georgia region and over the years between 1997 and 2010 from the distributed Active Archive Center (http://oceancolor.gsfc.nasa.gov/). From the same website, time-period and region we also retrieved SMI-L3 eight-day averages of SeaWiFs Photosynthetically Active Radiation (PAR).

Daily QuikSCAT (Quik SCATterometer) Level-4 wind-speed measurements available between 1999 and 2009 were retrieved for the South Georgia region from the Center for Satellite Exploitation and Research (CERSAT, http://www.ifremer.fr/opendap/cerdap1/cersat/wind/l4/quikscat/daily/).

To evaluate how SST, PAR and wind-speed influence the temporal evolution of Chl a concentrations in the South Georgia Typical Bloom Area (see below) environmental measurements over the same area were averaged for the period 27 October - 02 April of each year and for a 15-day period prior to each year's bloom onset-date (i.e. first week in which Chl a were $\geq 0.75$ mg $m^{-3}$, see Table 3.2.1 and 3.2.2). From the 15-day averages we subtracted the climatological values over the same 15-day period to remove the effect of the seasonal cycle: towards the summer, SST and PAR are likely to increase, while wind-speed is likely to decrease. Hence, in the correlations with dates of bloom onset we used 15-day SST, PAR and wind-speed anomalies. All values used in the correlations (i.e. growth-season averages, 15-day anomalies and bloom onset-dates) as well as the obtained correlation coefficients are reported in Table 3.2.2 and discussed in section 3.2.4.

### 3.2.3 Results

#### Austral summer climatology

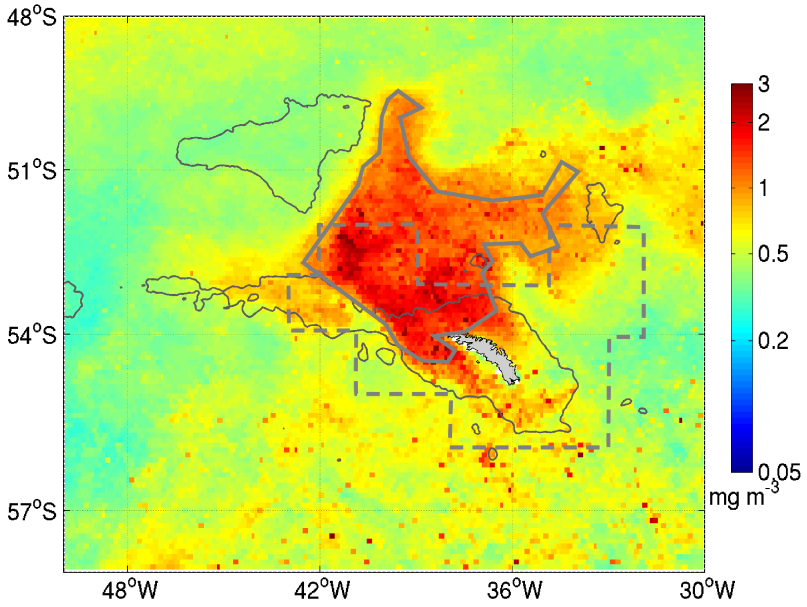


*Fig. 3.2.3. Surface Chl a climatology around South Georgia (detail from Fig. 3.2.1). The bold grey line marks the Typical Bloom Area (see below), and the dashed grey line marks the Georgia area utilized by Park et al. (2010). The 2000m bathymetry contour is indicated with thin lines.*

The Chl a climatological average constructed by averaging austral summer data (December to February) over the entire study period between 1997 and 2010 is depicted in Fig. 3.2.3. Chl a values greater than 0.75 mg $m^{-3}$ are present over the Georgia Basin and in the area west of the North East Georgia Rise, along the northern and southern shelf of the island as well as in the area surrounding Shag Rocks. Chl a concentrations greater than 3 mg $m^{-3}$ (shades of dark red) are indicated mostly in the south-western portion of the basin including the north-western shelf of the island. Overall, averaged Chl a values decrease in a north-easterly direction and reach values close to 0.75mg $m^{-3}$ in the area adjacent to the North East Georgia Rise.

#### Spatial and temporal variability

In Fig. 3.2.4 we show SeaWiFS Chl a data (colours) as well as satellite altimetry values (black contour lines) for four individual months. These four monthly composites were chosen because of reduced cloud cover within the South Georgia bloom area. Furthermore, each image provides examples of the major spatial Chl a patterns present in the SeaWiFS time series analyzed here and allows an examination of how bloom distributions relate to local circulation. Unsurprisingly, all composites reveal greater patchiness with respect to the previously described Chl a climatology (Fig. 3.2.3, see also Fig. 3.2.2 for a climatology of circulation around South Georgia).

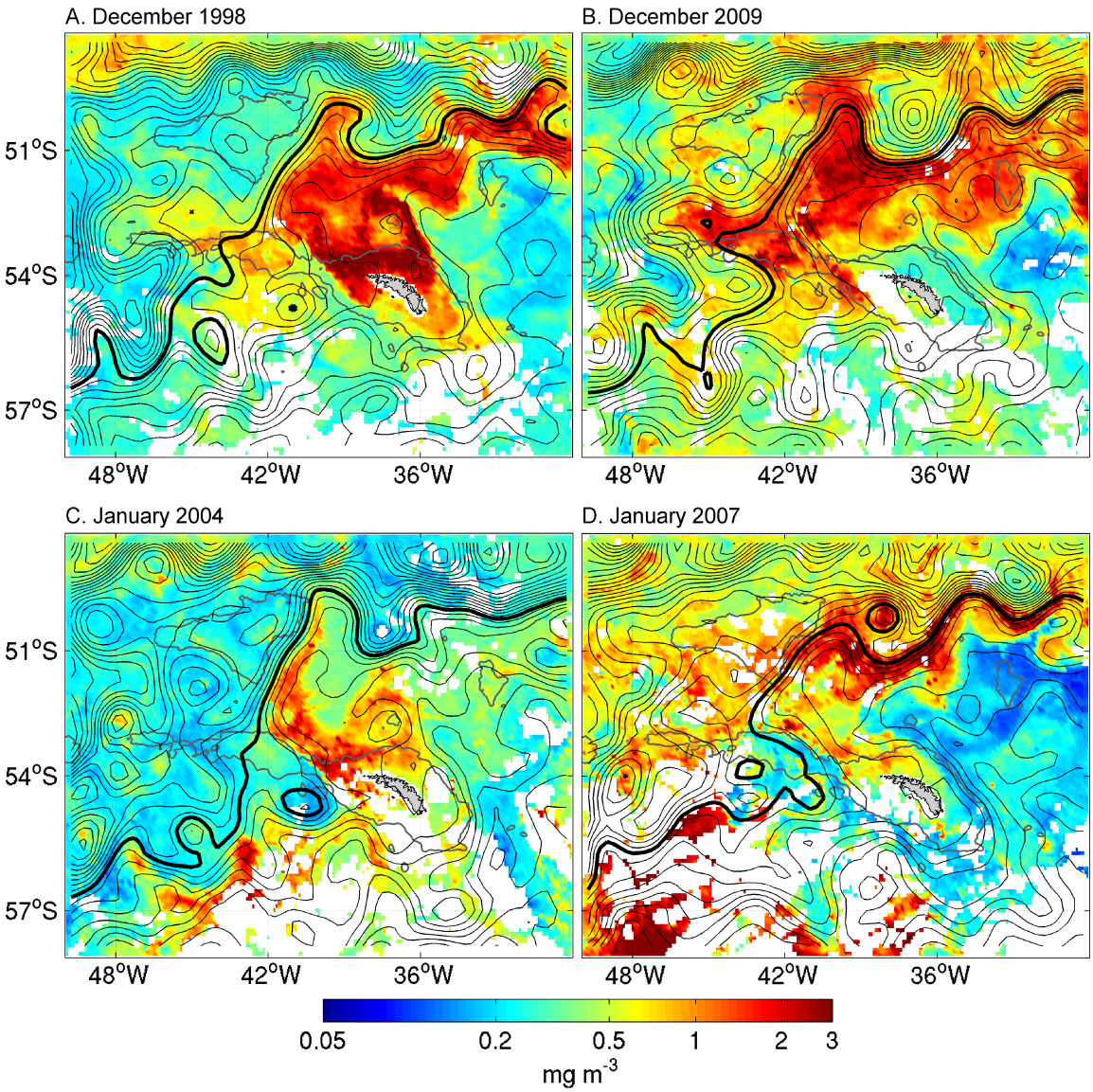


*Fig. 3.2.4. Monthly composites of Chl a concentrations (colour) and concomitant dynamic topography isopleths (black lines) for (A) December 1998, (B) December 2009, (C) January 2004 and (D) January 2007, respectively. Isopleths are equally spaced every 5 dyn cm to highlight the smaller scale features; values decrease from north to south. As reference, the -71 dyn cm contour is depicted with a bold line, to indicate, according to Venables et al. (2012), the southern limit of the Polar Front. Colour scale units are mg $m^{-3}$. Yellow to red colours depict bloom conditions (Chl a ≥ 0.75 mg $m^{-3}$). Regions in white correspond to data gaps due to the presence of persistent cloud cover. For reference, the 2000m bathymetry contour is also indicated with thin grey lines.*

In all chosen examples, a close match between Chl a distributions and surface flow fields (direction and intensity) is observed, also at the smaller scales. In December 1998 (Fig. 3.2.4a) for example, the phytoplankton bloom is clearly confined to the area comprising the shelf of the island and it extends over the southern and northern sectors of the Georgia Basin up to the southern limit of the Polar Front (bold line), here defined following Venables et al. (2012). All sides of the bloom are tightly contoured by closely spaced isopleths, which indicate strong currents. Similar phytoplankton blooms and circulation patterns are also observed in December 2001, January 2005 and January 2006 (not shown). Over the North West Georgia Rise (37°W, 52.5°S), amidst Chl a concentrations greater than 2 mg $m^{-3}$, a

patch with lower Chl a values (~0.70 mg $m^{-3}$) can be observed delineated by closed lines that indicate the presence of the anticyclonic eddy previously identified by Meredith et al. (2003). This eddy is present in most of the summer months considered for this study and is clearly captured by the circulation climatology of Fig. 3.2.2.

Compared to December 1998 (Fig. 3.2.4a), the periphery of the bloom observed in December 2009 (Fig. 3.2.4b) is less clearly defined and extends further to the west, following the pronounced meander kinking westwards. Most of the bloom is confined to the northern sector of the Georgia Basin and is missing around the island. Other examples of similar Chl a distributions are found in December 1999, January 2003 and December 2007 (not shown). Worth noting, is the anticyclonic eddy present north of the bloom area, with lower Chl a concentrations. This eddy, which is a recurrent feature of the region and is also present in the monthly images of December 2001 and December 2005 (not shown), is likely stabilized by bottom topography, which here is closely followed by the lines of flow (see also Fig. 3.2.2). In January 2004 (Fig. 3.2.4c) the phytoplankton bloom is much weaker and smaller and is confined to the area closer to the island; highest Chl a concentrations are found surrounding the North West Georgia Rise and over the northern shelf of the island up to the northern limits of the Maurice Ewing Bank–Georgia Basin (MEB-GB) margin. In January 2007 (Fig. 3.2.4d), bloom conditions are mostly limited to a narrow band of very closely spaced dynamic topography isopleths to the north of South Georgia, following the approximate position of the Polar Front (bold contour line). In this monthly composite, as in December 2000 (not shown), intense blooms (Chl a > 2 mg $m^{-3}$) are present far from the island shelf and at distances calculated along the direction of main flow that can be greater than 800 km. To the northwest of the island, and over the southern portion of the Georgia Basin Chl a concentrations are mostly below 1 mg $m^{-3}$ and in the proximity of the North West Georgia Rise Chl a values are close to 0.2 mg $m^{-3}$. The Chl a rich cyclonic eddy detaching from the northern tip of the South Georgia bloom is another recurrent feature of the region, and has been observed also in December 2000 and December 2004 (not shown).

Overall, we observe that protrusions and bends in regions of enhanced Chl a values generally coincide with meanders in the flow, while patches of higher or lower concentrations coincide with eddies. In most cases, largest concentration gradients are located along bands of rapid currents, which define the limits of the bloom area. This can be particularly seen along the -71dyn cm contour (i.e., the southern limit of the Polar Front, (Venables et al., 2012)), which in all cases closely delimits the western extent of South Georgia blooms to the MEB-GB margin and determines the formation of the clock-wise flowing meander located at the northern tip of the Georgia Basin (39°W,50°S). In these locations, the close correspondence between circulation and primary productivity patterns is well captured also by the climatologies depicted in Fig. 3.2.2 and 3.2.3. Furthermore, particularly recurrent appears to be the flow found along the northern flank of Shag Rocks and travelling from the north-western shelf of the island towards the MEB-GB margin. In most cases, this particular flow delimits the south-western extension of phytoplankton blooms occurring over the Georgia Basin.

Summarizing, phytoplankton blooms (i.e., Chl a concentrations greater than 0.75 mg $m^{-3}$) are observed on all occasions and they recur especially over the northern shelf of the island,

and in the south-western portion of the Georgia Basin extending to its northern periphery along MEB-GB margin. Outside these regions phytoplankton blooms show larger variability. In particular, to the west and to the north of the line delimiting the southern extent of the Polar Front and due east of the island, summer Chl a concentrations never rise above 0.5 mg $m^{-3}$.

Occasional small-scale pattern differences between surface flows and Chl a distributions shown in Fig. 3.2.4 can be affected by the different spatial resolution of the two datasets (1/4° for AVISO and circa 1/12° for SeaWiFS), or by the temporal average (here we show monthly composites). Such large averaging time period is dictated by the need for enough ocean colour measurements; the latter in fact are highly compromised by persistent cloud cover (white regions in the panels of Fig. 3.2.4).

### Frequency of bloom occurrences and the Typical Bloom Area

Ocean colour estimates utilized to construct the climatological average depicted in Fig. 3.2.3 were also elaborated with the pixel count algorithm; results provide information on the frequency of occurrence of summer phytoplankton blooms recorded in the South Georgia region. The colour of each image-pixel (~60 $km^2$) represents the total number of years when Chl a concentrations exceeded 0.75 mg $m^{-3}$ (i.e., bloom conditions).

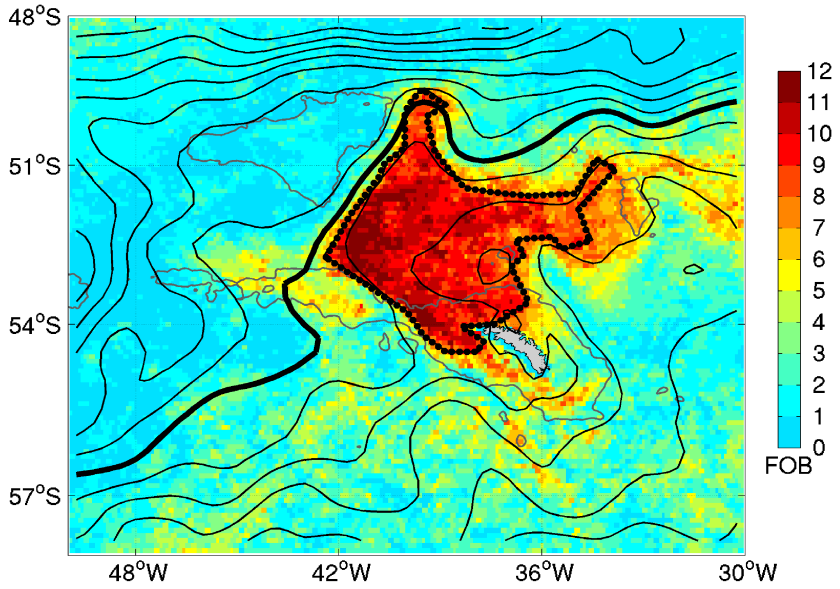


*Fig. 3.2.5. Phytoplankton bloom occurrences in the South Georgia region obtained from SeaWiFS estimates and calculated for austral summer (Dec-Feb, from 1997-2010). Colour indicates the frequency of occurrence of bloom conditions (Chl a ≥ 0.75 mg $m^{-3}$). Regions coloured in shades of red correspond to pixels where summer blooms have been recorded at least 8 times out of the 12 sampled seasons while regions in shades of blue indicate more rare bloom events. Black lines correspond to AVISO dynamic topography isopleths for the summer climatology (Dec-Feb, from 1997-2010); isopleths are drawn every 10 dyn cm. For reference, the bold black line corresponds to -71 dyn cm, and is indicated by Venables et al. (2012) as the southern limit of the Polar Front. The polygon drawn with a dotted black line indicates the extension of the Typical Bloom Area. The 2000m bathymetry contour is also indicated.*

In the South Georgia region, the area where blooms occurred in at least 8 out of the 12 yr (coloured with shades of red) is largely confined to the Georgia Basin and the northern shelf of the island with highest values close to the western and northern periphery of the basin (FBO equal or greater than 10). Worth noting are the presence of high FBO also at the northernmost tip of the Georgia Basin (39°W, 50°S) which has often been excluded from ocean colour and in situ investigations. Bloom conditions were more variable over Shag Rocks and the southern shelf of South Georgia, where FBO values mostly range between 4 and 7. Furthermore, FBO ranging between 1 and 4 indicate that summer blooms have occurred also south of the island, although only on few occasions (pixels coloured in shades of green and blue). Just outside the periphery of the Georgia Basin, especially to the west and north of the basin, as well as along the eastern shelf of the island, frequency values remain very low (FBO<2), indicating that in almost all years blooms were absent.

Utilization of the pixel count algorithm with the objective to locate and enumerate the occurrence of Chl a concentrations greater than 0.75 mg $m^{-3}$ in 12 summer seasons, has allowed for identifying a sector of the South Georgia region in which phytoplankton blooms have been most recurrent (FBO equal or greater than 8), and where, therefore, blooms can be considered predictable in time. This region, which we consider to be representative of South Georgia phytoplankton blooms, and which we hereafter refer to as the Typical Bloom Area, has been outlined in Fig. 3.2.5 (dotted black line) but also in Fig. 3.2.3 (solid grey line) to allow a comparison with the Chl a climatology described above. The results on temporal variability of surface Chl a concentrations and phytoplankton blooms shown below (Fig. 3.2.6 and Fig. 3.2.7) are restricted to this area.

The Typical Bloom Area defined by applying the pixel count algorithm agrees in shape with the area of enhanced Chl a concentrations indicated in the summer climatology (Fig. 3.2.3). Similarly in both the frequency plot and in the Chl a climatology, the core of the South Georgia bloom is found to the northwest of the island and is centred over the deep waters of the Georgia Basin (depths greater than 3000 m, Fig. 3.2.2); moreover, in both cases there is a clear indication of the narrow bloom protrusion extending north of the 50°S parallel (39°W, 50°S).

However, as only regions characterized by FBO greater or equal to 8 were considered in the successive steps of our analysis, most of the southern and eastern shelf of the island, as well as the area surrounding Shag Rocks and the area adjacent to the North East Georgia Rise were not included in the Typical Bloom Area. Although in these latter regions the Chl a climatology averages are above 0.75mg $m^{-3}$, frequency calculations indicate that phytoplankton blooms have occurred less regularly or only on few occasions; this is especially valid for the area over Shag Rocks, where FBO are mostly close to or below 6. Portions of the South Georgia region where climatological Chl a averages indicate values below 0.75 mg $m^{-3}$ (areas shaded in green and blue) are never part of the Typical Bloom Area.

The Typical Bloom Area (~145000 $km^2$) contains the bloom region shown by Korb et al. (2008), but includes the area lying north of 50°S, where FBO indicate recurrent summer phytoplankton blooms. It is important to note that the Typical Bloom Area differs considerably from the South Georgia area illustrated by Park et al. (2010) (outlined in their

Fig. 3.2.5a, and in Fig. 3.2.3 of the present contribution), which was obtained from an empirical orthogonal function analysis and k-means classification. Compared to the Typical Bloom Area, their area was centred on South Georgia and hence excluded the northern portion of the Georgia Basin, and included the low chlorophyll waters found to the southwest and east of the island. The sensitivity of the Chl a concentration time series on the specific area under consideration is discussed below.

### Temporal variability across the Typical Bloom Area

All SeaWiFS eight-day Chl a values between September 1997 and September 2010 were averaged over the Typical Bloom Area to construct the time series shown in Fig. 3.2.6a. For comparison with previous work, we also constructed a time series based on the median of the above Chl a values (Fig. 3.2.6b). Pixels with no data were excluded from the calculations. Chl a average and median values that were obtained from less than 30% of all pixels included in the Typical Bloom Area are marked with red dots in Fig. 3.2.6. Cloud cover, especially between late March and the first weeks of September, and low light levels between June and July are the main causes of reduced data coverage. The time series of average and median values are very similar, hence in the following we considered only average values. In order to investigate at greater detail the seasonal and intra-seasonal variability of phytoplankton blooms, in the second step of our analysis the time series obtained from Chl a averages (Fig. 3.2.6a) was split into separate seasons (coloured lines in Fig. 3.2.7a). The time series of Chl a concentrations was also used to derive the regression line depicted in blue in Fig. 3.2.6a.

Despite the pronounced inter-annual variability in the time series shown in Fig. 3.2.6a, phytoplankton blooms (i.e., Chl a $\geq$ 0.75 mg $m^{-3}$) occurred every year. Concentrations above 2 mg $m^{-3}$ were reached in 7 yr, with values exceeding 3 mg $m^{-3}$ in November 1999, December 2001 and February 2002, as well as in April 2006. Least productive growth seasons were in 1997/1998, 2000/2001 and 2006/2007 (see also Table 3.2.1). The very small slope of the regression line (0.009 ± 0.01 mg $m^{-3}$ $yr^{-1}$, blue line in Fig. 3.2.6a) indicates that in the time period analyzed here, Chl a concentrations did not follow an evident long term temporal trend.

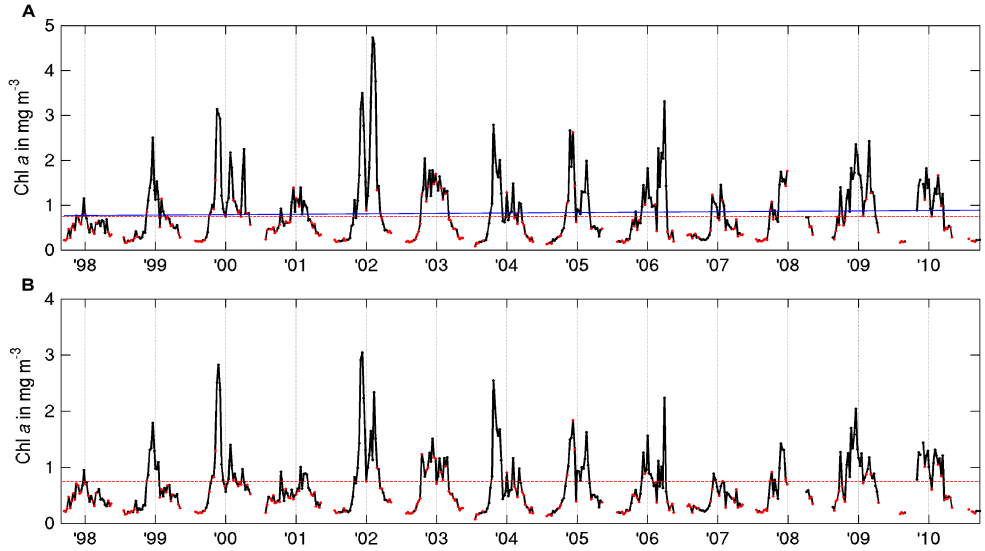

*Fig. 3.2.6. Chl a time series obtained from the mean (A) and the median (B) of all Chl a values available from eight-day composites of the Typical Bloom Area between September 1997 and September 2010. In (A) the regression line calculated along time is illustrated in blue. In both cases, as pixels with no data were excluded, we distinguish values that were obtained from more (black) or less (red) than 30% of all pixels contained in the Typical Bloom Area. Between 9 January and 28 March 2008 no SeaWiFS data were available. Chl a concentrations are expressed in mg $m^{-3}$. Vertical grid-lines indicate the first week of each year. The dashed red horizontal lines denote 0.75 mg $m^{-3}$.*

*Table 3.2.1. Column 2 and 3: phytoplankton bloom duration; Column 4: growth-season's maximum Chl a value and its timing (date of week); Column 5: year's specific seasonal Chl a average (based on the growth-season durations indicated column 2); Column 6: Chl a seasonal average based on the average growth-season length (i.e., from 27 October to 02 April). All concentrations values are expressed in mg $m^{-3}$.*

| Year | Date of first and last week when Chl *a* ≥0.75 mg $m^{-3}$ | Days with Chl *a* ≥0.75 mg $m^{-3}$ | Value and date of maximum Chl *a* | Growth-season Chl *a* average (year specific) | Growth-season Chl *a* average (27 Oct-02 Apr) |
|---|---|---|---|---|---|
| 1997/1998 | 20 Nov 1997 - 04 Jan 1998 | 32 | 1.15 / 30 Dec. 1997 | 0.78 | 0.62 |
| 1998/1999 | 20 Nov 1998 - 21 Feb 1999 | 96 | 2.51 / 22 Dec. 1998 | 1.22 | 0.96 |
| 1999/2000 | 11 Oct 1999 - 03 May 2000 | 208 | 3.14 / 20 Nov. 1999 | 1.34 | 1.42 |
| 2000/2001 | 18 Oct 2000 - 01 Mar 2001 | 96 | 1.4 / 28 Jan. 2001 | 0.91 | 0.87 |
| 2001/2002 | 04 Nov 2001 - 17 Mar 2002 | 136 | 4.73 / 05 Feb. 2002 | 2.19 | 1.97 |
| 2002/2003 | 19 Oct 2002 - 01 Mar 2003 | 144 | 2.04 / 04 Nov. 2002 | 1.45 | 1.29 |
| 2003/2004 | 11 Oct 2003 - 16 Mar 2004 | 120 | 2.79 / 27 Oct. 2003 | 1.18 | 1.15 |
| 2004/2005 | 03 Nov 2004 - 09 Mar 2005 | 128 | 2.67 / 27 Nov. 2004 | 1.34 | 1.21 |
| 2005/2006 | 04 Nov 2005 - 10 Apr 2006 | 136 | 3.31 / 02 Apr. 2006 | 1.31 | 1.27 |
| 2006/2007 | 06 Dec 2006 - 05 Feb 2007 | 56 | 1.45 / 20 Jan. 2007 | 1.03 | 0.69 |
| 2007/2008 | 03 Oct 2007 - NA | >72 | 1.76 / 30 Dec. 2007 | 1.2 | 1.3 |
| 2008/2009 | 02 Oct 2008 - 02 Apr 2009 | 176 | 2.43 / 01 Mar. 2009 | 1.37 | 1.47 |
| 2009/2010 | 04 Nov 2009 - 17 Mar 2010 | 136 | 1.82 / 22 Dec. 2009 | 1.29 | 1.2 |
| Average | 27 Oct - 02 Apr | 160 | 1.53 / 14 Dec. | 1.19 | 1.19 |

The annual cycle of average Chl a concentrations over the Typical Bloom Area and the timing of the phytoplankton blooms is given for each year in Fig. 3.2.7a, together with the climatological annual cycle (solid bold black line in Fig. 3.2.7b) and the one standard error interval (dashed black lines in Fig. 3.2.7b). The one standard error interval is depicted also in Fig. 3.2.7c to allow for greater detail. Additionally, Table 3.2.1 provides for each year as well as for the climatological annual curve the phytoplankton bloom duration (expressed as the first and last week in which calculated Chl a averages were ≥0.75 mg $m^{-3}$) and the total number of days in which Chl a concentrations averaged over the Typical Bloom Area were ≥0.75 mg $m^{-3}$. In addition, for each year are also indicated the Chl a value and the date of the week when the season's maximum value was recorded, as well as the growth-season Chl a average.

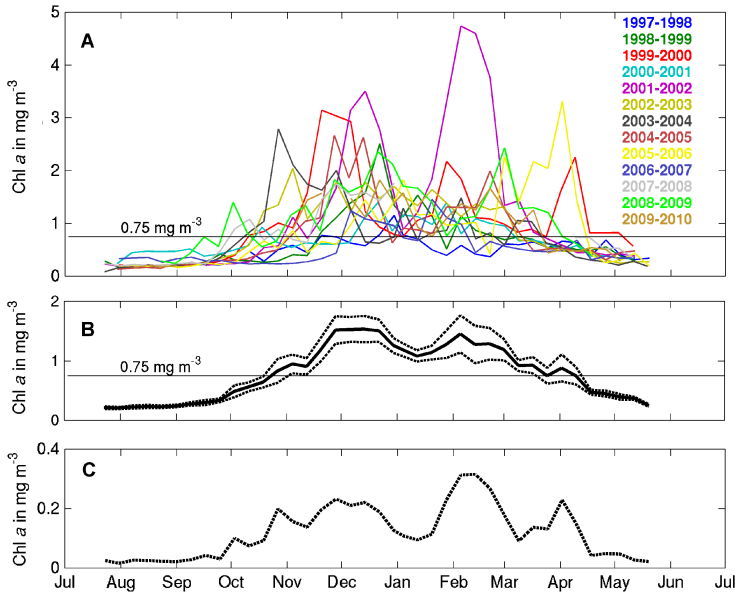


*Fig. 3.2.7. Seasonal variability of Chl a concentrations and bloom occurrences in the Typical Bloom Area. (A) Every year included between September 1997 and June 2010 is colour-coded differently; refer to Fig. 3.2.6 for data-coverage in each data-point and Table 3.2.1 for growth-season Chl a averages and bloom duration. (B) Chl a concentration climatological average (solid line) and the one standard error interval (dashed line) as obtained from all curves depicted in panel A. (C) The dashed line indicates the one standard error interval (as in panel B). Horizontal black lines in panels A and B mark 0.75 mg m$^{-3}$.*

As described above and depicted in Fig. 3.2.6 and 3.2.7a, Chl a concentrations reach phytoplankton bloom levels in all years. Typically, until late winter or early spring (i.e., mid September) averaged Chl a values remain low (≤0.2 mg m$^{-3}$); after September Chl a concentrations increase progressively and in most cases peak between mid November and the end of December, although austral spring peaks are observed also earlier in the season, as in October 2008, October 2003 or November 2002 (1.4, 2.8 and 2.04 mg m$^{-3}$, respectively). After the spring peaks terminate, as is occurring in most cases by the beginning of January, Chl a values gradually decrease and by the beginning of April (exceptions are April 2006 and April 2000) fall below ~0.75 mg m$^{-3}$. During the first weeks of May Chl a concentrations are very low, except in May 2000 and May 2005 when concentrations were still close to 0.4 mg m$^{-3}$. In contrast with this progressive decrease in Chl a concentrations, during several years, and especially between late summer and early autumn, a second or even a third intense peak in Chl a values (Chl a >2 mg m$^{-3}$) was observed (i.e., in the seasons of 2001/2002, 2008/2009, 1999/2000 or 2004/2005). At times, the second peak appears to be more intense than the preceding spring peak. In particular, a total of three Chl a concentration peaks were observed in the 1999/2000 season (red curve in Fig. 3.2.7a), at the end of November 1999, during late January/early February 2000 and in April 2000, respectively. Between mid May and mid July, the very low light levels preclude satellite estimates of winter Chl a concentrations.

Comparison between each seasonal curve and the chosen threshold (black horizontal line in Fig. 3.2.7a) indicates that in 9 out of 12 yr, phytoplankton blooms lasted more than four months (see also Table 3.2.1). The shortest phytoplankton bloom seasons were recorded

during the 1997/1998 and the 2006/2007 seasons, when phytoplankton bloom conditions were maintained for less than three months (Table 3.2.1).

The climatological growth season, obtained after averaging all years considered in this study, is characterized by two distinct productivity peaks (Fig. 3.2.7b). The first Chl a peak (~1.52 mg $m^{-3}$ ± 0.21 mg $m^{-3}$) is recurrent and occurred regularly between late November and the first weeks of December. The second peak (~1.8 mg $m^{-3}$ ± 0.31 mg $m^{-3}$) instead, is a less regular feature (both in timing and magnitude) and occurred between late January and early April. A transition phase, included between the last week of December and mid January, can be observed between the peaks. Just before this trough, which appears as a regular feature of the seasonal cycle (standard error interval ~0.1 mg $m^{-3}$, Fig. 3.2.7c), spring Chl a concentrations declined by about 30%, from 1.52 mg $m^{-3}$ to 1.08 mg $m^{-3}$.

### 3.2.4 Discussion

The trajectories of the Polar Front and the Southern ACC Front in the South Georgia region (Venables et al., 2012; Park et al., 2010) together with the patterns of local circulation (Fig. 3.2.2 and 3.2.4) play a major role in controlling the location and extension of the blooms which develop to the north and northwest of the island and tend to reflect the geometry of the Georgia Basin. In particular, the southern limit of the Polar Front, identified following Venables et al. (2012), and the flow that travels westward from the northern shelf of the island along the northern flank of Shag Rocks generally separated bloom from impoverished waters outside the Georgia Basin. Hence, the boundaries of the Typical Bloom Area are clearly demarcated and vary little over time because the flow field is constrained by bottom topography.

The veritable absence of blooms along the eastern shelf of the island and their recurrence to the west and far north of the Typical Bloom Area can be explained by rapid transport of island and shelf-derived iron by intense currents (20-40 cm/sec (Ward et al., 2005)) that flow to the northwest of the island and subsequently turn east. This circulation regime explains, e.g., the distribution of enhanced Chl a concentrations in Fig. 3.2.4c, where highest concentrations are found along the western periphery of the basin up to the northern limits of the MEB-GB margin. The importance of hydrography in controlling the extent of South Georgia phytoplankton blooms has been reported at the climatological level (i.e., Park et al., 2010) or for averages of a few years (Venables et al., 2012), but not at the high temporal and spatial resolution over 13 yr that we present here.

Phytoplankton blooms always occurred within the Typical Bloom Area but their locations, intensities and time of onset (i.e. first week in which Chl a were ≥ 0.75 mg $m^{-3}$, Table 3.2.1) exhibited pronounced inter-annual variability. This is not surprising given the various independent factors that can influence surface Chl a concentrations. Among these: mixed layer depth and its effects on bloom dilution (Smetacek and Naqvi, 2008), dust input (e.g. Gassó et al., 2010), composition of the bloom (diatoms versus flagellates) and grazing (Whitehouse et al., 2009). Variations in flow intensity and pathways of the ACC fronts around South Georgia (Thorpe et al., 2002; Park et al., 2010; Boehme et al., 2008) are also among the most important factors likely influencing the inter-annual variability of the bloom: circulation

around and then downstream of shallow topographic features is believed to control the magnitude of sediment-derived iron input to the water column (i.e. due to re-suspension processes) as well as its transport to more distant regions (Blain et al., 2008; de Jong et al., 2012; Nishioka et al., 2011; Planquette et al., 2007).

In particular, we investigated the roles of SST, PAR and wind speed in regulating the observed inter-annual variability. Growth-season averages (i.e. from 27 October to 02 April, in Table 3.2.1) of each environmental variable were correlated with those obtained from Chl a concentrations. All growth-season averages used in the correlations as well as the obtained correlation coefficients are reported in Table 3.2.2. The positive correlations coefficients we obtained for Chl a/SST (R=0.48, n=10) and for Chl a/PAR (R=0.24, n=13), indicate the positive effect of warmer temperatures, which likely reflect a shallower mixed layer depth, and higher PAR levels on surface Chl a concentrations. For example, the presence of warmer temperatures and higher PAR levels could explain the particularly high Chl a concentration averages during the 2001-2002 season (Fig. 3.2.6). Conversely, no relationship was found between Chl a and wind speed (R~0, n=10); this is likely because of the pronounced irregularity of wind speeds over the Typical Bloom Area during summer (wind speed time series not shown). When we analyzed the correlations of SST, PAR and wind speed with the timing of bloom onset (values in Table 3.2.2), we found negative correlation coefficients, i.e. R=-0.19, n=10 for date of onset/SST and R=-0.37, n=13 for date of onset/PAR; these negative values indicate that phytoplankton blooms started earlier in years when SST and PAR levels were higher than the respective climatologies. Conversely, the correlation between the date of bloom onset and wind speed is inconclusive because the correlation coefficient is negative or positive depending on the number of pairs used in the correlation (i.e. R=-0.30, n=10 and R=0.12, n=9).

The expected intrinsic variability of top-down and bottom-up controls, as well as the fact that these may have additive or contrasting effects on pigment biomass accumulation, as would be the case for the controls mentioned above, may explain the absence of a prominent decadal trend in the Chl a time series (Fig. 3.2.6a). Similar conclusions were reached by Arrigo et al. (2008) who analyzed annual primary production in the Southern Ocean. However, the very small yet positive slope of the regression line ($0.009 \pm 0.01$ mg $m^{-3}$ $yr^{-1}$) that suggests a slow increase in Chl a concentrations (i.e. 0.09 mg $m^{-3}$ in ten years), appears to be in line with Whitehouse et al. (2008b) who expected an increase in productivity as a response to the gradual warming documented around South Georgia.

Pronounced variability in Chl a concentrations around South Georgia was also reported by Park et al. (2010). They used ocean colour estimates from SeaWiFS for the period September 1997 - December 2007 and ocean colour estimates from MODIS for the period January 2008 - August 2008. They applied an empirical orthogonal function analysis to the 11 yr-period of satellite observations and then used the k-means algorithm to delimit, among others, a polygonal area around South Georgia (outlined in their Fig. 3.2.5a, and in Fig. 3.2.3 of the present contribution); across this area they studied temporal patterns of Chl a concentrations.

*Table 3.2.2. SST, PAR and wind speed growth-season averages (from 27 Oct to 02 April) and 15-day anomalies prior to each year's date of bloom onset. Coefficients obtained from their correlations with the Chl a growth-season average (in Column 2) and the date of bloom onset (in Column 3) are also reported.*

| Year | Chl *a* growth-season average | Date of bloom onset | SST(°C) | | PAR (mol photons m-2 d-1) | | Wind Speed (m/s) | |
|---|---|---|---|---|---|---|---|---|
| | | | avg[1] | 15-day[2] | avg[1] | 15-day[2] | avg[1] | 15-day[2] |
| 1997-1998 | 0.62 | 20 Nov 1997 | N/A | N/A | 33.26 | -6.51 | N/A | N/A |
| 1998-1999 | 0.96 | 20 Nov 1998 | N/A | N/A | 34.98 | -3.23 | N/A | N/A |
| 1999-2000 | 1.42 | 11 Oct 1999 | N/A | N/A | 32.22 | 1.58 | 9.1 | 0.22 |
| 2000-2001 | 0.87 | 18 Oct 2000 | 2.75 | -0.09 | 33.78 | 3.93 | 9.49 | -0.68 |
| 2001-2002 | 1.97 | 04 Nov 2001 | 3.64 | -0.27 | 35.68 | 1.26 | 9.27 | 1.33 |
| 2002-2003 | 1.29 | 19 Oct 2002 | 2.71 | -0.56 | 33.67 | -1.67 | 8.97 | -0.37 |
| 2003-2004 | 1.15 | 11 Oct 2003 | 3.63 | 0.1 | 35.06 | -0.81 | 9.18 | -0.24 |
| 2004-2005 | 1.21 | 03 Nov 2004 | 3.63 | 0.22 | 35.54 | 2.61 | 9.14 | 0.62 |
| 2005-2006 | 1.27 | 04 Nov 2005 | 3.17 | -0.4 | 35.44 | -0.92 | 8.62 | -1.78 |
| 2006-2007 | 0.69 | 06 Dec 2006 | 3.27 | 0.06 | 35.37 | -2.63 | 8.99 | -1.62 |
| 2007-2008 | 1.3 | 03 Oct 2007 | 3.08 | 0.2 | 39.6 | -0.56 | 8.97 | 0.15 |
| 2008-2009 | 1.47 | 02 Oct 2008 | 3.77 | 0.38 | 35.87 | 4.77 | 9.04 | -0.72 |
| 2009-2010 | 1.2 | 04 Nov 2009 | 3.07 | 0.18 | 35.15 | 10.46 | N/A | N/A |
| Correlation coeff. for growth-season averages | | | 0.48 | | 0.24 | | -0.007 | |
| Correlation coeff. with date of bloom onset | | | | -0.19 (-0.39)[3] | | -0.37 (-0.30)[3] | | -0.3 (0.12)[3] |

[1] Growth-season averages (from 27 Oct to 02 April); [2]15-day anomalies prior to each year's date of bloom onset; [3] Values obtained if averages from the 2006/2007 are removed from the calculations

Their results showed that in only six of the 11 yr-period, Chl a concentrations exceeded 0.75 mg $m^{-3}$ and that in all cases they remained below 2 mg $m^{-3}$. Our time series, based on average or median values (Fig. 3.2.6a and Fig. 3.2.6b) provide a different picture, indicating bloom levels in all years and Chl a concentrations exceeding 2 mg $m^{-3}$ in at least five years.

Differences between the Typical Bloom Area and the South Georgia area used by Park et al. (2010) are most likely causing these contrasting results (both areas are outlined in Fig. 3.2.3). While the Typical Bloom Area is located to the north and northwest of the island only, where phytoplankton blooms are pronounced and most recurrent (i.e., over the Georgia Basin), the area defined by Park et al. (2010) occupies the south-western portion of the Georgia Basin and includes waters to the southwest and east of the island, where Chl a values are generally below 0.5 mg $m^{-3}$ and in some months even as low as 0.2 mg $m^{-3}$ (i.e., in January 2007). Therefore, their analysis did not include the phytoplankton blooms occurring over the northern and eastern portion of the Georgia Basin, such as those observed in December 1998, December 2009 or January 2007 (Fig. 3.2.4), and introduced a systematic negative bias by including the impoverished waters to the southwest and east of the island. Consequently, differences between their time series and the one presented here are more pronounced when maximum Chl a concentrations were recorded only over the northern sector of the Georgia Basin, as in 2005/2006 and 2006/2007. Hence, the area across which Chl a concentrations are extracted is of critical importance and averaging areas that differ significantly from the

Typical Bloom Area can yield different conclusions on the recurrence of phytoplankton blooms but also on their annual cycle.

Phytoplankton dynamics in the Southern Ocean are characterized by a pronounced annual cycle with a growth and non-growth season constrained by the combined effects of the solar cycle, shallowing and deepening of mixed layer depth and timing of sea-ice retreat and advance (Smith et al., 2008; Venables and Moore, 2010). Chl a concentrations peaks have been observed in the first half of the growth season, while in the second half concentrations were progressively lower, resulting in an unimodal pattern mostly centred between late spring and early summer (Mongin et al., 2008; Moore and Abbott, 2000; Thomalla et al., 2011). Conversely, over the Typical Bloom Area Chl a concentrations remained high throughout the entire growing seasons, and in many years followed a bimodal pattern.

Double Chl a concentration peaks are well known for the North Atlantic phytoplankton growth season (Martinez et al., 2011) but to our knowledge have been reported only on few occasions from the open Southern Ocean (Trull et al., 2001; Jouandet et al., 2011). Trull et al. (2001) reported a double peak in the Sub-Antarctic Zone south of Australia for the 1997/1998 season only, while Jouandet et al. (2011) observed two regular peaks in the Kerguelen Plateau phytoplankton bloom over the period between October 1997 and October 2007. Jouandet et al. (2011) observed a first peak in late spring (i.e. between November and December), and a second peak mostly around January. Over the Typical Bloom Area the timing of the first Chl a concentration peak occurred mostly around December, similarly to the first Chl a peak in the Kerguelen region. However, as observed in Fig. 3.2.7, the second bloom peak reported over the Typical Bloom Area exhibited higher variability in timing but also magnitude than the first peak, presumably due to variability in the factors responsible for its build-up. Amongst these we exclude light levels, which are sufficient to support pigment biomass accumulation till mid May (Venables and Moore, 2010), but also mixed layer depth, which according to available climatologies (i.e. Monterey and Levitus, 1997; Dong et al., 2008) remains shallow until the end of April (<70 m). Hence, variability in nutrient availability as shown in Fig. 3.2.8 below is likely to play the major role.

Iron input and availability is one of the major factors influencing build-up of phytoplankton blooms in the Southern Ocean (Martin et al., 1990; Blain et al., 2008; Boyd et al., 2007). The main sources of iron to the Typical Bloom Area are: dust (Gassó et al., 2010), sediment input from the island or from the deeper enriched layers, through horizontal and vertical advection (Holeton et al., 2005; Nielsdóttir et al., 2012) and island runoff and glacier melt (Korb et al., 2008; Young et al., 2011). Dust events from South America are sporadic, likely increasing in austral summer (Gassó et al., 2010), whereas the input of sediment-derived iron could be considered relatively steady because dependant on circulation; the flow originating from the north-western shelf of the island and travelling westward along the northern flank of Shag Rocks and then along the MEB-GB margin shows in fact reduced variability (see Fig. 3.2.4 and Korb et al., 2008). Hence, of the three iron sources only runoff is expected to have a pronounced seasonality during the growth season, with its peak coinciding with maximum rate of ice melt in mid summer when Chl a concentrations actually tend to decline. Therefore, because several concomitant mechanisms can be proposed as

supplying iron to the Typical Bloom Area during austral summer, one could expect iron-replete conditions (see also (Nielsdóttir et al., 2012; Hinz et al., 2012)).

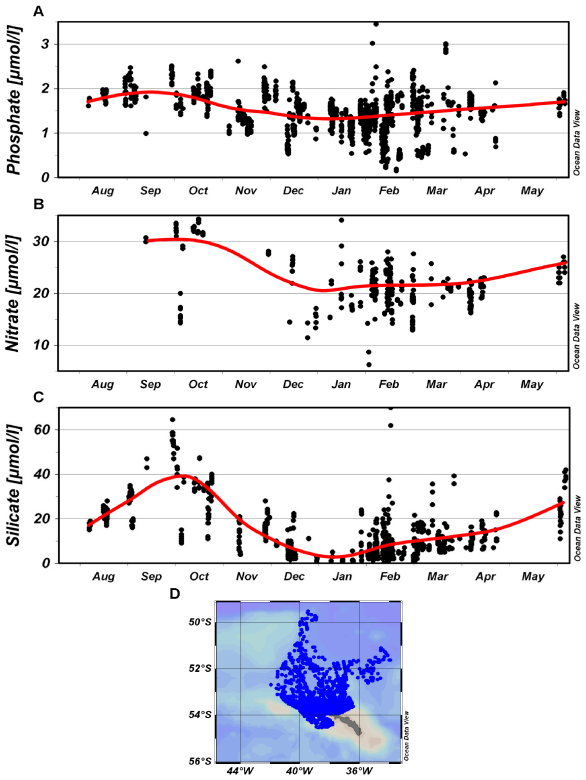


***Fig. 3.2.8.*** *Seasonal cycle of phosphate (A), nitrate (B) and silicate (C) in the Typical Bloom Area (D). All values are from the surface layer (0-50m) and were extracted from the World Ocean Database 2009 (Boyer et al., 2009). In all panels black dots indicate individual original measurements, while red lines represent running averages. All panels were created using Ocean Data View (Schlitzer, 2012).*

In order to examine the role of macronutrient availability during the growth season, we present in Fig. 3.2.8 surface (0-50m) nutrient concentrations for the Typical Bloom Area from the World Ocean Database 2009. Although phosphate and nitrate concentrations vary greatly, they are always high and can be excluded as a limiting factor (Fig. 3.2.8a and Fig. 3.2.8b). However, silicate concentrations decrease rapidly after October and reach limiting values between December and January (Fig. 3.2.8c).

Because the spring bloom is dominated by diatoms (Korb et al., 2012; Korb et al., 2008; Korb et al., 2010) silicate exhaustion is the most likely cause of bloom termination reflected in the January minimum. Groups other than diatoms, e.g. Phaeocystis or coccolithophorids, that could thrive under silicate limiting conditions and potentially form the second bloom also contribute to Southern Ocean blooms, e.g. in the Ross Sea (Arrigo et al., 1999) and in the Crozet region (Poulton et al., 2007) but were rare or have not been reported from the South Georgia region (Korb et al., 2012; Korb et al., 2008). These groups seem more susceptible to virus infection and grazing by zooplankton and krill than diatoms (Smetacek et al., 2004), however, inter-annual variation in grazing pressure could result in build-up of their biomass and account for the Chl a increase observed in the second half of the growth season during some years. This needs to be verified by future ship-based investigations.

It is also possible that the moderate to high Chl a concentrations in the second phase of the growth season is due to diatoms responding to the progressive increase in silicate concentrations recorded after January (Fig. 3.2.8c). The sources of silicate at this time of the growth season could be due to deeper intrusions of SACCF water into the Georgia Basin

(Korb et al., 2008; Boehme et al., 2008) but also due to a likely increasing number of end-summer storms, which would favour mixing of surface waters with the deeper enriched ones. Reduced uptake of silicate upstream of the island, where phytoplankton blooms are short lived and terminate earlier in the season depending on iron availability (Whitehouse et al., 2012), could also have an effect on the amount of silicate advected in the Typical Bloom Area.

Because data coverage in ocean colour and nutrient measurements in the Typical Bloom Area are not concomitant nor at equal resolution, the processes responsible for the characteristic double peak in Chl a concentrations remain uncertain and need more direct investigations. Indeed, a silicate/iron co-limitation cannot be excluded, especially farther downstream of South Georgia where iron concentrations can be two orders of magnitude lower than those measured over the shelf (Nielsdóttir et al., 2012).

The progressive increase of Chl a concentrations in spring followed by several months of high phytoplankton biomass (Fig. 3.2.7) is likely to reflect the rate of dissolved inorganic carbon (DIC) consumption, and the consequent enhancement of $CO_2$ uptake from the atmosphere. Progressive reduction of $CO_2$ fugacity and DIC with increasing surface Chl a concentrations has been reported for the Kerguelen Plateau region (Lourantou and Metzl, 2011; Jouandet et al., 2008), the Crozet Plateau (Bakker et al., 2007) as well as downstream of South Georgia (Jones et al., 2012; Boutin and Merlivat, 2009). In particular, Jones et al. (2012) estimated a summertime (February 2008) DIC deficit of 4.4 +- 0.8 Tg C when the bloom was about 80000 $km^2$ in size, equivalent to ~ 55% of the Typical Bloom Area (~145000 $km^2$). Therefore, one would expect that the summertime DIC deficit estimated by Jones et al. (2012) is likely to be a low estimate of the $CO_2$ drawdown that would derive when particularly intense phytoplankton blooms occupied the entire Typical Bloom Area (i.e. December 1998 in Fig. 3.2.4a).

### 3.2.5 Conclusions

The time series of Chl a concentrations averaged across the Typical Bloom Area (~145000 $km^2$) shows that the South Georgia phytoplankton bloom, defined by Chl a values ≥ 0.75 mg $m^{-3}$, occurred regularly every year between 1997 and 2010. This result is in line with other sub-Antarctic islands, i.e., those of the Kerguelen or Crozet plateaus, where shelf-sediment interactions and local circulation provide a reliable annual supply of iron to the bloom region. The described regularity, size and intensity of South Georgia phytoplankton blooms will indeed lead to an atmospheric $CO_2$ drawdown potentially greater than what previously estimated from smaller scale studies. Chl a concentrations invariably peaked around December, and in many years peaked a second time between late January and April. Given the predominance of diatoms in the spring bloom and a most likely continuous advection of iron from the island, we attribute the second peak to a renewed supply of silicate which in January are reaching limiting concentrations and hence terminate the first (i.e., spring) bloom. To date only very few regional studies have reported bimodal bloom patterns in the open Southern Ocean and more studies, including biogeochemical modelling, are needed to help investigate the environmental controls behind it.

The recurrence and regularity of blooms described here is in marked contrast with Park et al. (2010) who showed a time series of weak and unpredictable South Georgia phytoplankton blooms. We point out that these significant differences arise from differences in location and extent of the study areas chosen. In fact, because the local flow is strongly constrained by topography and hence the bloom boundaries vary little in time, averaging areas substantially different from the Typical Bloom Area used here will necessarily exclude bloom waters or include others where blooms are rare or missing, hence introducing a systematic bias in the Chl a concentration analysis.

## Acknowledgements

The authors thank P. Assmy, O. Aumont, C. Klass, V. Strass, M. R. v. d. Loeff and C. Völker for valuable discussions. Particular thanks go to Victor Smetacek for sharing his insight into the ecology and dynamics of phytoplankton blooms in the Southern Ocean. Dr. Jouandet and the anonymous reviewer are also acknowledged, as their comments greatly improved the technical and scientific quality of the present manuscript. Financial support was provided by the Earth System Science Research School at the Alfred Wegener Institute for Polar and Marine Research and the EU FP7 project CARBOCHANGE under grant agreement no. 264879.

## *3.3 Primary productivity and circulation patterns downstream of South Georgia: a Southern Ocean example of the Island mass effect*

Ines Borrione[a,*], Olivier Aumont[b], Reiner Schlitzer[a]

[a]Alfred Wegener Institute for Polar and Marine Research, Am Alten Hafen 26, 27568 Bremerhaven, Germany

[b]Laboratoire de Physique des Océans, Centre IRD de Bretagne, 29280 Plouzané, France

Published as:

I.Borrione, Aumont O. and Schlitzer R. in "Bridging the Gaps between Disciplines: Perspectives from a Multi-disciplinary Helmholtz Graduate Research School", Series: SpringerBriefs in Earth System Sciences. Lohmann, G.; Grosfeld, K.; Wolf-Gladrow, D.; Unnithan, V.; Notholt, J.; Wegner, A. (Eds.) 2013, 38-41, 138 p. ISBN 978-3-642-32234-1; Springer, Heidelberg. 2013.

### Abstract

Growth of phytoplankton in the Southern Ocean (SO) is largely limited by insufficient concentrations of the micronutrient iron, so that despite the large macronutrient reservoir, the SO is considered a High Nutrient Low Chlorophyll region. Therefore, phytoplankton growth is enhanced where exogenous iron is introduced to the system, for example downstream from islands. These confined regions sustain very rich ecosystems and are hot spots for atmospheric carbon dioxide drawdown. In this study, a combination of satellite derived measurements and model simulations are used to investigate the biological and physical environmental disturbances of the island of South Georgia (37°W, 54°S), which is located in the southwestern part of the Atlantic sector of the SO. We show not only that the island shelf is an important source of dissolved iron to the system, but also that the characteristic surface circulation patterns found downstream of the island play an important role in maintaining the shape and distribution of the developing phytoplankton bloom.

**Keywords:** Southern Ocean South Georgia Island mass effect Satellite observations Primary productivity High nutrient low chlorophyll regions Biogeochemical modeling Iron ROMS PISCES.

### 3.3.1 Introduction

The Southern Ocean (SO, latitudes south of 40° S) covers 20% of the global ocean, and surrounds the Antarctic Continent. The main hydrographic component is the Antarctic

Circumpolar Current (ACC), an intense eastward flowing current encircling uninterrupted the continent.

The SO is a fundamental component of the Earth system and of its response to climate change (Marinov et al. 2006). Along portions of the Antarctic coast, the seasonal sea-ice formation generates intermediate and bottom waters which provide a major forcing to the global thermohaline overturning circulation, hence promoting heat, nutrient and gas fluxes with the other oceans.

Along the path of the ACC, upwelling of deeper waters replenishes surface waters with high concentrations of macronutrients (e.g., phosphates and nitrates) necessary for the growth of phytoplankton. However, due to insufficient concentrations of the trace metal iron, which is necessary for photosynthesis, algal growth in the SO is reduced, a reason why it is defined as a High Nutrient Low Chlorophyll (HNLC) region (Sarmiento and Gruber 2006).

Higher algal biomass is found where exogenous iron is introduced to the surface layers; among others, noteworthy sources are continental margins and atmospheric dust depositions (Tagliabue et al. 2009a), as well as sea-ice melting (Lannuzel et al. 2007).

In situ investigations of the remote SO are generally limited to Austral summer, when most oceanographic cruises can be conducted. Consequently, satellite observations and modeling experiments are necessary tools to integrate with available in situ measurements. The former provide a quasi-synoptic view of regions as large as the SO, while the latter, albeit the necessary simplifications, allow for a virtual laboratory where to test hypothesis and better understand processes. Both tools were combined in the current study to investigate how and to what extent the sub-Antarctic Island of South Georgia generates an “Island Mass Effect”, in other words, influences the surrounding physical and biogeochemical environment.

South Georgia (SG) is a relatively small island of the southwest Atlantic sector of the SO, lying between two of the major ACC fronts: the Polar Front (PF) to the north, and the Southern ACC Front (SACCF) to the south. Amidst HNLC waters, downstream from the island develops an intense phytoplankton bloom, which is clearly detectable from satellite ocean color imagery (Fig. 3.3.1, refer also to (Park et al. 2010)) and in situ measurements (Korb and Whitehouse 2004). This highly productive system sustains a rich ecosystem and one of the largest commercial krill fisheries (Atkinson 2001); furthermore, due to the enhanced phytoplankton growth, which promotes the biological carbon pump, it is identified as one of the most important Antarctic regions of atmospheric carbon drawdown (Schlitzer 2002).

### 3.3.2 Data and Methods

Chlorophyll-a concentration (chl-a) estimates were derived from the satellite Sea-viewing Wide Field-of-View Sensor (SeaWiFS) at 9km resolution. Due to the large number of data gaps caused by frequent cloud cover, only monthly composites were used. Ocean color images were retrieved between November and February (austral summer) and between 1997 and 2010.

Surface circulation patterns were estimated from the AVISO Satellite Absolute Dynamic Topography (ADT) measurements. Weekly products were retrieved, and averaged to form a monthly climatology corresponding to the same time period of the SeaWiFS observations.

Model simulations were carried out with a coupled configuration of ROMS, a free surface, topography following, primitive equation regional model (Shchepetkin and McWilliams 2005) and PISCES, a 24-compartment biogeochemical model, where the cycles of carbon and the main nutrients (including iron) are resolved (Aumont and Bopp 2006). Simulations were run at 1/6° resolution (~12 km).

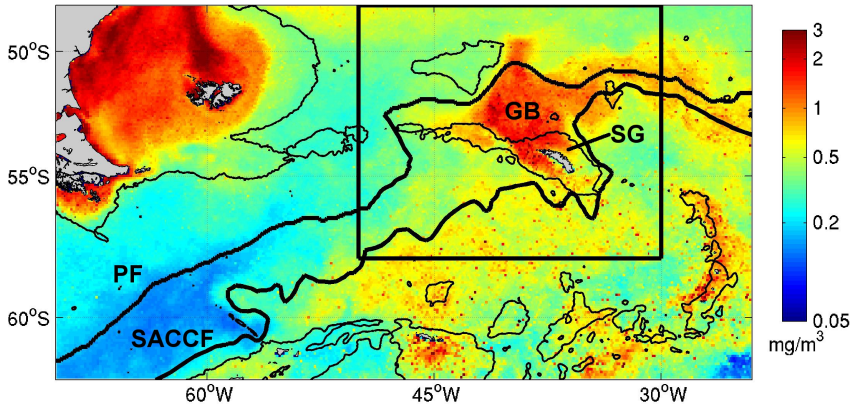


*Fig. 3.3.1. November-February chlorophyll-a climatology from 1997 until 2010 in the southwest Atlantic sector of the SO from satellite ocean color estimates. Bold lines indicate the Polar Front (PF) and the Southern ACC Front (SACCF), SG indicates the island of South Georgia, and GB stands for Georgia Basin, the rectangle depicts the South Georgia region; thin black lines indicate the 2000m isobaths.*

### 3.3.3 Results and Discussion

According to the climatology shown in Fig. 3.3.1, a large phytoplankton bloom develops in the South Georgia region; the position of the bloom appears to be confined over the Georgia Basin while outside the basin borders, chl-a remains mostly below 0.5 mg/m$^3$ hence indicating typical HNLC conditions.

Measurements of ADT in the SG region, allow for estimating the main pathways and intensities of surface circulation; the former are parallel to ADT contour lines, while the latter are more intense when contour lines are closer. As indicated by ADT contours (black lines in Fig. 3.3.2a), the flow encounters the island from the southwest and then continues northeast embracing the Georgia Basin at all sides. Furthermore, it is possible to infer intense currents along the borders of the basin (especially along the northern periphery, where contour lines are closely spaced) and a weaker circulation regime in the region found directly above the basin.

The similarity between surface circulation patterns depicted in Fig. 3.3.2a and the bloom distribution shown in Fig. 3.3.1 suggests that the surface circulation in the SG region plays an important role in maintaining the shape and position of the phytoplankton bloom developing downstream from SG. Therefore, circulation patterns are such that phytoplankton cells remain

entrained in a favorable region where the flow is weaker and nutrient reservoirs may be continuously replenished.

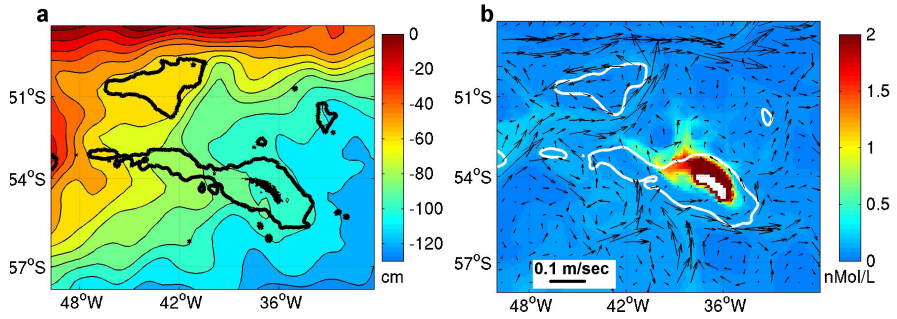


*Fig. 3.3.2. a Absolute dynamic topography in the South Georgia region between November and February according to the 1997-2010 climatology. Contour lines indicate direction of main flow and distance between isolines provides an estimate of flow intensity. b Simulated distribution of surface dissolved iron (color code) and circulation (arrows) during December of model year 3. In both panels, 2000m isobaths are indicated with bold contour lines.*

The importance of SG as a source of dissolved iron is suggested by model simulations (Fig. 3.3.2b), which show the presence of a plume originating from the island that follows the direction of the main flow (arrows). However, the characteristic circulation patterns depicted in Fig. 3.3.2a remain difficult to resolve, possibly due to the sensitivity of the system to the adopted boundary conditions or the chosen model resolution which does not allow for a full representation of the physical environment (i.e., eddies, which at the chosen resolution are not resolved).

### 3.3.4 Conclusions

Although our results indicate that downstream from SG the observed phytoplankton bloom results from a characteristic physical environment, being SG a source of dissolved iron, a comprehensive understanding of the system, where a patchwork of top-down (i.e., grazing) or bottom-up (light or nutrient co-limitation) controls come into play, requires further in situ investigations and model experiments. The former would provide additional biogeochemical measurements which to date remain scarce, while the latter would help assess the relative importance of physical processes other than surface circulation (for example performing simulations where tidal effects and/or eddies are included) or additional nutrient sources in determining the observed biological response to the South Georgia “Island Mass Effect”.

## *3.4 Sedimentary and atmospheric sources of iron around South Georgia, Southern Ocean: a modelling perspective*

I. Borrione[1], O. Aumont[2], M. C. Nielsdóttir[3,*] and R. Schlitzer[1]

[1] Alfred Wegener Institute for Polar and Marine Research, Columbusstrasse, 7568 Bremerhaven, Germany

[2] Laboratoire de Physique des Océans Institut Européen de la Mer, 29280 Plouzané, France

[3] University of Southampton, National Oceanography Centre, European Way, SO14 3ZH, Southampton, United Kingdom

[*] Presently at Old Dominion University, Department of Ocean, Earth and Atmospheric Sciences, 4600 Elkhorn Avenue, Norfolk VA 23529

Correspondence to: I. Borrione (Ines.Borrione@awi.de)

Published as:

I. Borrione, O. Aumont, M. Nielsdóttir and R. Schlitzer, Sedimentary and atmospheric sources of iron around South Georgia, Southern Ocean: a modeling perspective, Biogeosciences Discuss., 10, 10811-10858, doi:10.5194/bgd-10-10811-2013, 2013.

### Abstract

In high-nutrient low-chlorophyll waters of the western Atlantic sector of the Southern Ocean, an intense phytoplankton bloom is observed annually north of South Georgia, most likely due to an enhanced supply of the limiting micronutrient iron. Shallow sediments and atmospheric dust deposition are believed to be the main iron sources. However, their relative importance is still unclear and in the South Georgia region have yet not been ascertained because iron measurements are very few. In this study, we use austral summer dissolved iron (dFe) data around South Georgia (January and February 2008) with a coupled regional hydrodynamic and biogeochemical model to investigate natural iron fertilization around the island. The biogeochemical component of the model includes an iron cycle, where sediments and dust deposition are the sources of iron to the ocean. The model captures the characteristic flow patterns around South Georgia, hence simulating a large phytoplankton bloom to the north, i.e., downstream, of the island. Modelled dFe concentrations agree well with observations (mean difference and root mean square errors of ~0.02 nM and ~0.81 nM) and form a large plume to the north of the island that extends eastwards for more than 800 km. In agreement with observations, highest dFe concentrations are located along the coast and decrease with distance from the island. Sensitivity tests indicate that most of the iron measured in the main bloom area originates from the coast and the very shallow shelf-sediments (depths < 20m) while dust deposition plays a minor role, with almost no effects on surface chlorophyll a concentrations. Iron sources such as run-off not represented explicitly in

the model, but that likely contribute to the iron plumes observed around South Georgia, are also discussed together with the potential effects their temporal variability may have on the system.

### 3.4.1 Introduction

The island of South Georgia is located in the western Atlantic sector of the Southern Ocean at the northeastern limit of the Scotia Sea, along the North Scotia Ridge (Fig. 3.4.1), and lies between two of the main fronts of the easterly flowing Antarctic Circumpolar Current (ACC): the Polar Front (PF) and the Southern ACC Front (SACCF). The PF crosses the North Scotia Ridge at Shag Rocks Passage and then flows east remaining always due north of the island; the SACCF reaches South Georgia from the southwest, it flows along the southern shelf of the island and then veers anticyclonically towards the Georgia Basin before resuming its eastwards course (Orsi et al., 1995; Thorpe et al., 2002). Because of this large meander in the SACCF, waters downstream of South Georgia are transported to the northwest and north of the island. The ACC and its fronts control the physical and chemical properties of the waters surrounding South Georgia (i.e., Whitehouse et al., 1996; Korb and Whitehouse., 2004). In particular, the PF traces the boundary between the silicate poor waters observed to its north and the silicate rich waters to its south. Consequently, at the beginning of the growth season all macronutrients are at excess concentrations for phytoplankton growth: nitrates and silicates normally range 20-30 nM, whereas phosphates concentrations are close to 1.3-2 nM (CARS 2009; Ridgway et al., 2002 ).

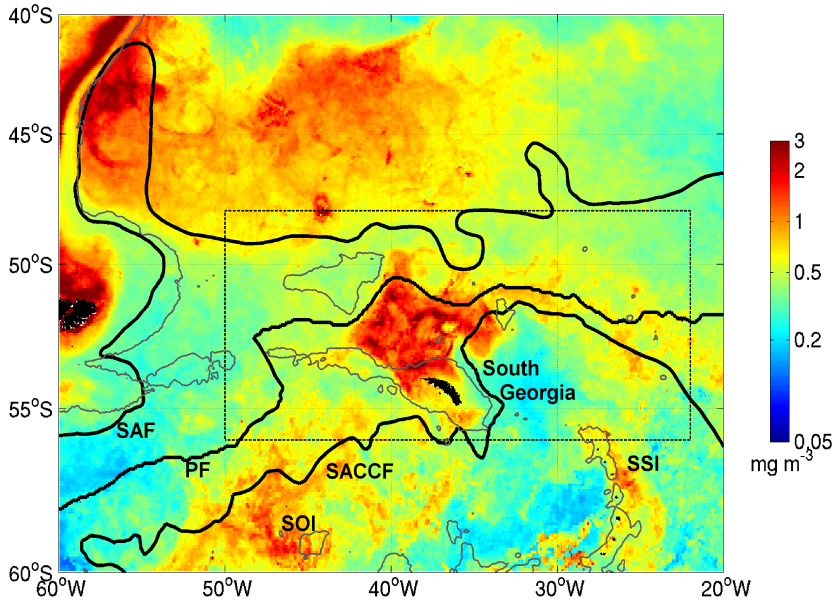


*Fig. 3.4.1. Austral summer (January-February) chlorophyll a climatology derived from MODIS for the 2006-2011 time-period in the southwestern sector of the Atlantic Southern Ocean. Bold lines indicate the Subantarctic Front (SAF, Orsi et al., 1995), the Polar Front (PF, Moore et al., 1999) and the Southern ACC Front (SACCF, Thorpe et al., 2002). The position of the South Orkney Islands (SOI) and the South Sandwich Islands (SSI) are also indicated. The rectangle indicates the South Georgia area mentioned in the text.*

Despite South Georgia's relatively small size (~ 3700 km$^2$), satellite ocean colour imagery from the north and northwest of the island reveal a large (~ 145 000 km$^2$, Borrione and Schlitzer, 2013) and long-lived phytoplankton bloom with chlorophyll a (Chl a) concentrations often greater than 10 mg m$^3$ (Korb et al., 2004) leading to one of strongest seasonal atmospheric-carbon uptake in the open Southern Ocean (Jones et al., 2012). These very high levels in pigment biomass concentrations are in sharp contrast with the surrounding high-nutrient low-chlorophyll (HNLC) waters, where, despite the presence of high macronutrient concentrations, phytoplankton blooms are observed only on few occasions (Fig. 3.4.1).

The environmental conditions behind South Georgia's very high primary productivity are still investigated; ongoing research has indicated that a continuous supply of iron from the island's shelf is most likely one of the most important drivers (Nielsdóttir et al., 2012). The currents flowing along and over the wide (30-100 km) continental shelf of the island could pick-up iron from shelf sediments and would then transport the iron-enriched waters towards the Georgia Basin, where intense blooms are regularly found (Nielsdottir et al., 2012; Korb et al., 2008; Borrione and Schlitzer, 2013). Clearly, sources of iron other than the South Georgia coastal region are possible. Among these there is atmospheric deposition of dust particles originating from the Patagonian Desert (Meskhidze et al., 2007; Johnson et al., 2010). Nevertheless, it is still impossible to ascertain from in situ data the magnitude and relative contribution of coastal processes and dust deposition on natural iron fertilization around the island because measurements of iron from the coast of the island are still very few (Holeton et al., 2005; Nielsdóttir et al., 2012) and direct estimates of dust-deposition are absent. In our current state of knowledge biogeochemical modelling remains the key tool, however to date such studies are absent for South Georgia, as they mostly considered the Southern Ocean as a whole (i.e., Tagliabue et al., 2009a; Moore and Braucher, 2008).

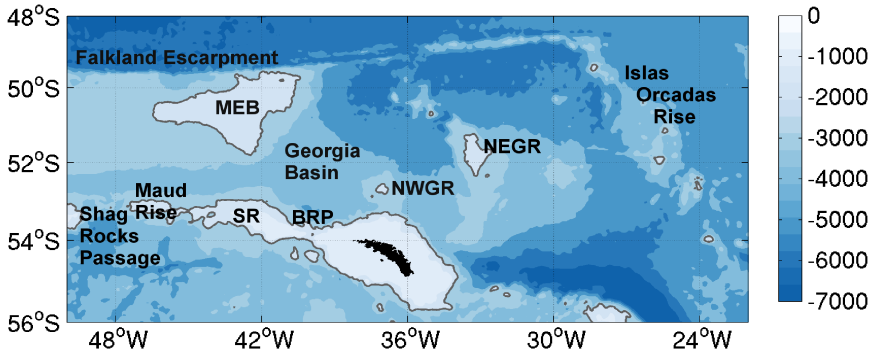


*Fig. 3.4.2. Bathymetry and main topographic features in the South Georgia area: MEB: Maurice Ewing Bank; SR: Shag Rocks; BRP: Black Rocks Passage; NWGR: North West Georgia Rise; NEGR: North East Georgia Rise. Bathymetric contours for the 2000m are indicated with thin lines.*

In this study we investigated iron fertilization around South Georgia using a coupled model including the hydrodynamic regional model ROMS (i.e., Regional Oceanic Modelling System; Shchepetkin and McWilliams, 2005) and the biogeochemical model PISCES (i.e., Pelagic Integration Scheme for Carbon and Ecosystem Studies; Aumont and Bopp, 2006). In addition to the source of iron from dust deposition accounted for alone in previous models

(i.e., Parekh et al., 2004; Aumont et al., 2003), PISCES also includes a sedimentary source of iron to the ocean. According to Moore and Braucher (2008) and Elrod et al. (2004), both iron sources must be present in ocean biogeochemical models including iron-limitation.

After introducing the modelling tools and observational datasets, we evaluate the model's performance in the South Georgia area and in particular the model's ability to simulate surface dissolved iron (dFe) concentrations. Finally, we present results from sensitivity runs, performed to identify the main sources and distribution-pathways of dFe concentrations in the region. These results provide an opportunity to investigate natural iron fertilization around and downstream of South Georgia complementing the current lack of spatially-uniform in situ dFe measurements.

### 3.4.2 Model description

#### The hydrodynamic model ROMS

The hydrodynamic model used for this study is the version of ROMS (Shchepetkin and McWilliams, 2005) which makes use of the Adaptive Grid Refinement in Fortran (AGRIF) procedure, (i.e., ROMS_AGRIF; Debreu and Blayo, 2008; Penven et al., 2006).

ROMS_AGRIF is a three-dimensional, split-explicit, free-surface, primitive equation model. Vertical and horizontal coordinates are discretized in coastline and terrain-following curvilinear coordinates (i.e., sigma-layers) using high-order numerical methods. ROMS_AGRIF is based on the Boussinesq approximation and hydrostatic vertical momentum balance and solves the free surface primitive equations in an Earth-centred rotating environment. The model's code (version V1.1) and the pre- and post-processing routines (Penven et al., 2008) used in this study, together with the biogeochemical model PISCES described below, were obtained from the webpage of the Institut de Recherche pour le Développement (http://www.romsagrif.org/). To date, ROMS_AGRIF has been utilized for several oceanographic settings (i.e., Karakas et al., 2006; Penven et al., 2006), but never for a region of the Southern Ocean.

#### The biogeochemical model PISCES

PISCES (Aumont and Bopp, 2006) is a 24-compartment biogeochemical model. It simulates the biogeochemical cycles of oxygen, carbon and the cycle of the main micro- and macronutrients controlling phytoplankton growth, i.e., iron, phosphate, nitrate, ammonia and silicate. The phytoplankton compartment comprises nanophytoplankton and diatoms; of the two, only the latter requires silicate for growth. Moreover, PISCES includes a grazer compartment (i.e., micro- and meso- zooplankton) as well as a non-living detritus compartment, consisting of big and small organic particles. In all living compartments the total biomass in carbon is calculated explicitly and the Redfield C/N/P ratios are assumed constant and equal to 122/16/1. Additionally, for the phytoplankton compartment PISCES explicitly calculates values for chlorophyll (Chl), iron and, for diatoms only, silicate; consequently, the internal ratios for Fe/C, Chl/C, and Si/C, which are allowed to vary, are

always known. Conversely, for the zooplankton compartment these ratios are kept constant. The bacterial pool is not modelled explicitly.

The presence of an iron cycle (briefly described below and schematically represented in Fig. 3.4.3) is the key aspect of PISCES when performing biogeochemical modelling in the iron-limited HNLC Southern Ocean.

In PISCES iron is supplied to the ocean in dissolved form from atmospheric dust-deposition and sediment mobilization. Aeolian deposition of iron to the ocean has been estimated from the climatological monthly maps of dust deposition modelled by Tegen and Fung (1995). Their annual estimates of dust deposition around South Georgia (i.e., 1-5 g $m^{-2}$ $yr^{-2}$) are comparable to those obtained with more recent modelling experiments (Mahowald et al., 2005; Ginoux et al., 2001). In the current configuration of PISCES, the iron content and its solubility in dust particles is constant and set to 3.5%, and 2% respectively. Similar percentages were used in previous biogeochemical models including iron (Moore and Braucher, 2008; Parekh et al., (2004)). Once in the water column, dust particles sink at 5 m $day^{-1}$ and undergo remineralisation until they reach the sea-floor and are lost to the sediments (Aumont and Bopp, 2006).

The flux of dFe from the sediments to the water column is calculated adapting the meta-model of Middelburg et al. (1996), here used to estimate the reductive mobilization of iron. The dFe flux depends on the maximum iron-flux at the sediment-water interface (parameterized to 1 μmol dFe $m^{-2}$ $day^{-1}$, which is close to 2 μmol dFe $m^{-2}$ $day^{-1}$ used by Moore and Braucher, (2008)) and depth. In the calculations depth is used as a proxy for how well the sediments are oxygenated.

Dissolved iron in free inorganic form (Fe' in Fig. 3.4.3) can undergo complexation with one type of ligands (L' in Fig. 3.4.3), which are present at uniform concentrations (i.e., 0.6 nM, see also Johnson et al., 1997) or scavenging on particles; the latter depends on the total load of organic particles and together with aggregation processes leads to the formation of particulate organic iron. Particulate organic iron is reintroduced into the dissolved iron pool via remineralization, or it is lost to the sediments with sinking particles. Previous simulations including the biogeochemical model PISCES have shown its ability to reproduce adequately global dFe and pigment biomass distributions proving it to be an appropriate tool for a variety of studies concerning ocean biogeochemistry, including those in the Southern Ocean (Aumont and Bopp, 2006; Slemons et al., 2009; Tagliabue et al., 2009a).

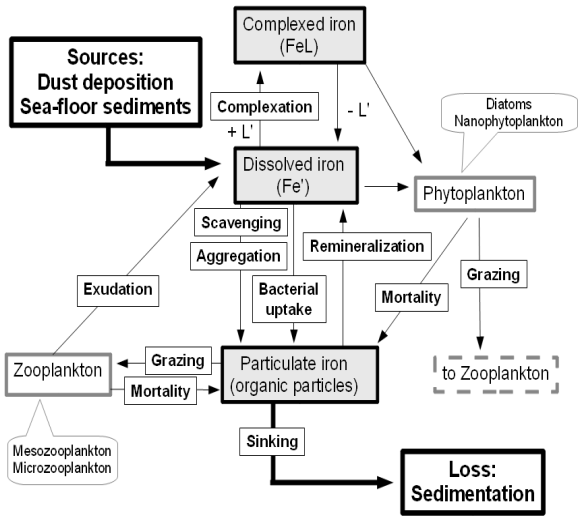


*Fig. 3.4.3. Schematics of the iron cycle in PISCES as implemented in the current application (modified from Slemons et al., 2009). Fe' indicates free inorganic dissolved iron, L' are ligands, while FeL indicates dissolved iron complexed to ligands.*

## Model configuration and simulations

In the present configuration, the coupled ROMS_AGRIF-PISCES model was implemented over the ocean domain depicted in Fig. 3.4.1, defined between (60°W-20°W) and (60°S-40°S) with a resolution of approximately 11 km. The size of the domain was chosen in order to maintain sufficient distance between South Georgia and the domain-boundaries, thus limiting the effects of the four open-boundary conditions on the solutions (see also Young et al., 2011). At the average latitude and longitude of the model-domain, the Rossby radius is ~15 km (Chelton et al., 1998), indicating that the current resolution is eddy permitting. Along the vertical dimension we used 32 sigma-coordinate layers stretched to increase vertical resolution near the surface.

ETOPO2 (Smith and Sandwell, 1997) was used to construct the model bathymetry. To prevent horizontal pressure gradient errors, the ETOPO2 topography was smoothed. In our configuration, the variable that controls the maximum value of the r-parameter measuring the slope of the sigma-layers is set to 0.25 (Beckmann and Haidvogel, 1993). Water temperature, salinity, sea level and velocity fields used at the boundaries and for the model's initial conditions derive from the Simple Ocean Data Assimilation reanalysis (SODA, Carton and Giese, 2008). The SODA physical ocean properties were retrieved from the web ( http://iridl.ldeo.columbia.edu/) and elaborated with the ROMSTOOLS pre-processing toolbox (Penven et al., 2008) to construct the climatology used in the simulations.

The model is forced with fresh water and heat fluxes from the Comprehensive Ocean-Atmosphere Data Set (COADS05, Da Silva et al., 1994), while the surface wind stress climatology for the 2000-2007 time-period derives from QuikSCAT measurements (Quick scatterometer, http://www.ifremer.fr/opendap/cerdap1/cersat/wind/l4/quikscat/daily/). A climatology of sea surface temperatures from Pathfinder satellite observations (Casey and Cornillon, 1999) was utilized to restore modelled surface temperatures.

PISCES boundary and initial conditions for dissolved iron, macronutrients (i.e., nitrate, phosphate, silicate) and oxygen were derived from the World Ocean Atlas 2005 climatological datasets (Conkright et al, 2002) included in the ROMSTOOLS pre-processing

toolbox, while the boundary and initial conditions for chlorophyll a, phytoplankton and zooplankton biomass were obtained from existing ORCA2 model simulations (Aumont and Bopp, 2006), and successively adapted to the current domain size, grid structure and resolution.

Model spin-up was carried out for 20 yrs, until quasi-equilibrium was reached, and then ran for 10 more yrs. In addition to the reference simulation, hereafter called SEDDUST, in which boundary conditions, surface forcings and iron sources are equivalent to those described above, we performed sensitivity runs in which we modified the iron sources present in the last three modelling years. All sensitivity runs are listed in Table 3.4.1. In two sensitivity runs either sedimentary or aeolian sources of iron were removed from the system (simulations are named NOSED_DUST and SED_NODUST, respectively). In each of the other sensitivity runs, atmospheric sources of iron were kept identical to those utilized in the SEDDUST scenario, whereas the reductive mobilization of iron was limited to sediments present at selected 5m-thick ocean depth intervals. Six simulations resolved the top 0-30m surface layer, while in two additional runs reductive mobilization of iron was limited to the sediments present at the 50-55m and 100-105m ocean depths intervals only. When compared to the reference SEDDUST scenario, these sensitivity simulations provide information on the relative importance of dust and sedimentary sources, but also provide an indication of the depth of the sedimentary sources contributing most of the dFe observed at the surface. Results are presented in Sect. 4.5 below.

All model results shown in the following are obtained from the averages of January and February of the last modelling year, because for these months in situ surface dFe data are available for the validation of our results (Nielsdóttir et al., 2012).

### 3.4.3 Observational dataset

#### Ocean colour measurements

Freely available Aqua MODIS (Moderate Resolution Imaging Spectroradiometer) Standard Mapped Images - Level 3 products, for the ocean-colour monthly composites of January and February from the 2006-2011 time-period, processed by the Goddard Space Flight Center and projected on a regular spatial grid of 9 km, were retrieved from the Distributed Active Archive Center (http://oceancolor.gsfc.nasa.gov/). The full dataset was used to construct the climatology depicted in Fig. 3.4.1, while the averages obtained from the monthly composites of January and February 2008, corresponding to the sampling-period of in situ surface dFe concentrations (Nielsdóttir et al., 2012, see below), and the averages obtained from the monthly composites of January and February 2011 were used for comparisons with model outputs (Fig. 3.4.6). Ocean colour estimates depicted in Figs. 6a and 6b were interpolated onto the model's coarser grid resolution (~ 11 km).

#### Surface water circulation

Surface circulation patterns in the South Georgia area (region outlined with a rectangle in Fig. 3.4.1) were estimated from Aviso satellite altimetry

(http://www.aviso.oceanobs.com/duacs/). The Aviso altimeter product is based on multiple altimeter missions (Jason-1&2, T/P, Envisat, GFO, ERS-1 & 2 and Geosat) and provides a consistent and homogeneous dataset. Weekly delayed-time values for the zonal and meridional components of surface current velocity computed from absolute topography, re-sampled on a regular 0.25° grid, were extracted for the months of January and February of 2008 for comparisons with modelled surface (0-30 m) velocities (in Fig. 3.4.4), but also for January and February of 2011 (Fig. 3.4.6b).

### Macronutrients

Surface (0-30m) concentrations of nitrate, phosphate and silicate, distributed by the CSIRO Atlas of Regional Seas (CARS; http://www.marine.csiro.au/~dunn/cars2009/; Ridgway et al., 2002) and available at a 0.5° grid resolution, were retrieved and then averaged for the area centred around the main South Georgia bloom region (45°-32°W; 56°-50°S in Fig. 3.4.7a). The annual cycles of the three macronutrients were compared with those obtained with the model during the last modelling year (Fig. 3.4.5).

### In situ surface dFe measurements

Underway surface dFe measurements around South Georgia were obtained during an oceanographic cruise to the Scotia Sea aboard the RRS James Clark Ross, as part of the British Antarctic Survey Discovery 2010 FOODWEBS programme. DFe concentrations used in this study are from the period between 23 January and 10 February of 2008. All dFe underway samples were treated and determined as described in detail by Nielsdóttir et al. (2012). Sample locations and measured values are shown in Fig. 2c of Nielsdóttir et al. (2012) and in Figs. 3.4.7a and 3.4.8a of the present manuscript.

## 3.4.4 Results

In the following, we first assess the ability of the model to reproduce environmental conditions around South Georgia by comparing physical and biogeochemical conditions obtained from model simulations with available observational data. For consistency with the time period of the available surface dFe concentration dataset (Nielsdóttir et al., 2012), surface circulation and ocean colour pertain to January-February of 2008, while model results are from surface (0-30m) averages of January-February of the last modelling year. To assess the sensitivity of the results to the chosen period, we also considered previous years but found comparable results in all cases. Similar results are obtained because the model was in a quasi-equilibrium state but also because boundary conditions and forcing fields derive from climatologies that are repeated cyclically in each year of the simulations. For the same reason, modelling results shown in the following cannot reproduce the details of any observational year. Second, we use model results to describe the potential distribution of surface dFe concentrations around South Georgia, as well as its principal sources.

## Circulation Patterns around South Georgia

Surface circulation patterns estimated from Aviso satellite altimetry during January and February of 2008 and those obtained from model simulations are compared in Fig. 3.4.4 to evaluate the ability of the model to reproduce the main features of circulation around South Georgia. Satellite altimetry (Fig. 3.4.4a) indicates that the ACC, the principal current around South Georgia, enters the South Georgia area from the southwest and crosses the North Scotia Ridge at three locations: close to Shag Rocks Passage (~ 48°W, 53°S), at Black Rock Passage, which is located between Shag Rocks and South Georgia (~ 40°W, 54°S), and to the east of the island following closely the 2000 m bathymetry contour (Fig. 3.4.4). The latter branch of the ACC turns west along the northern flank of the island flowing towards the Georgia Basin. On its way the current is joined by the flow through Black Rock Passage at first and subsequently also by part of the flow that crosses the North Scotia Ridge through Shag Rocks Passage. Over the Georgia Basin, the circulation is cyclonic and characterized by intense currents along the margins of the basin (~ 20-25 cm $s^{-1}$), and by weaker currents over the central portion of the basin (often below 10-15 cm $s^{-1}$). Once the flow exits the Georgia Basin it continues east along a convoluted route close to NEGR and the Islas Orcadas Rise (refer to Fig. 3.4.2 for topographic features in the region).

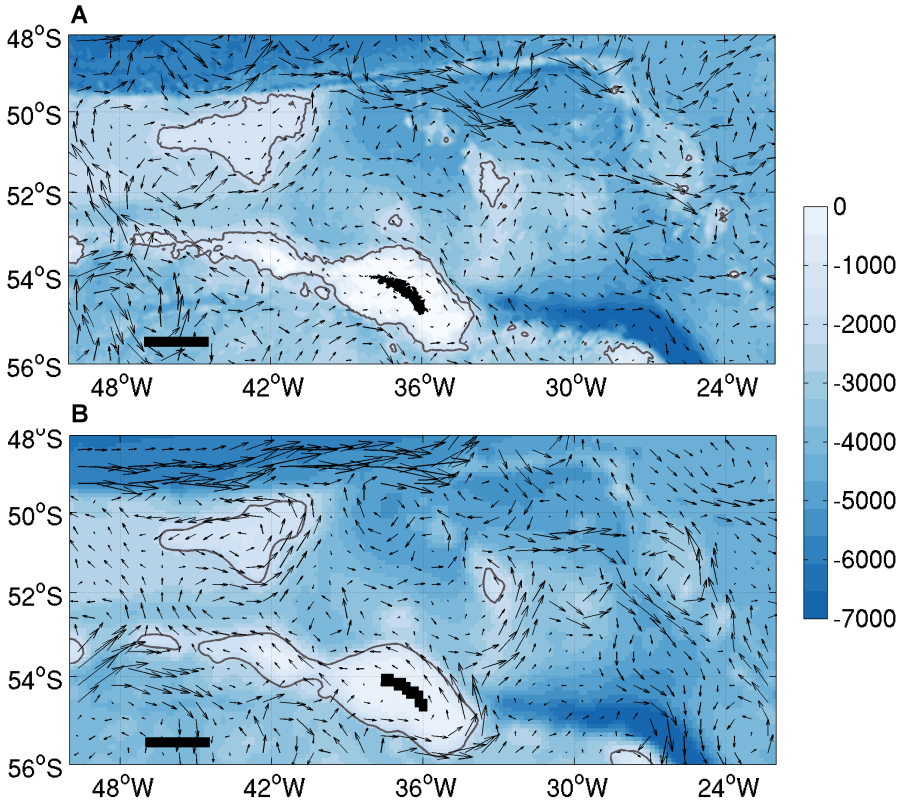


*Fig. 3.4.4. Surface circulation (black arrows) in the South Georgia area, as obtained from (A) Aviso satellite altimetry for January-February 2008 and from (B) model results for January-February of the last modelling year. Background colours indicate bottom topography. For reference, the 2000m bathymetry is indicated with thin grey lines. In both panels, the horizontal bar in the bottom-left corner indicates 1 m $s^{-1}$, and corresponds to approximately 160 km. Modelled surface circulation is interpolated onto the coarser grid resolution of satellite altimetry.*

For the purposes of this study, which aims at understanding sources but also potential transport pathways of iron from and then around South Georgia, particularly important circulation features are (i) the current that flows westwards along the northern shelf of the island towards the Georgia Basin, believed to transport iron-enriched waters from the shelf region towards the bloom area (Nielsdóttir et al., 2012); (ii) the intense cyclonic circulation along the borders of the Georgia Basin, which confine South Georgia blooms to the basin (see Borrione and Schlitzer, 2013) and (iii) the flow across Black Rock Passage which delimits the southwestern border of South Georgia blooms separating them from the waters adjacent to Shag Rocks (see Venables et al., 2012). The level of realism reached by the simulated surface circulation during January and February (Fig. 3.4.4b) will be assessed considering these specific currents. Smaller scale features, like eddies, filaments or meanders in the flow, are not considered in the comparison between altimetry and modelling results because they reflect the natural variability of the system, and can be very different according to the years considered.

During January and February of the last model year (Fig. 3.4.4b), surface circulation patterns around the island are strongly steered by bottom topography, and reflect in many ways circulation patterns described from satellite altimetry (Fig. 3.4.4a). In fact, the model reproduces the current that after flowing along the southeastern and then the northeastern shelf of the island splits into a branch that flows northeast of the island, along the southern flank of the NEGR, or veers west travelling along the northern shelf of the island towards the Georgia Basin. Moreover, the model reproduces the northwards current flowing across Shag Rock Passage or across the Black Rock Passage.

Along the margins of the Georgia Basin the current is relatively intense (20-40 cm $s^{-1}$) whereas over the central portion of the basin the current is generally weaker (10-15 cm $s^{-1}$), except for a fast rotating anticyclonic eddy that is formed to the south west of the basin (40°W, 53°S). This eddy is not present in the Aviso observations for January-February of 2008.

Modelled current intensities reproduce the general spatial variability observed in satellite altimetry. For example, in both the modelled and satellite-based circulation fields, surface currents are stronger along the margins than over the central part of the basin; overall, however, the model tends to overestimate absolute circulation velocities.

### Macronutrient concentrations

Macronutrient surface (0 - 30m) concentrations averaged over the domain centred around the main South Georgia bloom area, defined between 45°-32°W and 56°-50°S (shown in Fig. 3.4.7a) follow a clear annual cycle both in the CARS2009 and modelled data (Fig. 3.4.5). For both datasets and all macronutrient variables, maximum values occur between winter and early spring, while minimum values are recorded in early austral summer; furthermore, in all cases surface macronutrient concentrations averaged over the chosen domain are above concentrations that are limiting for phytoplankton growth. In the following, maximum and

minimum values are reported with their corresponding standard deviation (SD) and one standard error interval (SE).

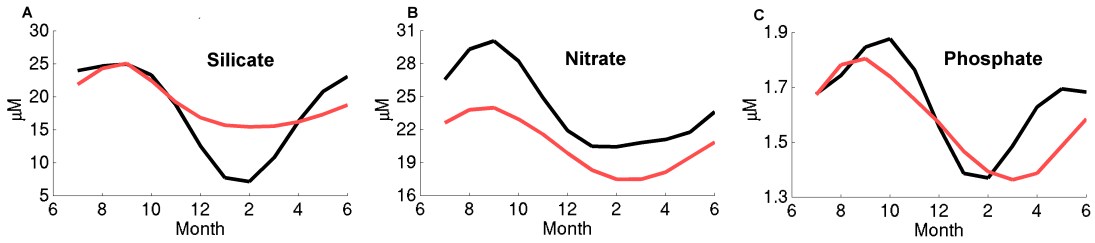


*Fig. 3.4.5. Annual cycles of surface (0-30m) silicate (A), nitrate (B) and phosphate concentrations averaged over the South Georgia domain defined between 45°-32°W and 56°-50°S (shown in Fig.* 3.4.*7a) from the CARS2009 climatology (black lines) and from model outputs from the last modelling year of the SEDDUST scenario (red line).*

In the two datasets, the timing of maximum and minimum values in the annual cycles of silicate coincide (Fig. 3.4.5a). During September surface silicate concentrations reach their annual maximum value and rise to ~ 25 μM in the CARS2009 dataset (SD ~8.9 μM and SE ~0.47 μM) and in the model (SD ~8.63 μM and SE ~0.12 μM ). In February, however, when silicate surface concentrations are at their minimum, concentrations are significantly different: in the CARS2009 dataset concentrations are close to 7.16 ± 5 μM (SE = 0.34 μM ) and correspond to approximately 28% of the maximum value recorded in September; conversely, in the model silicate concentrations during February are almost twice those of the CARS2009 dataset; modelled silicate concentrations are close to 15.45 ± 7.7 μM (SE ~0.11 μM) and correspond to 62% of the maximum value recorded in September. Therefore, in the model there is a significantly weaker winter-summer reduction of silicate concentrations than in the CARS2009 observations, possibly due to the model's tendency to underestimate total Chl a (see below) or to the model's range of admitted Si/C ratios.

As shown in Fig. 3.4.5b, the model matches the timing of maximum and minimimum nitrate concentrations observed in the CARS2009 dataset (i.e., September and February in both datasets). However, compared to the CARS2009 surface nitrate concentrations, which range between ~20.44 ± 1.65 μM in February (SE ~0.09 μM) and 30.1 ± 2.5 μM in September (SE ~0.13 μM), the annual cycle of modelled surface nitrate concentrations averaged over the South Georgia domain are approximately 4 μM lower than observations: in the model, nitrate concentrations range between 17.5 ± 2.22 μM in February (SE = 0.03 μM L) and 24 ± 1.66 μM in September (SE = 0.03 μM). Despite the negative bias in modelled concentrations, like in the observations modelled minimum values during summer derive from a ~30% reduction of the maximum winter values.

The annual cycles of CARS2009 and modelled phosphate concentrations averaged over the South Georgia area are indicated in Fig. 3.4.5c. Observational and modelled phosphate concentrations range between very similar values: minimum values are respectively 1.37 ± 0.13 μM and 1.36 ± 0.12 μM, while maximum concentrations are respectively 1.88 ± 0.08 μM and 1.8 ± 0.01 μM. In the two datasets however, the months of minimum and maximum

values differ: in the CARS2009 dataset, they occur respectively in February and October, while in the model minimum and maximum values are observed respectively in March and September.

### Surface Chl a concentrations

During January-February of 2008, MODIS satellite estimates of surface Chl a concentrations (Fig. 3.4.6a) reveal the presence of a large and intense phytoplankton bloom over the southern and northwestern shelf of South Georgia, and to the northwest and north of the island (Chl a > 2 mg $m^{-3}$). The bloom reflects the geometry of the typical bloom area described by Borrione and Schlitzer (2013). Outside all borders of the Georgia Basin and due east of the island Chl a values fall close to or below 0.5 mg $m^{-3}$ (HNLC waters). In this specific period of observations, exceptions to the HNLC waters observed outside the main bloom area are the patches around (42°W, 55°S), (43-49°W, 48°S) and (24°W, 53°S) where Chl a concentrations are above 0.75 mg $m^{-3}$. The latter Chl a rich patch, which is more than 700 km east of the NEGR, is much larger in size than the previous patches, and appears to be connected to the main bloom area by a narrow filament with Chl a concentrations ~1 mg $m^{-3}$.

Arrows in Fig. 3.4.6a represent contemporaneous surface circulation patterns from Aviso satellite altimetry (see also Sect. 4.1 and Fig. 3.4.4a). The joint analysis of the two datasets shows that the location and shape of the South Georgia bloom is strongly related to local circulation, which seems to also generate the narrow tongue of Chl a rich waters connecting the main bloom area to the Chl a rich patch observed around (24°W, 53°S). Moreover, over the shelf of the island variability in flow intensity is reflected in the distribution of Chl a concentrations. In fact, over the western and southern shelf of the island, where Chl a concentrations are highest, surface circulation is very weak (< 5 cm $s^{-1}$ ), while over the northeastern portion of the shelf region, where Chl a concentrations are low (< 0.2 mg $m^{-3}$) surface currents flowing parallel to the shelf-break are above 10-15 cm $s^{-1}$.

During January-February of 2011 (Fig. 3.4.6b), Chl a concentrations were mostly below 1.5 mg $m^{-3}$ and provide an example of a weaker South Georgia phytoplankton bloom. Nevertheless, patterns in Chl a concentrations (i.e., location of bloom and non-bloom waters) and surface circulation around the island have many similarities with the patterns described for January-February of 2008 (Fig. 3.4.6a).

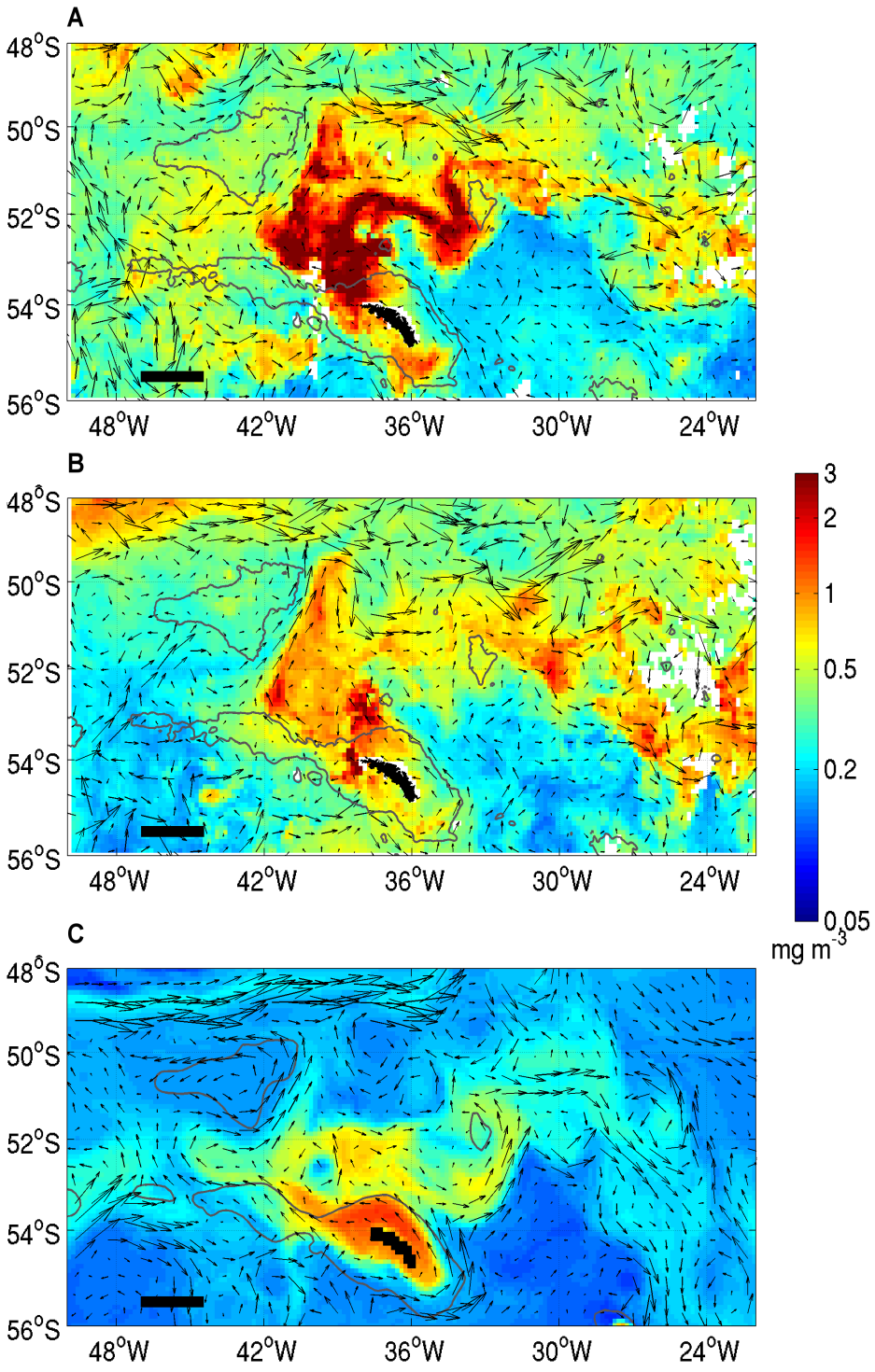


*Fig. 3.4.6. Surface Chl a concentrations in the South Georgia area as obtained from MODIS ocean colour estimates for January-February 2008 (A) and January-February 2011 (B). Satellite estimates are interpolated onto the model's coarser grid resolution. In (C ) surface (0-30m) averages of Chl a concentrations from January-February of the last modelling year. In all cases, black arrows report contemporaneous surface circulation patterns either from Aviso altimetry (in A and B) or from the model (in C). Circulation patterns in panels A and C are equivalent to those depicted in Fig.* 3.4*.4. In all panels the 2000m bathymetry is indicated with thin grey lines; the horizontal bar in the bottom-left corner indicates 1 m s $^{-1}$, and corresponds to approximately 160 km.*

Surface Chl a concentrations obtained from the average of January and February from the last modelling year (SEDDUST scenario) are shown in colour in Fig. 3.4.6c. In the same Fig., black arrows depict contemporaneous modelled surface circulation partterns. Comparison between modelled surface Chl a concentrations and surface velocities (Fig. 3.4.6c) with satellite observations (Fig. 3.4.6a) shows the ability of the model to capture the main features of primary productivity in the South Georgia region: in the modelling and observational datasets highest productivity levels are observed over the Georgia Basin and the shelf of the island, where Chl a concentrations are one order of magnitude higher than in the surrounding waters. Moreover, in both datasets the phytoplankton bloom extends in the west-east direction between the area north of Shag Rocks and the NEGR, and it extends in the north-south direction between the 50°S parallel and the southern shelf-break of the island. In agreement with satellite ocean colour imagery, ROMS_AGRIF-PISCES reproduces the long (~800 km) Chl a rich plume extending eastwards of the NEGR, but also a region of higher productivity along the Falkland Escarpment, to the northwest of the South Georgia phytoplankton bloom. Although the current model configuration does not allow for a reproduction of a specific year of observations, it must be noted that overall the model can capture adequately the relative magnitude of Chl a concentrations between bloom and non bloom waters. However the model tends to under-estimate absolute Chl a concentrations as shown by comparing model results with Chl a concentrations observed in 2008 (Fig 3.4.6a), but also those observed during the less productive austral summer of 2011 (Fig. 3.4.6b). In the model in fact, highest Chl a concentrations are mostly between 0.7-1.5 mg $m^{-3}$ in the main bloom area, while in the relatively wide plume extending downstream of the NEGR, Chl a concentrations never rise above 0.3 mg $m^{-3}$.

Similarly to our description of MODIS Chl a concentrations and Aviso altimetry (Figs. 3.4.6a and b), also in the modelled fields (Fig. 3.4.6c) there is a clear correspondence between productivity patterns and local circulation. In fact, in the simulations the South Georgia phytoplankton bloom is confined at all sides by bands of rapidly flowing currents (20-40 cm $s^{-1}$), while the two Chl a rich plumes observed along the Falkland escarpment and downstream of the NEGR correspond to regions of very high flow velocities (30-80 cm $s^{-1}$), which most likely are responsible for the position, shape and extension of the two Chl a rich plumes. Over the southern portion of the Georgia Basin (40°W, 53°S), amidst waters with high Chl a concentrations, an anticyclonic eddy encircles waters with very low Chl a concentrations (~ 0.1 mg $m^{-3}$). Analysis of circulation and Chl a concentration fields from previous modelled months, indicates that the anticyclonic eddy detaches from a meander extending southwards from the Chl a poor waters to the north of the Georgia Basin. A similar meander is observed in satellite imagery of January 2004 (Borrione and Schlitzer, 2013).

### Surface dissolved iron concentrations

Surface (~ 3 m) underway dFe concentrations (in Fig. 3.4.7a, see also Nielsdóttir et al., 2012) were measured between January and February 2008 in the area south of South Georgia (~ 41°W, 55°S), along a transect across the Georgia Basin, and over the northern shelf of the island. Surface dFe concentrations were highest over the shelf of the island, ranging between 2.5 and 6.9 nM and then decreased to concentrations of approximately 1 nM close to the 2000

m bathymetry contour. Over the Georgia Basin, concentrations were variable and ranged between values close to the instrumental detection limit (0.027 ± 0.018 nM) and high concentrations (i.e., 2 nM at 38°W, 52.5°S). South of South Georgia, i.e., upstream of the island, dFe concentrations were very low (≤ 0.1 nM ) at all sampled locations.

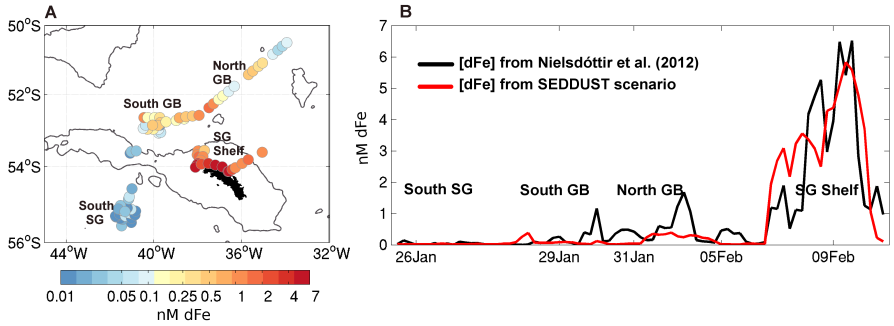


*Fig. 3.4.7. (A) location and concentrations of dFe underway measurement from January and February of 2008 (Nielsdóttir et al., 2012). B) Underway measurement of dFe (red line) and simulated surface dFe concentrations (black line); model values were interpolated onto the dFe sampling locations shown in panel A. For reference, the x-axis indicates dates of in situ dFe sampling. The main geographical areas are also indicated, and correspond to those marked in panel A.*

DFe concentrations measured in the locations marked in Fig. 3.4.7a, are also depicted in Fig. 3.4.7b following their sampling progression for a more detailed comparison with model results. Modelled surface (0-30 m) dFe concentrations from January and February of the last model year (SEDDUST scenario; Fig. 3.4.7b) were interpolated onto the same sampling locations in order to maintain in both datasets the correspondence of dFe concentrations with local topography (i.e., distance from the island or ocean depth). As in the current model configuration, boundary conditions and forcing fields derive from a cyclical climatology, and hence model results cannot be representative of any specific observational year, we will compare the relative variability of dFe concentrations in the region, and not absolute dFe concentrations. In both datasets dFe concentrations increase progressively from the area upstream of South Georgia (on average, dFe < 0.1 nM), to the Georgia Basin (on average, dFe concentrations between 0.5 nM and 2 nM) and finally to the area over the shelf of the island, where concentrations are maximum in both datasets (on average, dFe concentrations between 1.5 nM and 6 nM). Differences in the absolute measured and sampled dFe concentrations, as for example over the southern part of the Georgia Basin (indicated as South GB in Fig. 3.4.7), depend on differences between surface circulation patterns in the two datasets: comparing Fig. 3.4.6c with Fig. 3.4.6a, it can be seen that around (40°W, 53°S) model results indicate the presence of an anticyclonic eddy which is not present in the surface circulation patterns obtained from satellite altimetry for 2008.

On average, the difference between modelled and measured dFe concentrations in the locations marked in Fig. 3.4.7a is ~ 0.02 nM, with root mean square (RMS) close to 0.81 nM. Similar values were also obtained when dFe concentrations were extracted from the austral summers of the two previous modelling years (data not shown): in the previous years the calculated mean difference is ~ 0.01 nM and the RMS is close to 1 nM. These low values

demonstrate that in the present configuration, the model can reproduce adequately the main features of the distribution of dFe concentration in the region; moreover, similarly to the in situ dataset, modelled dFe concentrations are at their minimum values to the south, i.e., upstream, of the island and reach their maximum concentrations along the coastal area.

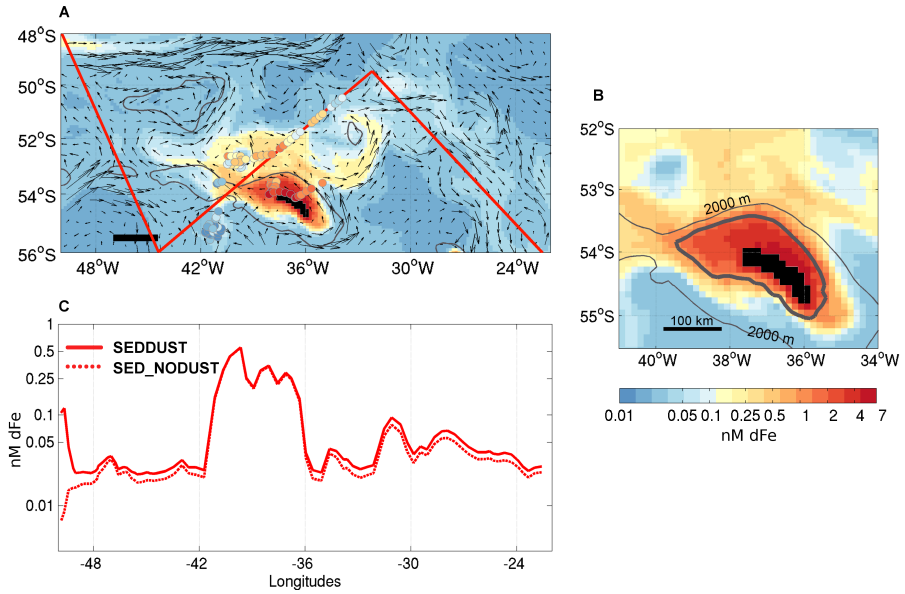


*Fig. 3.4.8. Simulated surface (0-30 m) dFe concentrations for January-February of the last modelling year. In (A) dFe concentrations (colour-scale as in B) are obtained from the SEDDUST scenario; coloured dots indicate in situ surface dFe concentrations measured by Nielsdóttir et al. (2012), shown also in Fig. 3.4.7a. The red line marks a virtual transect along which are extracted modelled dFe concentrations depicted in C; black arrows represent the contemporaneous surface circulation as depicted in Fig. 3.4.4b; the horizontal bar indicates 1 m $s^{-1}$ and corresponds to approximately 160 km. (B) dFe concentrations from the SEDDUST scenario (detail from panel A); the thick contour line indicates dFe concentrations equal to 1.35 nM, here marked to estimate dFe scale lengths; see text for more details. (C) modelled dFe concentrations for points along the red line drawn in A. Solid line depicts values obtained from the SEDDUST scenario (i.e., including sedimentary and atmospheric deposition of dFe), dashed line depicts dFe values obtained from the SED_NODUST scenario where there is no atmospheric deposition of dFe.*

Clearly, modelling results can provide a picture at uniform spatial resolution (~11 km) of surface dFe concentrations also outside the locations indicated in Fig. 3.4.7a. During January and February of the last modelling year, surface dFe concentrations (Fig. 3.4.8a) are <0.1 nM in most of the South Georgia domain, except for a large area over the shelf and to the north and northeast of the island and over a narrow area along the Falkland Escarpment, located to the northwest of South Georgia.

Over the shelf of South Georgia dFe concentrations are overall > 2 nM, with highest values along the coast (2-8 nM ). An iron rich plume (~ 0.5 nM) originates from the northwestern corner of the shelf and extends westwards along the northern flank of Shag Rocks; a second dFe plume originates from the northeastern shelf of the island and extends northeastwards along the flanks of the NEGR. The latter plume continues further east along the Islas Orcadas Rise for approximately 800 km, until dFe concentrations reach background values (< 0.1 nM). Both plumes are clearly dependant on the direction of flow (black arrows),

which here moves away from the island, and its high velocities (~ 20-50 cm $s^{-1}$). Conversely, to the south and east of the island, surface dFe concentrations decrease rapidly to background concentrations (< 0.1 nM), remaining high only along a narrow band over the southern shelf of the island; such limited extension is due to the local currents which here move northwards pushing surface waters towards the coast, and then in the easterly direction.

The scale length (Johnson et al., 1997) provides a way to quantify the decrease of iron with distance; its value accounts for all processes acting to increase or decrease surface dFe concentrations, without discriminating between them. The scale length of dFe transport is defined as the distance over which an initial reference concentration (RC) drops to 1/e*RC. For our calculations, as reference we use the average dFe concentration along the coast of the island (i.e., 3.68 nM). In Fig. 3.4.8b (detail of Fig. 3.4.8a) the position of dFe concentrations equal to 1/e * 3.68 nM (i.e., 1.35 nM) is traced with a thick contour line. The dFe scale length corresponds to the distance between the coast of the island and the 1.35 nM contour line.

In the chosen time-period, modelling results clearly show that the scale length of dFe concentrations is a dynamic property, and that it can vary of a factor of ~5 depending on the direction and intensity of local circulation. In fact, to the south of the island, where the flow pushes surface waters towards the coast and then in the easterly direction, the scale length is at its minimum values (~20 km), while to northwest of South Georgia, where local circulation is directed away from the island towards the Georgia Basin, the scale length reaches its maximum values (~ 110 km).

## Iron sources around South Georgia

### Atmospheric sources of iron

Scale lengths ranging between 20 and 110 km have clearly shown that South Georgia is the core of the dFe plume observed in the region. However, as South Georgia is located along the main trajectory of dust plumes originating from the Patagonian desert (Mahowald et al., 2005: Ginoux et al., 2001; Johnson et al., 2010) dust deposition may also be a source of iron to the surface waters around the island.

The importance of dust-derived dFe to the surface layer was evaluated by comparing results from the reference SEDDUST scenario with the SED_NODUST sensitivity run. Surface dFe concentrations obtained with the two simulations and extracted along the virtual transect line traced in Fig. 3.4.8a are marked respectively with a solid and dashed red line in Fig. 3.4.8c. The transect line was chosen in order to consider regions of the South Georgia domain which are closer or farther from the island or the Patagonian desert, and hence likely differ on the relative importance of sedimentary or dust sources of iron. Results depicted in Fig. 3.4.8c indicate that along the transect east of ~48°W, the contribution of dFe from dust deposition is approximately 0.01 nM, hence negligible when compared to surface concentrations from the SEDDUST run, especially over the Georgia Basin. Conversely, in the area around (49°W, 48°S), at the northwestern corner of the South Georgia domain, atmospheric deposition is the principal source of dFe to the region; in fact, in the SEDDUST simulation, dFe concentrations are ~ 0.1 nM, but drop to values close to zero when the dust source of iron is removed.

The greater importance of sedimentary versus atmospheric sources of iron in the domain centred around the main bloom area (Fig. 3.4.7a) is confirmed by averaged surface dFe and Chl a concentrations obtained either with the SEDDUST or SED_NODUST simulation. As shown in Table 3.4.1, average values from the SED_NODUST simulation are only slightly lower than those obtained with the SEDDUST run. Moreover the integrated dust deposition of dFe over the same domain (~2200 km away from South America) is ~6.27 x $10^{9}$ µM day $^{-1}$ while the flux of sedimentary iron released into the water column from all sediments shallower than 100m is 1.35 x $10^{11}$ µM $day^{-1}$. Nevertheless, it must be remarked that although the flux estimates presented above are useful for an estimate of the relative importance of the two main iron sources around South Georgia, their absolute values must be considered with care because model results rely on our current knowledge (and uncertainties) of the iron cycle, and may largely depend on the chosen model parameters (i.e., content and solubility of iron in dust, or maximum dFe flux from the sediments).

### Sedimentary sources of iron

Results presented in the previous section have indicated that in the model, sediments around South Georgia release almost all of the iron observed around and then downstream of the island. Therefore sensitivity runs were used to estimate the depth of the most significant sedimentary sources. For this purpose, in each sensitivity run sediments from a selected depth range only could act as sources of iron, while at all other depths the iron flux was set to 0 µM $m^{-2}$ $day^{-1}$ (see Sect. 2.3). Surface dFe and Chl a concentrations obtained from the reference SEDDUST simulation and each sensitivity run and then averaged over the domain centred around the main bloom area (Fig 3.4.7a) are compared in Table 3.4.1 and depicted in Fig. 3.4.9.

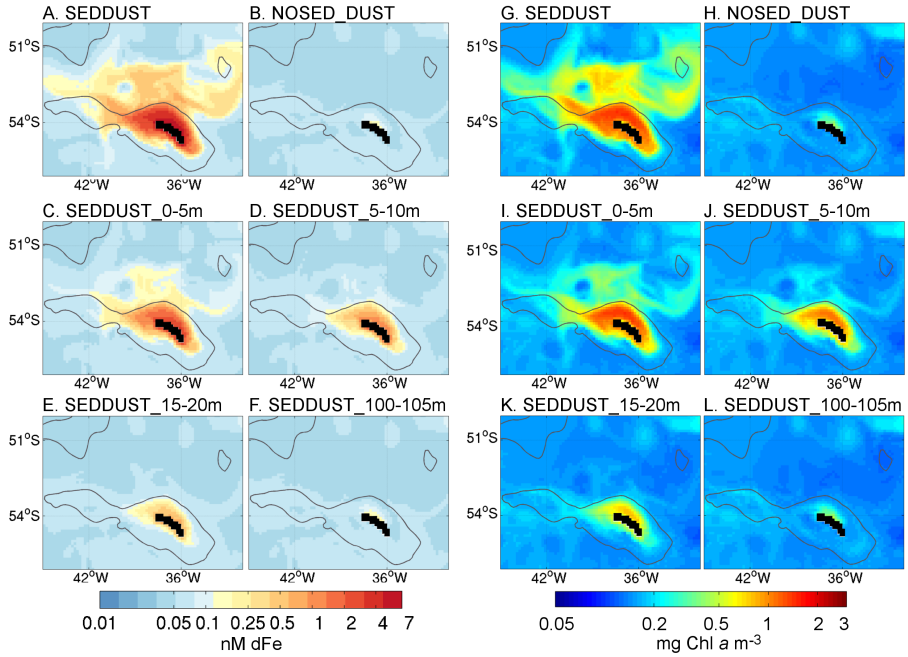


*Fig. 3.4.9. Surface (0-30 m) dFe concentrations (panels a-j on the left) and Chl a concentrations (panels g-l on the right) for January-February of the last modelling year obtained with simulations including different sedimentary sources of iron. Results for the reference runs (i.e., SEDDUST and*

*NOSED_DUST) are shown in the first row. See also Table 3.4.1 and Sect. 2.3 for further details on each simulation.*

Results suggest that the island's coast and very shallow sediments (i.e., depths ≤ 5 m) account for most of the surface dFe and Chl a concentrations simulated with the SEDDUST scenario, followed in importance by sedimentary sources from the 5-20 m depth interval. Conversely, when the release of dFe occurs at greater depths only, the model generates a weak and localized surface dFe and Chl a concentration plume (not shown), reflected in dFe and Chl a values that become progressively similar to those obtained with the NOSED_DUST simulation (Table 3.4.1). Moreover, surface dFe and Chl a concentrations obtained with the SEDDUST_100-105m simulation (Figs. 3.4.9f and 9l) are almost identical to those obtained with the NOSED_DUST simulation (Figs. 3.4.9b and 9h). The similarity of results, is further confirmed by RMS and mean differences calculated between the two runs (last row of Table 3.4.1).

*Table 3.4.1. Averages of surface dFe and Chl a concentrations from each sensitivity run and from the domain around South Georgia depicted in Fig.* 3.4.*7a. RMS and mean differences between each sensitivity run and the SEDDUST scenario are also indicated.*

| Name of scenario | Average ± std (nM $10^{-1}$ dFe) | Average ± std (mg Chl *a* $m^{-3}$) | RMS / mean diff. (nM dFe) | RMS / mean diff. (mg Chl *a* $m^{-3}$) |
|---|---|---|---|---|
| SEDDUST[1] | 1.98 ± 6.01 | 0.33 ± 0.28 | / | / |
| SED_NODUST | 1.92 ± 5.90 | 0.31 ± 0.29 | 0.01 / -0.01 | 0.02 / -0.02 |
| NOSED_DUST[1] | 0.25 ± 0.05 | 0.15 ± 0.02 | 0.62 / -0.18 | 0.33 / -0.18 |
| SEDDUST_0-5m[1] | 0.82 ± 2.32 | 0.25 ± 0.22 | 0.39 / -0.12 | 0.14 / -0.09 |
| SEDDUST_5-10m[1] | 0.42 ± 0.84 | 0.2 ± 0.14 | 0.54 / -0.15 | 0.23 / -0.14 |
| SEDDUST_10-15m | 0.35 ± 0.51 | 0.18 ± 0.1 | 0.57 / -0.16 | 0.26 / -0.15 |
| SEDDUST_20-25m | 0.30 ± 0.31 | 0.17 ± 0.07 | 0.59 /-0.17 | 0.29 /-0.16 |
| SEDDUST_25-30m | 0.3 ± 0.28 | 0.17 ± 0.06 | 0.6 /-0.17 | 0.29 /-0.16 |
| SEDDUST_50-55m | 0.26 ± 0.10 | 0.16 ± 0.03 | 0.61 /-0.17 | 0.32 /-0.17 |
| SEDDUST_100-105m[1] | 0.25 ± 0.05 | 0.15 ± 0.03 | 0.62 / -0.17 | 0.33 / -0.18 |
| SEDDUST_100-105m[2] | 0.25 ± 0.05 | 0.15 ± 0.03 | 0.001 / ~ 0 | 0.002 / 0.001 |

[1] Surface (0-30m) averages of dFe and Chl *a* for these simulations are shown in Fig. 3.4.9

[2] RMS and mean-differences are calculated with respect to the NOSED_DUST simulation.

Although these results are very useful for an estimate of the relative importance of sedimentary sources of iron at different depths, it must be stressed that because in the present model configuration there is no effect of tidal mixing, and the chosen resolution does not allow the representation of vertical mixing generated at the meso and sub-mesoscale, the contribution from the deeper layers could be largely underestimated (Blain et al., 2008).

### 3.4.5 Discussion

#### The South Georgia island mass effect

The work presented here derives from the first regional biogeochemical modelling study that investigates natural iron fertilization and its effects on Chl a concentrations around South Georgia.

Results obtained with ROMS_AGRIF-PISCES show that enhanced Chl a concentrations are only found downstream of South Georgia, i.e., to the north and then northeast of the island, suggesting that the South Georgia island mass effect, and not processes acting upstream of the island, stimulate the observed blooms. A similar conclusion was reported by Korb et al. (2004) who investigated the spatial variability of phytoplankton blooms with in situ and satellite-based observations. In the model, South Georgia phytoplankton blooms extend in the easterly direction for more than 800 km following the direction of the main flow and decrease in magnitude with distance from the island. Such long ranges are in agreement with previous satellite-based studies, and in particular with those of Korb et al. (2004) who observed that the South Georgia bloom can extend till the 0° meridian, for distances > 2700 km aligned to the main path of the Polar Front (see also Venables et al., 2012). Moreover modelling results, which we have shown to be able to capture the main features of dFe

distribution revealed by available measurements, but also to reproduce relatively well absolute dFe concentrations (Fig. 3.4.7 and 3.4.8; root mean square 0.81 nM), can provide a comprehensive view of surface dFe concentrations in the region during the productive season, hence complementing the current lack of large scale and spatially-uniform in situ measurements.

As one could hypothesize observing surface Chl a concentration patterns, the modelled dFe plume extends over a large area to the north and then northeast of the island following local circulation. As previously measured around South Georgia (Nielsdóttir et al., 2012), but also in other regions of the Southern Ocean (e.g., Ardelan et al., 2010; Bucciarelli et al., 2001; Planquette et al., 2007) the model indicates highest dFe concentrations in near-shore waters (> 5 nM), decreasing with distance from the island. Our model results clearly show that the South Georgia island mass effect can reach regions located far away from the island (> 1000 km), where dFe concentrations may still be above background concentrations. A comparable long-range influence of coastal regions has been previously suggested in other open-ocean regions of the World's Ocean, including the Southern Ocean (Elrod et al., 2004; Lam et al., 2006; de Jong et al., 2012; Moore and Braucher, 2008).

DFe scale length values, calculated from our model results as the distances over which an initial reference concentration drops to 1/e of its initial value (Johnson et al., 1997), vary between 20 km and 110 km. These values include the wide range of scale lengths obtained from in situ dFe observations in the open ocean and near-shore regions of the Southern Ocean. Smallest values were obtained by Ardelan et al. (2010) around the Antarctic Peninsula, and by Planquette et al. (2007) around the Crozet Islands (~ 25 km in both studies); larger scale lengths were calculated around South Georgia by Nielsdóttir et al. (2012) and in the vicinity of the Kerguelen Islands by Bucciarelli et al. (2001) (scale lengths respectively 102 km and 151 km). As shown in our model results around South Georgia (Fig. 3.4.8a) and by Ardelan et al. (2010) and Planquette et al. (2007) from in situ estimates, dFe scale lengths are variable and dependant on the direction and speed of local circulation. Clearly, it is important to keep in mind that scale length values do not depend on surface circulation only, but can be influenced by all processes that decrease or increase dFe concentrations between the source region and the points where scale lengths are measured (i.e., dilution, biological uptake; Nielsdóttir et al., 2012). Nevertheless, scale length calculations alone cannot discriminate between them.

### Atmospheric and sedimentary sources of iron

In PISCES, dissolved iron is supplied to the ocean from atmospheric dust-deposition and sediment mobilization (Fig. 3.4.3; Aumont and Bopp, 2006). Compared to the reference SEDDUST scenario, model results obtained removing atmospheric sources of iron (SED_NODUST simulation), show that there is a very small reduction (< 1%) in surface iron concentrations over the main phytoplankton bloom area (Fig. 3.4.8c), reflected in a negligible change in surface Chl a concentrations. To the best of our knowledge, in situ measurements of dust-derived iron deposition around South Georgia are presently not available for a comparison with our results. However, similar results were obtained by Meskhidze et al.

(2007): combining model-based fluxes of mineral dust deposition and satellite-based surface Chl a concentrations between March 2000 and January 2004, they observed that the sole deposition of dust from the Patagonian desert, considered the major source of dust deposited to the Atlantic Ocean (Johnson et al., 2010), does not provide the major input of iron to the South Georgia region.

The limited effect of dust-deposition on the iron budget and hence also on phytoplankton growth downstream of South Georgia suggested by our study and by Meskhidze et al. (2007) mostly likely resides on the fact that local circulation provides a continuous supply of sedimentary iron that can maintain high dFe concentrations throughout the productive season. In these conditions, any additional input of iron, unless particularly conspicuous, will have negligible effects on existing dFe concentrations. Conversely, outside the area influenced by any sedimentary input of iron from the island, surface background dFe concentrations are very low (< 0.1 nM) and any additional input of iron, including from dust deposition, can modify initial concentrations and stimulate phytoplankton growth. Similar conditions may explain the isolated patches of Chl a rich waters observed outside the main South Georgia bloom area (Fig. 3.4.6a). The importance of aeolian deposition of iron in regions that are land-remote and upstream sedimentary sources is in agreement with previous observations or modelling results for larger scale or global studies (Tagliabue et al., 2009a; Moore and Braucher, 2008). However, as reviewed by Mahowald et al. (2005) there are still many uncertainties in the current knowledge of the life cycle of dust particles, from their release into the atmosphere to their deposition on the ocean's surface, as well as on their interaction with the biological compartment (i.e., bacterial, phytoplankton or grazers activity; Baker et al., 2010).

As described in Sect. 4.4 (Figs. 3.4.7b and 3.4.8a), model results are able to capture the main features of dFe concentrations around the island, and suggest that the very shallow sediments provide most of the iron observed around and downstream of the island. Clearly, the absence of tidal forcing as well as the current coarse model resolution and smoothed topography will likely lead to an underestimation of all the fine scale mechanisms that can dilute the highly enriched coastal waters and control the spatial variability of biogeochemical properties around the island (i.e., continental shelf waves, cross-shelf or vertical mixing; Young et al., 2011). The absence of these processes may also explain the relatively homogeneous distribution of dFe concentrations around most of the island (Fig. 3.4.8a), reflected in a similar distribution of Chl a concentrations (Fig. 3.4.6c).

With the current model configuration we cannot discriminate between all potential physical and chemical processes introducing iron around the island. However, considering the characteristic topography, landscape and circulation around South Georgia, we expect the concomitant effect of the processes schematically represented in Fig. 3.4.10. We can distinguish two major categories: processes acting on land or along the coast (i.e., precipitation and run-off) responsible for the input of iron present or deposited on land, and processes acting in the ocean, due to physical, biological or chemical processes occurring in the water-column or at the sediment-water interface.

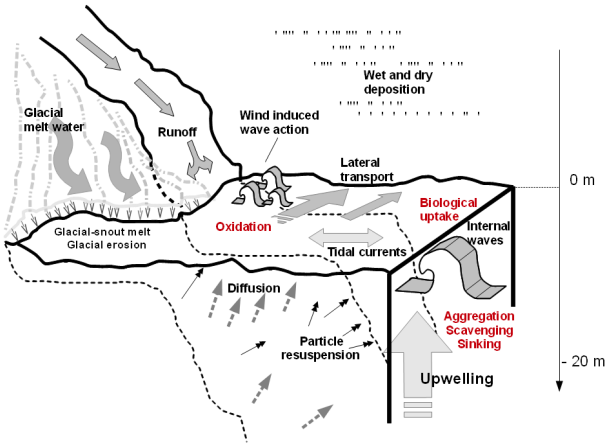


*Fig. 3.4.10. Schematic overview of the potential coastal and shelf processes leading to the surface distribution of dFe observed around South Georgia (i.e., Fig.* 3.4.*8). Processes removing dFe from the water column are indicated in red.*

South Georgia is a mountainous and largely barren island, with an irregular coastline and rugged topography. Most of the island's surface is recurrently or permanently covered by snow and ice; many glaciers terminate at the coast or calve directly into the sea (Gordon et al., 2008). During austral summer, rain, melting snow and glaciers most likely have a double effect on iron input to the ocean: melt-water not only can carry dust particles accumulated during winter, but, together with rain, it can feed local creeks, which hence have a stronger erosion effect on soil. All around the island, fine-sized particles and glacial-flour generate extensive plumes that are clearly visible in Landsat satellite images of South Georgia (see Fig. 3 in Young et al., 2011). Indeed, because many glaciers terminate at the coast or calve into the sea, glacier-scoured debris and glacier calving can determine an additional input of trapped soil particles and/or dust to the ocean (i.e., Raiswell et al., 2008).

In PISCES the sedimentary sources of iron are simulated considering reductive mobilization (Aumont and Bopp, 2006), which has been recognized as a significant source of dFe to the oceans; recent studies (i.e., de Jong et al., 2012; Klunder et al., 2011) suggest that the increase in dFe concentrations observed in measurements closer to the sea-floor most likely derive from reductive mobilization of iron. In particular, below very productive surface waters as those observed around South Georgia, the bacterial oxidation of deposited organic matter accentuates reductive conditions at the sediment surface, consequently reducing the oxygen penetration depth and hence increasing benthic dFe fluxes (Elrod et al., 2004). However, reductive mobilization of iron from the sediments is only one of the mechanisms believed to introduce dFe to the ocean interior. At the sediment-water interface, in fact, the remineralisation of sediments resuspended by bottom or tidal currents (Young et al., 2011; Blain et al., 2008), internal wave's activity (Blain et al., 2008) or wind-induced wave-action (Gargett et al., 2004; de Jong et al., 2012) can introduce additional dFe to the water column.

The total amount of dFe that ultimately leaves the bottom layer towards the surface depends on multiple concomitant factors, including the magnitude of bottom friction resuspending sediment particles, oxygen concentrations in the bottom water, the concentration and type of organic ligands actively stabilizing dissolved iron, or the presence of dFe-scavenging particles settling to the bottom (de Jong et al., 2012; Klunder et al., 2011). Once dissolved iron (in free inorganic or ligand-complexed form) leaves the bottom layer closer to

the sediment-water interface, the combination of diffusion and vertical advection brings dissolved iron to the surface where lateral transport distributes it in the region. Of the three mentioned processes, previous studies in the Southern Ocean (i.e., de Jong et al., 2012; Planquette et al., 2007) agree that lateral advection is the most important and efficient long-distance supplier of dFe (see also Lam et al., 2006). The importance of lateral transport around South Georgia has been suggested by several authors (i.e., Korb et al., 2008) and is evident from our modelling results (Fig. 3.4.8a).

Whitehouse et al. (2008a) and Nielsdóttir et al. (2012) point also to upwelling to the southwest of the island or in relation to eddies. Our sensitivity runs suggest that only a very small part of the total dFe measured at the surface derives from upwelling of deeper iron-rich waters. However, as noted previously, the lack of tidal forcing and the coarse grid resolution used in the modelling experiments presented here will not allow a full representation of vertical processes acting at the meso and sub-mesoscale or in relation to the presence of eddies and tides, better represented by higher resolution models (Naveira Garabato et al., 2002; Young et al., 2011).

At the surface the main mechanisms removing dFe are likely to be biological uptake by phytoplankton and bacteria, scavenging onto sinking biogenic particles (i.e., dead phytoplankton cells), oxidation of dFe and its adsorption to colloids. However, the high surface dFe concentrations measured around South Georgia, which result from the combination of all processes mentioned above, clearly indicate that dFe sources are far more effective than dFe losses. In fact, Borrione and Schlitzer (2013) suggest that the termination of the first peak observed in South Georgia phytoplankton blooms does not strictly depend on dFe availability, but rather it may be caused by insufficient silicate levels, rapidly exhausted by the spring and early summer phytoplankton blooms.

Iron-input mechanisms directly related to local hydrography, like lateral transport or tidal currents, are not expected to change significantly in time (i.e., at the seasonal or decadal scale), especially if they are steered by bottom topography (Borrione and Schlitzer, 2013). Conversely, iron-input mechanisms directly linked to weather or local climate (i.e., air temperature or precipitation) will likely follow a seasonal cycle, and possibly be modified in the future as a response to climate change. For example, during austral summer dust emission from the Patagonian desert and snow and ice-melt are at their maximum levels and hence coincide in timing with the main phytoplankton growing season (Johnson et al., 2010; Young et al., 2011; Borrione and Schlitzer, 2013): during this time of the year the growing and iron-demanding phytoplankton community can count on an additional exogenous source of iron other than the continuous supply of iron from sedimentary sources. An increase in dFe input can be expected at the longer time-scales due to the gradual but progressive increase in ocean and air temperatures which are leading to increased glacier melt (Gordon et al., 2008; Whitehouse et al., 2008b). Previous studies investigating the magnitude of climate-change induced dust emission and deposition from the world's deserts, provide contrasting results, depending on the models and initial scenarios used (Mahowald and Luo, 2003; Tegen et al., 2004). However, considering the stronger effect of sedimentary versus atmospheric sources of iron to the main South Georgia bloom area revealed by the current study, we suggest that

either an increase or decrease in future dust deposition, will have a negligible effect on primary productivity (see also Tagliabue et al., 2008; Aumont et al., 2008).

### Model uncertainties

Comparison of modelled surface dFe concentrations with recently published underway dFe concentrations measured around South Georgia (Figs. 3.4.7a and 3.4.8a) reconfirm the ability of PISCES (here coupled to ROMS_AGRIF) to reproduce the main distribution features of surface dFe, and, to an adequate level also absolute dFe concentrations. Results shown in Fig. 3.4.6 indicate that patterns in simulated and observed surface Chl a concentrations have many similarities because in both datasets location and size of the blooms clearly depend on local circulation, which is also reproduced adequately by **the** model. However, modelled and observed Chl a concentrations are significantly different in their absolute values: modelled Chl a concentrations are lower than those observed in January-February 2008, but also lower than the concentrations recorded during the less productive months of January-February 2011. Significant differences between the two datasets indicate that in the current configuration of PISCES applied to the region around South Georgia, certain biogeochemical processes may not be fully resolved.

The first important difficulty encountered in biogeochemical models applied to the iron-limited Southern Ocean, is the correct representation of the complex iron cycle, necessarily simplified because of the large number of uncertainties and limited number of observations (Aumont and Bopp, 2006). Observations in fact have shown that in seawater, iron is present in various oxidation forms, and that it interacts with several types and size classes of particles and ligands. In the current configuration of PISCES, iron is present in dissolved form and it is assumed to be all bioavailable (as in Moore and Braucher, 2008); moreover, in the model dFe may interact with biogenic particles only. Although recent investigations indicated the ubiquity of inorganic particulate iron, especially downstream of coastal regions (i.e., Lam et al., 2006), but also suggested its bioavailability (i.e., Raiswell et al., 2008), the inorganic form of particulate iron is currently not included in the model, as almost no quantitative information is available to parametrize this source (Aumont and Bopp, 2006). Furthermore, recent studies show that the concentration of ligands, which are responsible for the stabilization and hence prolonged bioavailability of dFe in the water column, is very variable in space, time and depth; in particular, ligands are present at higher concentrations where productivity is high (Hunter and Boyd, 2007; Moore and Braucher, 2008), as would likely be the case over the South Georgia main bloom area. In the model however, there is only one type of ligands, and they are present at constant concentrations throughout the whole water-column. Consequently, an underestimate of the total concentration of bioavailable iron, which is potentially also present in the form of inorganic particulate iron, or complexed to higher concentrations of ligands, may result in the low modelled Chl a concentrations. To date, there are no in situ measurements around South Georgia that could help better ascertain the role of particulate iron in the region, including its bioavailability and transport scale lengths. These measurements are fundamental to confirm or reject our hypothesis.

The lifetime of iron in the surface layer depends on the interaction between chemical, physical and biological processes removing or reintroducing iron. As mentioned above the presence of ligands is crucial to keep iron dissolved in seawater (Hunter and Boyd, 2007),

while diffusion, as well as lateral and vertical mixing or advection (Fig. 3.4.10) provide the means for iron supply from more enriched waters. Indeed, also the biological recycling of iron, due to phytoplankton, zooplankton and bacteria, will sensibly increase the lifetime of iron in the surface. Although these processes are represented in the model (Fig. 3.4.3), their relative importance may be affected by uncertainties in the rates of biological iron uptake, chemical processing, and its release into the water-column (Baker et al., 2010).

### 3.4.6 Conclusions

Natural input of iron around South Georgia, was investigated using the coupled physical-biogeochemical model ROMS_AGRIF-PISCES, implemented for the first time to a region of the Southern Ocean. The model captures the main features of circulation and primary productivity around the island, providing new evidence for the South Georgia island mass effect. In particular, the model can reproduce surface dFe distributions previously described with few discrete in situ measurements around South Georgia, and hence presents a large scale, yet detailed view of iron distribution, scale lengths and principal transport pathways around the island. To date this information was absent, and can now offer a useful tool to biogeochemists investigating the occurrence of phytoplankton blooms in the region but can also provide a base line for future in situ investigations. Clearly, some important questions remain open. Although the model captures adequately the overall distribution and magnitude of dFe distribution in the region as well as the main spatial patterns of phytoplankton blooms, modelled Chl a concentrations are significantly lower than in observations. This evident discrepancy may suggest that the total amount of iron bioavailable to phytoplankton, includes but is not limited to dissolved iron, and that recycling processes may be more efficient than currently simulated. Both aspects need to be verified by future investigations. In the mean time, as the model used in this study has proven its ability to simulate the South Georgia island mass effect in HNLC waters, additional model sensitivity tests could be performed in the future to estimate which levels of bioavailable iron are necessary to stimulate the particularly intense annual phytoplankton blooms observed downstream of South Georgia.

### Acknowledgements

J. Deshayes, T. Gorgues, Y. Jose, C. Klaas, E. Machu, M. Menzel, P. Penven, R. Timmermann and C. Völker are acknowledged for valuable discussions and help during the implementation of the models in a new study region. The Deutsches Klimarechenzentrum (DKRZ) hosting the model code is also thanked for their technical support. This work is part of Ph.D. research by I. Borrione, supported by the Earth System Science Research School at the Alfred-Wegener-Institut, Helmholtz-Zentrum für Polar- und Meeresforschung and the EU FP7 project CARBOCHANGE under grant agreement no. 264879. The PhD studentship grant to M.C. Nielsdóttir by the University of Southampton, the National Oceanography Centre, Southampton and by the Antarctic Funding Initiative under the Collaborative Gearing Scheme (CGS8/27 and CGS9/34) is also acknowledged. In particular, we acknowledge the late Gökay Karakaş, to whom this scientific contribution is dedicated.

## *3.5 Sensitivity of iron and Chl a concentrations in the South Georgia region to increased iron fluxes around the island*


### Abstract

Modelling experiments performed around South Georgia with the coupled hydrodynamic-biogeochemical model ROMS_AGRIF-PISCES have demonstrated its ability to simulate adequately the distribution and magnitude of in situ dissolved iron (dFe) concentrations. Although modelled surface chlorophyll a (Chl a) concentrations reflected in many ways spatial patterns observed in satellite ocean colour imagery, absolute Chl a values were underestimated by a factor of 2 to 4. A sensitivity run with increased iron fluxes around the island was performed to understand its effects on iron availability and hence primary productivity downstream of South Georgia. In the sensitivity run dFe concentrations rose significantly above available observations (i.e., RMS 2.7 nM, mean difference -1.3 nM), however overall Chl a concentrations remained below observations by a factor of 2. Chl a and dFe spatial patterns were not significantly modified by increased dFe concentrations around the island confirming the important role played by surface circulation in controlling Chl a and dFe distributions around the island. Results from this pilot study suggest that in the current model configuration increased iron enrichment alone cannot generate the very high Chl a concentrations observed downstream of the island, possibly because in the model the efficiency of processes removing iron from the water-column, increase with increasing iron concentrations.


### 3.5.1 Introduction

The island of South Georgia (37°W, 55°S) is associated to one of the largest phytoplankton blooms in the open Southern Ocean. During austral summer, Chl a concentrations are often higher than 5 mg $m^{-3}$ and occupy an area that is typically 145 000 $km^2$ (Korb et al., 2004; Borrione and Schlitzer, 2013; see also Fig. 3.5.1). In several years Chl a rich plumes extend eastwards for more than 2700 km along the main path of the Polar Front (Korb et al., 2004). Pigment biomass concentrations to the north, i.e., downstream, of the island are in sharp contrast with the surrounding high-nutrient low-chlorophyll (HNLC) conditions where very low iron concentrations limit primary productivity to Chl a concentrations below 0.5 mg $m^{-3}$ (Moore and Abbott, 2002). High primary productivity around the island has evident implications on the surrounding ecosystem, which hosts large colonies of marine and land based predators and sustains an important commercial fishery (Atkinson et al., 2001). Moreover, primary productivity around South Georgia leads to one of strongest seasonal atmospheric-carbon uptake in the open Southern Ocean (Jones et al., 2012).

The environmental conditions behind South Georgia's very high primary productivity are still investigated. Earlier studies suggested that a continuous supply of iron from the island's shelf is possibly one of the most important drivers (Nielsdóttir et al., 2012; Korb et al., 2008).

This initial hypothesis could be verified with biogeochemical modelling in the region (Borrione et al., 2013, Section 3.4). In the latter study, modelled dFe concentrations were in good agreement with in situ measurements during January and Feburary 2008 (Nielsdóttir et al., 2012). The model was also able to capture the main spatial patterns of Chl a concentrations, however absolute values were significantly lower than in observations. The pilot study presented here was tailored to addresses this specific discrepancy and test the sensitivity of modelled dFe and Chl a concentrations downstream of South Georgia to increased iron fluxes around the island.

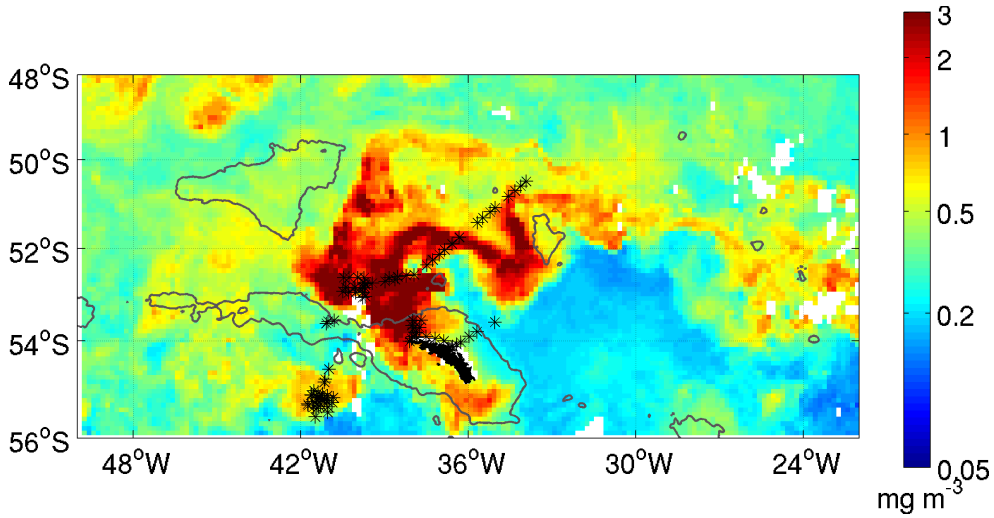


*Fig. 3.5.1. Surface Chl a concentrations in the South Georgia area as obtained from MODIS ocean colour estimates for January-February 2008. Black stars indicate the locations of dFe measurements used in this study (from Nielsdóttir et al., 2012). The 2000 m bathymetry is indicated with thin grey lines.*

### 3.5.2 Models and model configuration

The coupled hydrodynamic-biogeochemical model ROMS_AGRIF-PISCES and the observational datasets used for the comparison of our results (i.e., in situ dFe concentration and surface Chl a concentrations) are identical to those described in detail by Borrione et al., 2013 (Section 3.4). In the following we only report the most important features of the models used, as well as the configurations used here.

ROMS (Shchepetkin and McWilliams, 2005), is a three-dimensional, free-surface regional ocean model with coastline and terrain-following vertical and horizontal coordinates. The version of ROMS which makes use of the Adaptive Grid Refinement in Fortran (AGRIF) procedure, (i.e., ROMS_AGRIF; Debreu and Blayo, 2008; Penven et al., 2006) has been coupled to the 24-compartment biogeochemical model PISCES (Aumont and Bopp, 2006). PISCES, which includes two phytoplankton (nanophytoplankton and diatoms) and zooplankton (micro- and meso-zooplankotn) groups, as well as a detritus compartment with big and small particles, simulates the cycles of the main macronutrients limiting phytoplankton growth (i.e., silicate, phosphate, nitrate) but also iron, which is believed to control HNLC conditions in most of the Southern Ocean. In PISCES, the two sources of dissolved iron (dFe) to the ocean are dust deposition, estimated from the annual dataset of

Tegen and Fung (1995), and reductive mobilisation from the sediments. DFe in its free-inorganic and ligand-complexed form can be removed from the water column by biological uptake, but can also undergo scavenging onto sinking biogenic particles. In the water-column iron is recycled by phytoplankton and zooplankton. In the horizontal dimension the model's resolution is set to 1/6° (~11 km), while in the vertical dimension there are 32 sigma-layers stretched to increase resolution at the surface. Boundary and initial conditions as well as forcing fields are identical to those described in Section 3.4, and are summarized in the Table 3.5.1.

*Table 3.5.1: Datasets used in the model for the boundary and initial conditions, as well as for surface forcing*

| **Dataset** | **Data reference / source** | **Variables** | **Utilization in the model as** |
|---|---|---|---|
| COADS | Da Silva et al., 1994 | Heat and fresh water fluxes | Surface forcing |
| SODA | Carton and Giese., 2008 | Temperature, salinity, circulation (u, v), sea surface height | Boundary and initial conditions |
| PATHFINDER | Casey and Cornillon, 1999 | Sea surface temperature | Surface temperature restoring |
| WOA | Conkright et al., 2005 | Phosphate, silicate, nitrate, iron | Boundary and initial conditions |
| ORCA2 | Aumot and Bopp, 2006 | Phytoplankton, zooplankton | Boundary and initial conditions |
| Dust deposition | Tegen and Fung, 1995 | Iron content in dust | Surface forcing |
| QuikSCAT winds | http://www.ifremer.fr/opendap/cerdap1/cersat/wind/l4/quikscat | Wind fields | Surface forcing |

After 27 years of model spin-up, during which iron sources were identical to those described above, the model was ran for three additional years with two different configurations. In the first simulation, hereafter called SEDDUST, iron sources in the last three modelling years were identical to those utilized during spin-up. In the second simulation, hereafter called SED500_DUST, the total amount of iron released around the island was increased by introducing a virtual flux of dFe from each grid cell in the water column (i.e., near bottom to surface) and located between the coast and the 500 m bathymetry contour. The maximum flux of iron released from each grid cell is 1 μmol dFe $m^{-2}$ $day^{-1}$. In the following, all modelling results are from January and February of the last modelling year.

The objective of this set up was to increase dFe concentrations around the island to levels that were much higher than those obtained in the SEDDUST simulation. In this experiment the model is used as a testing environment, without claiming to reproduce real conditions. Nevertheless, vertical mixing due to tides or mesoscale processes (both not reproduced in the

current configuration of the model), could increase resuspension of sediments and hence iron concentrations around the island (Blain et al., 2008).

### 3.5.3 Observational dataset

Surface Chl a concentration estimates for January and February 2008 were obtained from Aqua MODIS (Moderate Resolution Imaging Spectroradiometer) Standard Mapped Images - Level 3 products. Data are available at a spatial resolution of 9 km from the Distributed Active Archive Center (http://oceancolor.gsfc.nasa.gov/).

Surface circulation patterns for January and February 2008 in the South Georgia area were obtained from the Aviso (http://www.aviso.oceanobs.com/duacs/) zonal and meridional components of surface current velocities, as derived from altimetry.

Underway surface dFe measurements around South Georgia are from the period between 23 January and 10 February of 2008 and were obtained from Nielsdóttir et al. (2012). Sampling locations of dFe measurements are shown in Fig. 3.5.1 together with contemporaneous satellite-derived Chl a concentrations.

### 3.5.4 Results and considerations

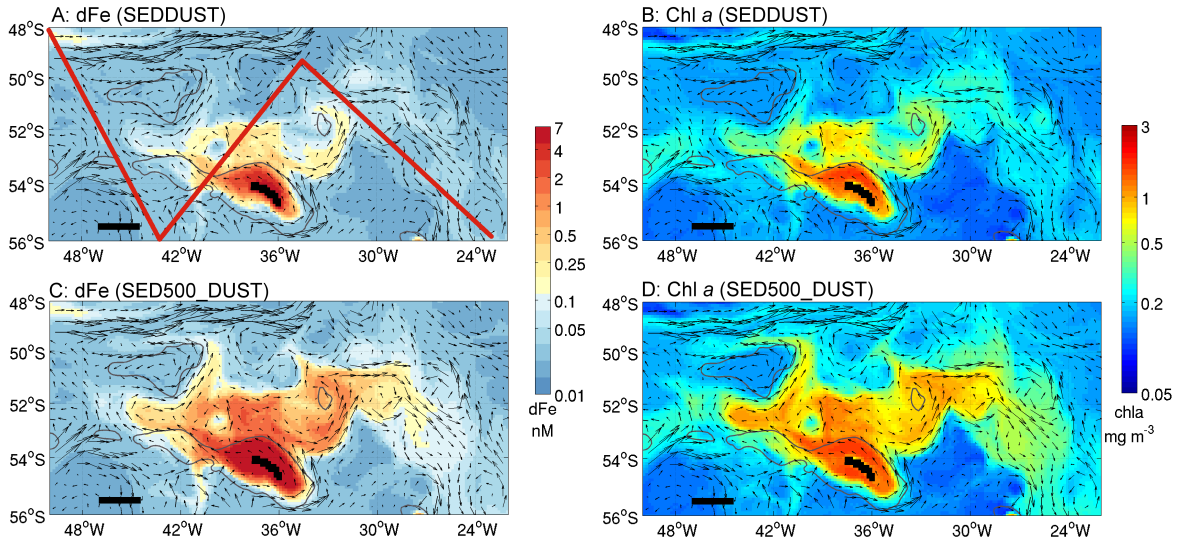


*Fig. 3.5.2. Simulated surface (0-30 m) dFe (left panels) and Chl a (right panels) concentrations for January-February of the last modelling year with the SEDDUST and SED500_DUST scenarios (top and bottom row, respectively). In all cases, black arrows represent the contemporaneous modelled surface circulation. The horizontal bar indicates 1 m $s^{-1}$ and corresponds to approximately 160 km.*

As one would expect, in the SED500_DUST simulation the increased flux of dFe around the island is reflected in dFe concentrations that are higher than those obtained in the SEDDUST simulation (Figs. 3.5.2 a-c). Along the island's coast dFe concentrations are more than twice those obtained in the SEDDUST simulation (i.e, 7.8 nM vs. 3.7 nM), while north of South Georgia and due east of the island dFe concentrations are 1-2 nM and 0.1-1 nM

respectively, and hence approximately two orders of magnitude higher than in the SEDDUST simulation.

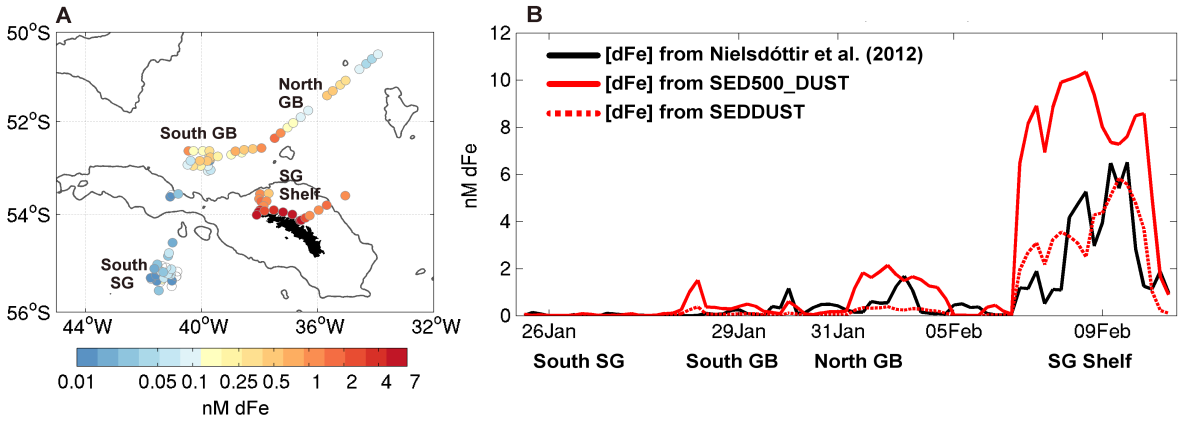


*Fig. 3.5.3. (A) location and concentrations of dFe underway measurements from January and February of 2008 (Nielsdóttir et al., 2012). B) Underway measurements of dFe (black line) and simulated surface dFe concentrations from the SED500_DUST (solid red line) and the SEDDUST (dashed red line) simulations; model values were interpolated onto the dFe sampling locations shown in panel A. For reference, the x-axis indicates dates of in situ dFe sampling. The main geographical areas are also indicated, and correspond to those marked in panel A.*

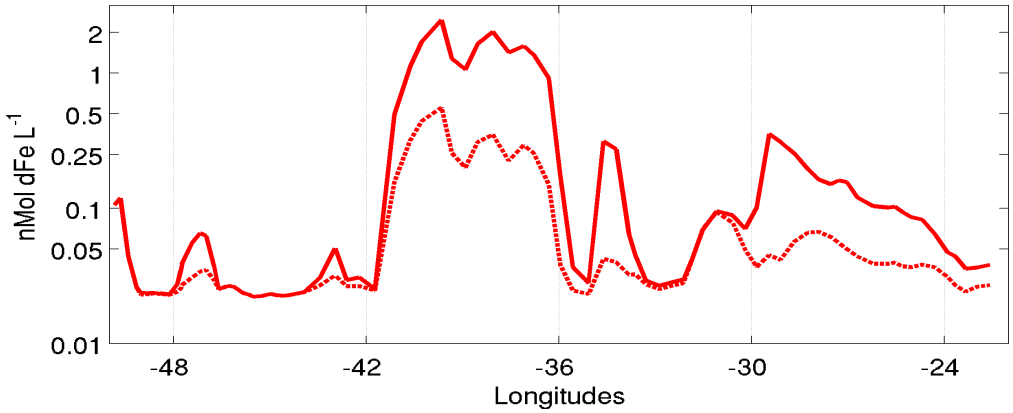


*Fig. 3.5.4: dFe concentrations extracted from the SEDDUST (dashed line) and SED500_DUST (solid line) along the transect traced in Fig. 3.5.2a. Note how very different initial dFe concentrations around 30°W (i.e., 0.5 and 0.05 nM in the SED500_DUST and SEDDUST scenarios respectively), drop to very similar values around 25°W (0.02-0.03 nM).*

Fig. 3.5.3b allows a more detailed comparison between dFe concentrations obtained from the two simulations (red lines), but also with the few available in situ dFe measurements around South Georgia (coloured dots in Fig. 3.5.3a, and black line in Fig. 3.5.b). As stated above, largest differences between the two runs are found along the island's coast and shelf region. In the same areas, dFe concentrations from the SED500_DUST simulation are well above observations, however, modeled dFe values from the Georgia Basin (regions indicated with North GB and South GB in Fig. 3.5.3) appear to better reproduce the spatial variability indicated by observations and in both cases dFe concentrations increase locally to 1-2 nM.

Observing higher dFe concentrations in the SED_DUST500 than in the SEDDUST scenario, one would also expect much larger and far-reaching iron plumes. This is not the case: as shown in Figs. 3.5.2a and c, as well as in Fig. 3.5.4, which displays dFe concentrations obtained from the two scenarios and extracted along a defined transect (red line in Fig. 3.5.2a), east of ~ 25°W dFe concentration drop to very similar values. This preliminary result suggests that in the two simulations along the way processes removing dFe from the water column may be acting differently, possibly more efficiently in the SED500_DUST scenario, as dFe decrease very rapidly to low values. Similar conclusions are drawn by comparing scale lengths for iron transport.

The scale length (Johnson et al., 1997) provides a way to quantify the decrease of iron with distance independently from all processes acting to increase or decrease surface dFe concentrations. The scale length of dFe transport is defined as the distance over which an initial reference concentration (RC) drops to 1/e*RC. Here RC is equal to the average coastal dFe concentration in the two simulations, i.e., 3.68 nM and 7.8 nM, in the SEDDUST and SED500_DUST respectively. In the panels of Fig. 3.5.4 the dFe scale length corresponds to the distance between the coast and the thick contour lines, which are traced along 1/e*RC.

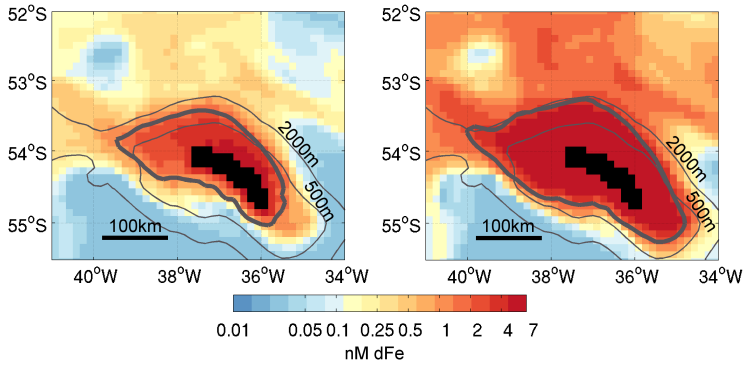


*Fig. 3.5.5. dFe concentrations from the SEDDUST scenario (A) and the SED500_DUST scenario (B) In both panels the thick contour line is traced along 1/e*RC (see text for more details) to define scale lengths. Thin lines mark the 500m and 2000m bathymetry contour.*

Despite the fact that coastal dFe concentrations in the SED500_DUST are approximately twice those in the SEDDUST simulation, scale length values do not increase proportionally. It must be remarked, however, that scale lengths in Fig. 3.5.5 could also be overestimated considering that in the SED500_DUST scenario dFe is released from bottom sediments but also from grid points located in the water column surrounding the island. In the SEDDUST simulation, instead, iron was introduced to the water-column from bottom sediments only. Therefore using the current model configurations a one-to-one comparison of length scale must be considered with care.

Variations in surface dFe concentrations (Fig. 3.5.2a and c) are reflected in similar variations of the contemporaneous surface Chl a concentrations (Fig. 3.5.2b and d). With respect to the SEDDUST scenario, Chl a values in SED500_DUST are generally higher, yet maintaining very similar spatial patterns. Largest magnitude variations are obtained over the

Georgia Basin where Chl a concentrations are twice those obtained with the SEDDUST scenario. Along the coast, instead, differences between the two scenarios are negligible, likely because in both simulations dFe are well above the requirements for maximum phytoplankton growth. In neither case, however, Chl a concentrations reach values that are comparable to observations (i.e., Fig 3.5.1).

Despite very different iron enrichment scenarios, comparable length scale values and dFe plume shapes and sizes suggest that in the model the strength of all processes removing iron from the surface layer may be increasing with initial iron concentrations, hence rapidly removing it from the water column and hence reducing the effect of increased dFe fluxes around the island on surface Chl a.

Indeed, results presented here are very preliminary. The chosen model setup in fact is not optimal to understand the sensitivity of iron concentrations in the South Georgia region to increased iron fluxes around the island. Nevertheless, these results may prove to be useful in future studies, as they show that by only increasing the input of iron from the region surrounding the island, iron plumes are not necessarily larger (and more intense), nor they travel significantly farther from the island. In the model in fact, several concomitant processes, other than input mechanisms and circulation, control dFe concentrations in the water column. Among these are dFe scavenging onto sinking and aggregating particles, complexation with ligands, biological uptake, and remineralization (Aumont and Bopp, 2006; See also Fig. 3.4.3). Therefore, future model experiments aimed at understanding the sensitivity of iron (and Chl a concentrations) to increased iron fluxes around South Georgia, will need to concentrate on the parameters controlling the iron cycle in the ocean, and not necessarily the magnitude of iron enrichment.

# 4 Conclusions and future perspectives

A multi-disciplinary approach integrating in situ and satellite observations with results from hydrodynamic-biogeochemical modelling was utilized to investigate spatial and temporal patterns in primary productivity around South Georgia, a sub-Antarctic island of the western Atlantic sector of the Southern Ocean. This integrated approach has provided the means for an insightful description of hydrography, biogeochemistry and primary productivity. Their interconnections could also be identified.

Using the pixel count algorithm, developed to identify recurrent phytoplankton blooms in 13 years (1997-2010) of satellite ocean colour images, we could define the South Georgia typical bloom area. In this study phytoplankton blooms were defined as regions where Chl a concentrations were $\geq 0.75$ mg $^{-3}$. Comparison with contemporaneous satellite altimetry has shown that the shape, size and location of the typical bloom area are strongly controlled by local circulation, which here closely follows bottom topography. The typical bloom area is new to research in the region, and can be a useful reference for future studies. In fact, the South Georgia typical bloom area marks the boundaries between two very different biogeochemical environments: in-bloom waters (i.e., high-nutrient high-chlorophyll) and out-bloom waters (i.e., high-nutrient low-chlorophyll). Future studies could take advantage of the regularity and hence predictability of this system. For example, in situ investigations could compare a set of multidisciplinary variables (i.e., macro and micro-nutrients, biology, carbon chemistry) in and out of the bloom.

The 13 year long time series of Chl a concentrations from the typical bloom area has indicated pronounced inter-annual variability in the magnitude and timing of blooms, which we could explain, at least in part, using contemporaneous satellite derived surface circulation patterns, sea surface temperature and light availability. Moreover, the same time series did not show any significant decadal temporal trend. The latter is a rather comforting result, considering that recent studies have documented rapid environmental changes during the past few decades. Indeed, 13 years of observations could be insufficient to resolve climate-change-driven trends in Chl a concentrations. According to Henson et al., 2010, due to the large inter-annual variability observed in the ocean colour data, as well as reduced spatio-temporal coverage, at least 20 years of observations would be necessary to identify an effect of climate change. Therefore, it would be interesting in the future to extend the current time series with new data, in order to verify (or not) these results or to increase the level of confidence of our conclusions. Encouraging, however, is the fact that very recent ocean colour imagery from the region (i.e., January 2013 in Fig. 4.1) confirm the observations made using data from 1997-2010.

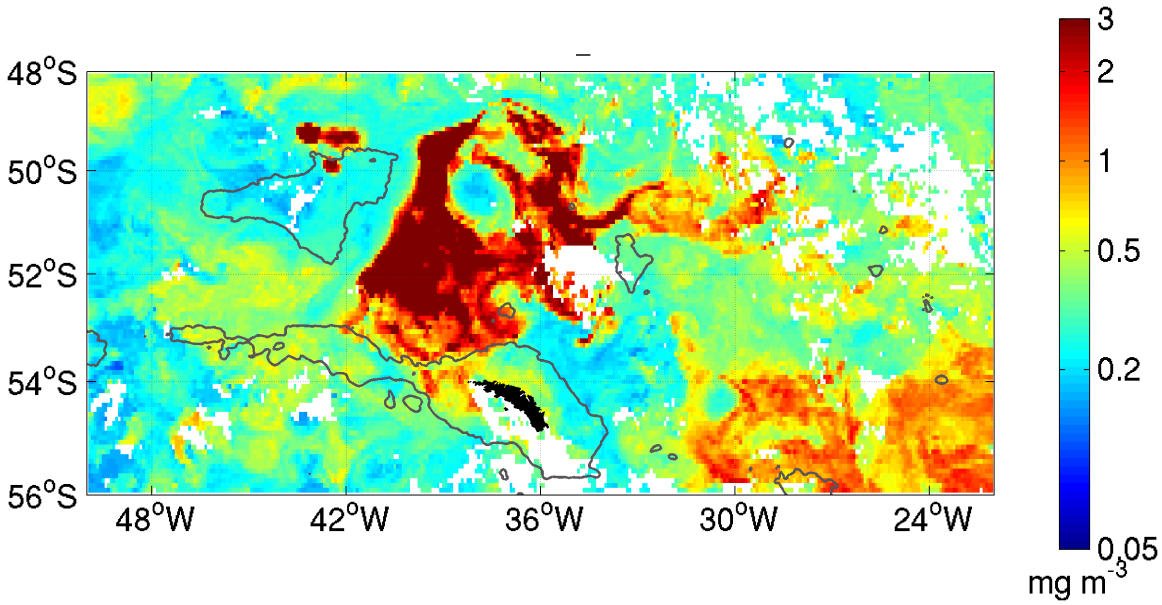


*Fig. 4.1 Surface Chl a concentrations in the South Georgia area as obtained from MODIS ocean colour estimates for January 2013.*

Over the typical bloom area phytoplankton blooms followed an unexpected bi-modal annual cycle with a first peak in Chl a concentrations in late austral spring (i.e., November-December) followed by a second peak during late austral summer and early fall (i.e., February-April). Our results suggest that the annual cycle of Chl a concentrations is modulated by the availability of silicate. Bi-modal annual blooms are likely to have important repercussions on the (eco)system. In fact, one would expect that enhanced productivity just before the onset of austral winter would provide an additional food resource to the ecosystem but also generate a second pulse in atmospheric $CO_2$ drawdown. Both hypothesis could also be interesting topics for future research.

To date only very few regional studies have reported bi-modal bloom patterns in the open Southern Ocean. Indeed, it would be interesting to repeat the analysis applied successfully to South Georgia, to other regions where seasonal blooms are observed regularly (i.e., in coastal regions, or other sub-Antarctic island mass effects). The combination of results could provide a more complete picture of the seasonality of phytoplankton blooms in the Southern Ocean, but also provide further details to our understanding of the factors controlling them. A ROMS_AGRIF-PISCES simulation conducted at a very early stage of the project has shown that the model is able to mimic a bi-modal pattern in annual Chl a concentrations. With the current model set-up however, it is not possible to investigate in detail the mechanisms leading to double peaks. Future work could pick up this issue with a modified model configuration and additional simulations.

After implementing the ROMS_AGRIF-PISCES coupled model to the South Georgia region, results from selected simulations were used to investigate sources of iron and its transport pathways in the region, complementing the still very limited number of in situ iron

measurements around South Georgia (Holeton et al., 2005; Nielsdóttir et al., 2012). Model results indicated that most of the iron measured in the main bloom area originates from the coast and the very shallow shelf-sediments surrounding the island (depths < 20m) while dust deposition plays a minor role, with almost no effects on surface Chl a concentrations. The large iron rich plume simulated to the north of the island, roughly matches the typical bloom area obtained from the analysis of satellite ocean colour images.

Among all processes likely playing an important role in regulating the amount of iron released around the island we highlighted run-off and tidal mixing. These processes however, are not explicitly represented in the current configuration of the model, and could thus be integrated in future simulations, together with an increased horizontal resolution (better than 1/6° used here). The new model configurations could thus improve the effects of finer scale physical processes, not well represented in this study, and that could increase vertical and horizontal mixing (i.e., eddies, mesoscale features or cross-shelf transport mechanisms). The AGRIF refinement technique (Debreu and Blayo, 2008; Penven et al., 2006) could also be tested to selectively increase resolution along the island's shelf region, while keeping unchanged the coarser resolution in the rest of the domain, hence optimizing the available computing resources. Higher resolution around the island would certainly improve the representation of topography, which at the current 1/6° resolution cannot capture the rugged and fiord-like coastline. An improved representation of topography, and the presence of finer scale physical processes, will surely provide a new point of view on the cycle of iron around South Georgia.

To conclude: the collection of results presented in this thesis has clearly shown that the South Georgia ecosystem is regulated by complex interactions between hydrography, biogeochemistry, primary and secondary productivity. The possibility of integrating multidisciplinary datasets from very different sources has proven to be a powerful tool to study a remote region of the Southern Ocean, allowing to overcome some of the weaknesses of each dataset taken alone. Modelling experiments presented here are the first of their kind for the South Georgia region. Hopefully they have paved the way towards new directions of research, and stimulated many more ideas for future research than those proposed here.

# 5 Annex



## A non-diatom plankton bloom controlled by copepod grazing and amphipod predation: Preliminary results from the LOHAFEX iron-fertilisation experiment

Maria Grazia Mazzocchi[1], Humberto E. González[2], Pieter Vandromme[3], Inès Borrione[4], Maurizio Ribera d'Alcalà[1], Mangesh Gauns[5], Philipp Assmy[4,6], Bernhard Fuchs[7], Christine Klaas[4], Patrick Martin[8], Marina Montresor[1], Nagappa Ramaiah[5], Wajih Naqvi[5], Victor Smetacek[4]

[1]Stazione Zoologica Anton Dohrn, Naples, Italy (grazia@szn.it)
[2]Universidad Austral de Chile, Institute of Marine Biology, Valdivia, and COPAS Center of Oceanography, Concepción, Chile
[3]Université Paris 06, UMR 7093, LOV, Observatoire océanologique, Villefranche-sur-mer, France
[4]Alfred Wegener Institute for Polar and Marine Research, Bremerhaven, Germany
[5]National Institute of Oceanography, Goa, India
[6]Bremen International Graduate School for Marine Sciences, University of Bremen, Bremen, Germany
[7]Max Planck Institute for Marine Microbiology, Bremen, Germany
[8]National Oceanography Centre, Southampton, UK

The most memorable LOHAFEX cruise came to an end on 17 March 2009 when RV *Polarstern* docked in the harbour of Punta Arenas (southern Chile) after successfully carrying out the longest iron fertilisation experiment so far (39 days). The two and a half month voyage, spent in the notorious Roaring Forties of the south-western Atlantic, was as close to an adventure as a research cruise can get these days. We first had to weather a totally unexpected political storm while we were selecting a suitable meso-scale eddy in which to conduct the experiment. Permission to go ahead with fertilisation came just as we had satisfied ourselves that we were indeed right in the centre of the selected eddy. After spreading 10 tonnes of dissolved ferrous sulphate over a patch of 150 km², we followed, with excitement, the chemical and biological changes stimulated by iron fertilisation while chasing the patch circling within the eddy (Fig. 1). Some weeks later, to our chagrin, the eddy started collapsing and ejected our patch, which, nevertheless, miraculously "waited" for two weeks, squeezed between other eddies, until our day of departure.

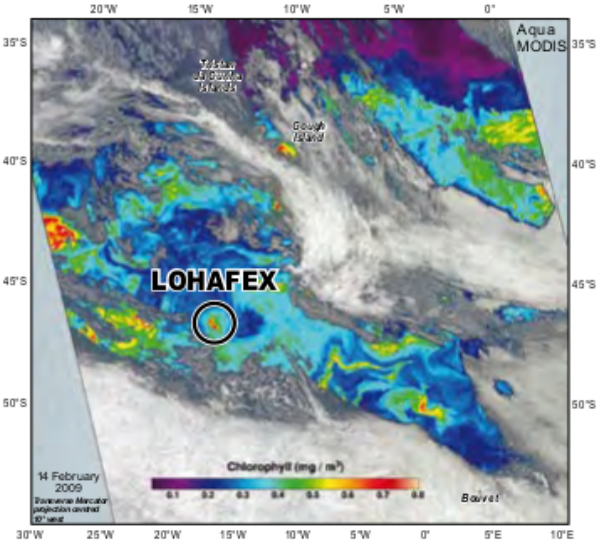


*Figure 1. Chlorophyll a satellite picture of the LOHAFEX bloom from the NASA website (http://oceancolor.gsfc.nasa.gov/cgi/image_archive.cgi).*

*Figure 2. Participants of the LOHAFEX cruise onboard the R/V Polarstern (photograph courtesy of T. Bresinsky).*

We also witnessed the spectacular collapse of a stately iceberg (from a safe distance) and were rocked to near-panic by a series of freak waves during our farewell party. In short, it was an exceptionally stimulating and emotionally rewarding experience.

The joint Indo-German venture LOHAFEX (Loha is the Hindi word for iron), for which preparations started in 2005, was targeted for the productive south-western sector of the Antarctic Circumpolar Current (ACC) where we expected to fertilise a different type of plankton community to those of the severely iron-limited ACC studied by the previous five experiments. LOHAFEX was carried out by an interdisciplinary group of 48 scientists (29 Indian, 10 German and nine from five other countries; Fig. 2): the physicists selected the eddy, pin-pointed its centre (based on altimeter images, drift trajectories of two surface buoys, and an Acoustic Doppler Current Profiler survey) and kept track of the patch while the chemists and biologists followed the processes within it and compared them with outside waters.

In contrast to the rest of the ACC, silicic acid in the south-western Atlantic is depleted by summer also well south of the polar front, clearly due to the extensive spring diatom blooms that occur there and are conspicuous in satellite images of chlorophyll distribution. The sources of iron fuelling these blooms are varied:

contact with landmasses and islands, Patagonian dust and the many icebergs characteristic of this region. The core water of the eddy in which we carried out the experiment had evidently experienced such a bloom because silicon concentrations were at limiting levels down to 100 m depth, so further growth of diatoms was not possible. In a previous experiment (European Iron Fertilization Experiment: EIFEX) conducted at the same latitude and season but in silicon-rich water 1,000 km further east, a massive diatom bloom developed and reached 3 mg Chl $m^{-3}$ within three weeks. Despite consistently high levels of primary production (~1.5 g C $m^{-2}$ $d^{-1}$), biomass accumulation stopped thereafter due to sequential fall-out of some early-response diatom species which was compensated by population growth of others that responded later. But the situation in the LOHAFEX bloom was different.

The phytoplankton community of mixed flagellates responded rapidly to the iron addition by increasing, as expected, Fv/Fm ratios (a measure of photosynthetic efficiency) above 0.4 and chlorophyll concentrations in the 60 m mixed layer doubled to 1.5 mg Chl $m^{-3}$ within two weeks but stopped increasing thereafter, although rates of primary production remained high (> 1.0 g C $m^{-2}$ $d^{-1}$). A second fertilisation three weeks later had no apparent effect indicating that the community was arrested in steady state despite abundant nutrients and sufficient light. However, there were changes in the composition of the phytoplankton that were not as easy to follow on board as in the case of large diatoms. The bulk of the biomass was contributed by small flagellates < 5 µm with the smallest size fraction (~2 µm) increasing towards the end of the experiment to densities measured by flow cytometer and corroborated with counts made with an inverted microscope as high as >15 x $10^6$ cells $L^{-1}$. A significant fraction of the larger flagellates (~5 µm) were *Phaeocystis* solitary cells that started making numerous colonies in the second week, so we were expecting a *Phaeocystis* bloom to develop (Fig. 3). Dense blooms of balloon-like colonies of this alga are commonplace around the continent, however, the colonies disappeared by the third week. Although the community was dominated by pico- and nanophytoplankton it was functioning differently to the bacteria-based microbial "loop" which is the paradigm for planktonic recycling systems.

There was no evidence, as in the case of the EIFEX diatom bloom, that the lack of biomass accumulation was due to a balance between new growth and sinking out of older cells. Low to moderate sinking fluxes with no difference between inside and outside the patch were indicated by transmissometer profiles, thorium measurements, catches of neutrally buoyant sediment traps and vertical particle profiles recorded with the Underwater Video Profiler, version 5 (UVP5; a camera system mounted on the CTD which records particles down to 0.06 mm diameter from the surface to 3,000 m depth). So the excess biomass due to iron fertilisation must have been retained in the surface layer but not as phytoplankton cells.

The relatively high ammonia levels in the surface layer compared to outside waters were indicative of higher remineralisation rates but these could not have been due to bacteria because their numbers were well below the average reported from the region and their growth rates were moderate. Besides, there was no significant difference between the bacterial communities inside and outside the patch. Why they were suppressed in the entire region and not revived, as in other experiments, by iron addition is a mystery in itself begging an explanation. The only processes of bacterial and phytoplankton cell removal left are grazing by proto- and metazooplankton respectively, or death and disintegration by viral attack as has been demonstrated for bacteria and flagellates. At this stage we can only speculate on the possible role of viruses, but there is a strong case for copepod grazing being the structuring factor in the LOHAFEX bloom.

Luckily for us, the structure of the grazer community was unusually simple: the stocks of flagellate-grazing protozooplankton (ciliates and dinoflagellates) were much lower than during EIFEX, apparently controlled by heavy copepod grazing pressure, as there was an abundant food supply. Copepods were dominated by one representative each of the large (*Calanus simillimus*), medium (*Ctenocalanus citer*) and small (*Oithona similis*) size groups. The other copepods common in the ACC (*Rhincalanus*, *Pleuromamma*) were also present but in low numbers. In the integrated 0-100 m water column, the highest abundances estimated, from preliminary counts conducted onboard, ranged from 199 x $10^3$ ind. $m^{-2}$ for *Oithona* spp. to 90 x $10^3$ ind. $m^{-2}$ for *C. simillimus*, and 31 x $10^3$ ind. $m^{-2}$ for *C. citer*, all recorded at in-patch stations within the 20th day after fertilisation.

*Figure 3. Small* Phaeocystis *colonies on* Corethron pennatum *spines (photograph courtesy of M. Montresor).*

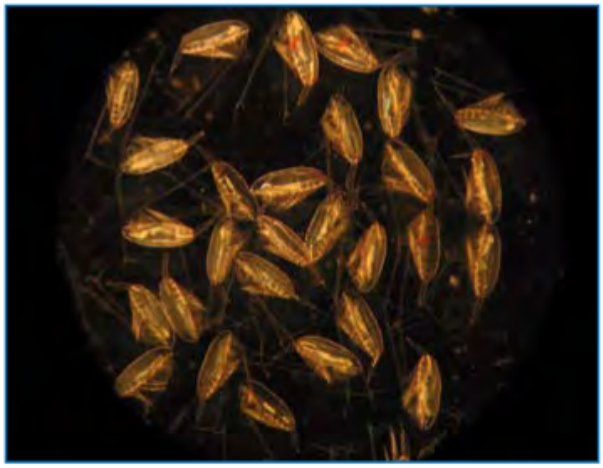

*Figure 4.* Calanus simillimus *copepodites (photograph courtesy of M.G. Mazzocchi).*

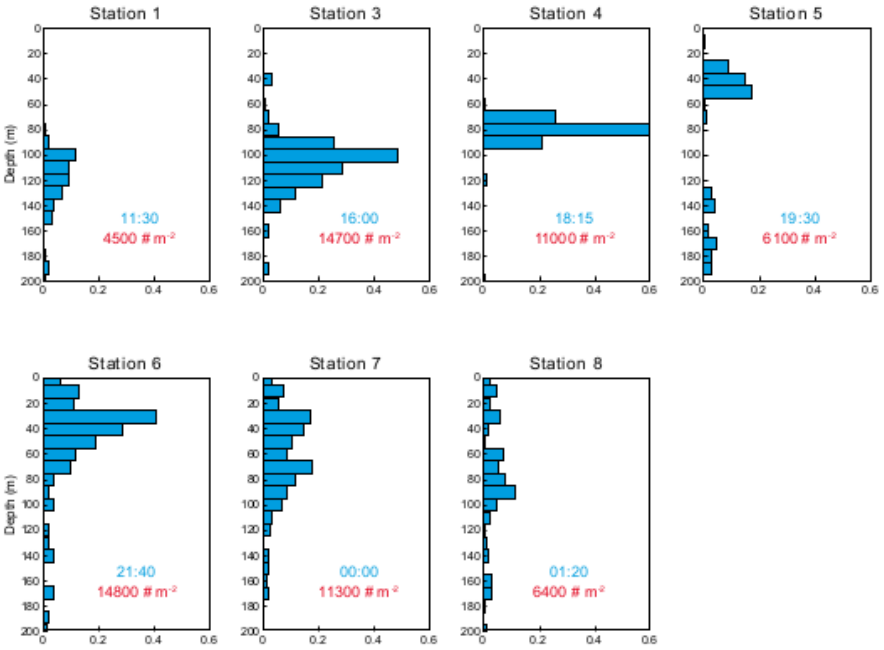


*Figure 5. Copepod vertical distribution (N ind. L$^{-1}$) measured at 10 m vertical resolution step with the Underwater Video Profiler 5 along a south-north transect through the patch. The first (Station 1) and last two stations (Stations 7 and 8) were outside the fertilised patch. Data are unavailable for Station 2. The ship time (UTC-1) is given in blue and the integrated number of copepods per m$^2$ for the first 200 m is shown in red.*

Clearly, *C. simillimus*, consisting almost entirely of late juvenile stages (CIV–CV copepodites) with large lipid sacs, overwhelmingly dominated copepod biomass (Fig. 4). Apparently, this population had developed during the previous bloom as there were very few adult females still present. The UVP5 images (Fig. 5) indicated that the bulk of the population was concentrated around 100 m depth during the day and dispersed within the 60 m mixed surface layer at night where they left behind large numbers of faecal pellets. There was a distinct decline over the course of the experiment in numbers and diversity of plankton collected by a 20 µm mesh net routinely examined on board. As many of the missing species were found in copepod pellets, particularly tintinnid loricae, diatom frustules, cell walls of a common, large dinoflagellate (*Ceratium pentagonum*), foraminifera shells, it is most likely that heavy grazing pressure exerted by the copepods was responsible. The shift to the smallest phytoplankton size class, in the veritable absence of ciliates, could also be attributed to "size escape" from copepod grazing pressure.

Since the *C. simillimus* population was not growing in numbers, the food was presumably being converted into lipid reserves by this deep diapausing species. Because lipids are hydrocarbons, the essential elements, including iron, were being recycled back to the phytoplankton. The necessary calculations will only be possible after all the samples from the various depth ranges sampled with the two multinets deployed at all major stations as well as the samples from grazing experiments have been processed. Due to marked spatial patchiness, reflected in wide variation in integrated standing stocks at both in- and out-stations, we cannot yet say whether copepod numbers were higher inside the patch due to congregation from the surroundings. However, the copepods inside the patch were eating more as indicated by the faecal pellet production rates expressed as volume of faecal pellets egested, which were about double inside as compared to outside the fertilised patch (67 and 39 x 10$^6$ µm$^3$ ind.$^{-1}$ d$^{-1}$, respectively) (Fig. 6). This could well have accounted for the fate of the extra biomass inside the patch because the community structures inside and outside, in contrast to diatom-dominated blooms, were essentially similar in all respects.

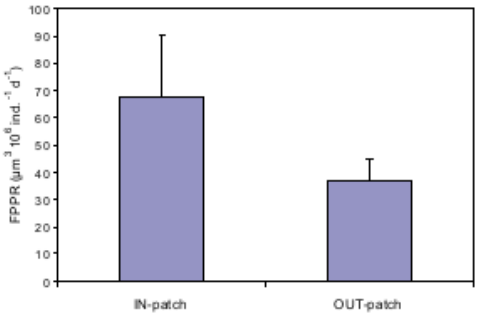


*Figure 6. Faecal pellet production rate (as volume, µm$^3$ x 10$^6$ ind.$^{-1}$ d$^{-1}$) in* Calanus simillimus *averaged at the stations inside the fertilised patch (days 4–36 after fertilisation) and outside the patch (days 16–35).*

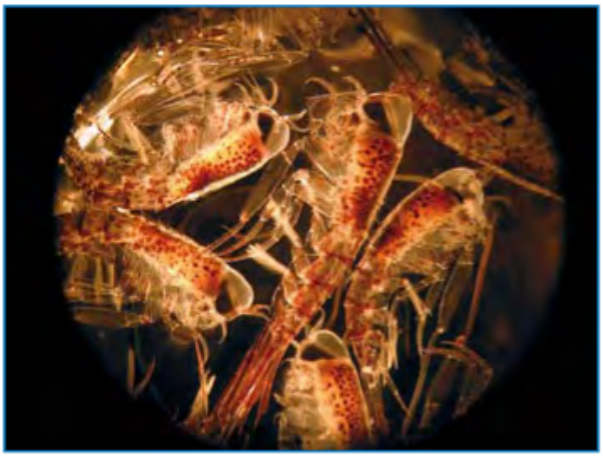

*Figure 7.* Themisto gaudichaudii *(photograph courtesy of H.E. González).*

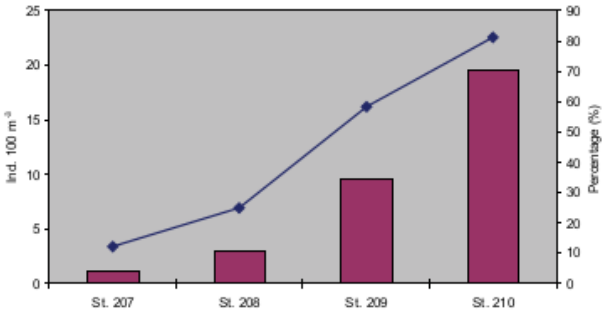


*Figure 8. Abundance of* Themisto gaudichaudii *(columns) and its percentage contribution (line) to macrozooplankton abundance in rectangular mid-water trawl samples along a transect.*

Macrozooplankton was dominated by the swarm-forming, hyperiid amphipod *Themisto gaudichaudii*, an active, aggressive, indiscriminate carnivore which attacks organisms much larger than itself with its formidable clawed appendages (Fig. 7). Its high densities in the region were the most likely reason why other large zooplankton, including euphausiids but in particular chaetognaths and salps, which thrive on copepods and small flagellates respectively, were present in relatively small numbers. The integrated average abundance of *Themisto gaudichaudi* in the upper 100 m water column (17 night catches with the rectangular midwater trawl) was two-fold higher inside (24 ind. 100 $m^{-3}$) than outside the patch (12 ind. 100 $m^{-3}$). This was confirmed by a transect of four trawls conducted from outside to inside the patch at the end of the experiment (Fig. 8). What attracted swarms of this species to the patch is not clear at this stage. As it is practically the only visual predator in this region, the strong diurnal migrations and remarkable transparency of its potential prey, in particular salps, can be attributed to selection by this predator. The impact of predation by *Themisto* on the copepods will be evaluated from the results of feeding experiments.

Surprisingly little is known about the biology and quantitative distribution of this interesting predator which is known to be the dominant zooplanktivore in productive regions of the northern ACC, extending northward along the Patagonian shelf in the southwest Atlantic. It seems to at least partially fill the niche occupied by small swarming fish almost everywhere else further north and is the major conduit from plankton to vertebrates and cephalopods, analogous to the role played by the much better known Antarctic krill (*Euphausia superba*) to the south of its range. Indeed *Themisto* has been called "krill of the north" and is reported to be the main food of the squid *Ilex argentinus* which is the target of the intense squid fishery along the Patagonian shelf break, prominent in satellite images of the world by night, because lights are used to attract squid. So why does only this region shine like an inhabited coastline in the night and why is there nothing similar in other parts of the ocean? Is it a bottom-up condition, driven by local hydrography mixing nutrient- with iron-rich waters along the shelf edge, or does the unique biology of *Themisto* hold the key to the explanation? Would long-term, larger-scale iron fertilisation in the ACC duplicate the processes along the Argentinean shelf edge?

A major conclusion from LOHAFEX is that, despite high growth rates, biomass of non-diatom phytoplankton can be kept in check by grazing pressure of oceanic copepods which can establish a recycling system analogous to, but different from, the classic microbial food web. The fact that copepods increased their feeding rates inside the patch indicates that they were food-limited in the surrounding waters. As a result, biomass accumulation was modest as was vertical flux of organic carbon, hence net uptake of atmospheric $CO_2$ by the fertilised phytoplankton was only marginally different to the unfertilised, surrounding water. This result conforms with observations that massive phytoplankton blooms in the ocean are almost exclusively due to diatoms (coccolithophorid blooms are prominent in satellite images but usually contain much less biomass than the spring and upwelling diatom blooms) and highlights a fundamental difference between oceanic and coastal waters where many non-diatom phytoplankton species (such as *Phaeocystis* and *Ceratium*) contribute to dense blooms. Presumably the larger zooplankton stocks on a square metre basis in oceanic as compared to coastal waters can exert top-down control on the structure of the ecosystem and, in the absence of silicon, prevent uptake of nutrients to limiting concentrations.

The main interest in iron fertilisation experiments has focused on the biological carbon pump because of its implications for sequestration of atmospheric $CO_2$. LOHAFEX has shown that an adequate supply of silicic acid is a prerequisite for significant, deep carbon sequestration, thereby restricting the region of the Southern Ocean where significant amounts of carbon dioxide can be sequestered from the atmosphere. Of course, we cannot say what happened to the system in the surface layer after the *C. simillimus* population departed for diapausing, how much carbon they took down with them and how much was retained in the deep ocean by predation at depth. Certainly, the C:N ratio of diapausing copepods will differ considerably from sinking diatom aggregates. Further experiments will yield new insights on physical, chemical and biological processes that govern the functioning of planktonic ecosystems. These fundamental control mechanisms can only be studied under *in situ* conditions as it is impossible to simulate natural grazing pressure under laboratory or mesocosm conditions. More open ocean perturbation experiments, analogous to the whole-lake experiments carried out by limnologists, are called for to study the impact of zooplankton grazing pressure in different regions and seasons on phytoplankton biomass and composition, hence ultimately the global carbon cycle.

**Acknowledgements**

The costs of the experiment were equally shared by the CSIR, India and the Helmholtz Foundation, Germany. We are deeply grateful to the LOHAFEX task team at the AWI, particularly Ulrich Bathmann, who skilfully countered the attack against us and to Nick Owens of BAS, Cambridge, UK and Doug Wallace and Ulf Riebesell of the Leibniz Institute of Marine Sciences, Kiel, Germany for taking on the onerous task of evaluating the LOHAFEX risk assessment in double-quick time. Our special thanks to the captain and crew of RV *Polarstern* for looking after us so well and all our colleagues for making LOHAFEX such a rewarding and successful cruise.

# 6 Bibliography


Achterberg, E. P., Holland, T. W., Bowie, A. R., Mantoura, R. F. C., and Worsfold, P. J.: Determination of iron in seawater, Anal. Chim. Acta, 442, 1-14, doi: 10.1016/S0003-2670(01)01091-1, 2001.

Allison, L. C., Johnson, H. L., Marshall, D. P., and Munday, D. R.: Where do winds drive the Antarctic Circumpolar Current?, Geophys. Res. Lett., 37, L12605, doi: 10.1029/2010gl043355, 2010.

Antonov, J. I., Seidov D., Boyer T. P. , Locarnini R. A., Mishonov A. V. , Garcia H. E., Baranova O. K., Zweng M. M., and Johnson D. R.. World Ocean Atlas 2009, Volume 2: Salinity. S. Levitus, Ed. NOAA Atlas NESDIS 69, U.S. Government Printing Office, Washington, D.C., 184 pp. 2010

Ardelan, M. V., Holm-Hansen, O., Hewes, C. D., Reiss, C. S., Silva, N. S., Dulaiova, H., Steinnes, E., and Sakshaug, E.: Natural iron enrichment around the Antarctic Peninsula in the Southern Ocean, Biogeosciences, 7, 11–25, doi:10.5194/bg-7-11-2010, 2010.

Arrigo, K. R., Robinson, D. H., Worthen, D. L., Dunbar, R. B., DiTullio, G. R., VanWoert, M., and Lizotte, M. P.: Phytoplankton Community Structure and the Drawdown of Nutrients and CO2 in the Southern Ocean, Science, 283, 365–367, doi:10.1126/science.283.5400.365, 1999.

Arrigo, K. R., and van Dijken, G. L.: Phytoplankton dynamics within 37 antarctic coastal polynya systems, J. Geophys. Res., 108, 3271, doi: 10.1029/2002jc001739, 2003.

Arrigo, K. R., van Dijken, G. L., and Bushinsky, S.: Primary production in the Southern Ocean, 1997-2006, J. Geophys. Res., 113, C08004, doi:10.1029/2007jc004551, 2008.

Atkinson, A., Siegel, V., Pakhomov, E. A., Rothery, P., Loeb, V., Ross, R. M., Quetin, L. B., Schmidt, K., Fretwell, P., Murphy, E. J., Tarling, G. A., and Fleming, A. H.: Oceanic circumpolar habitats of antarctic krill, Mar. Ecol. - Prog. Ser., 362, 1-23, doi:10.3354/meps07498, 2008.

Atkinson, A., Whitehouse, M. J., Priddle, J., Cripps, G. C., Ward, P., and Brandon, M. A.: South Georgia, Antarctica: a productive, cold water, pelagic ecosystem, Mar. Ecol.-Prog. Ser., 216, 279–308, doi:10.3354/meps216279, 2001.

Aumont, O., and Bopp, L.: Globalizing results from ocean in situ iron fertilization studies, Global Biogeochem. Cy., 20, GB2017, doi: 10.1029/2005GB002591, 2006.

Aumont, O., Bopp, L., and Schulz, M.: What does temporal variability in aeolian dust deposition contribute to sea-surface iron and chlorophyll distributions?, Geophys. Res. Lett., 35, L07607, doi: 10.1029/2007gl031131, 2008.

Aumont, O., Maier-Reimer, E., Blain, S., and Monfray, P.: An ecosystem model of the global ocean including Fe, Si, P colimitations, Global Biogeochem. Cy., 17, 1060, doi: 10.1029/2001GB001745, 2003.

Baker, A. R., and Croot, P. L.: Atmospheric and marine controls on aerosol iron solubility in seawater, Mar. Chem., 120, 4-13, doi: 10.1016/j.marchem.2008.09.003, 2010.

Bakker, D. C. E., Nielsdóttir, M. C., Morris, P. J., Venables, H. J.,and Watson, A. J.: The island mass effect and biological carbon uptake for the subantarctic Crozet Archipelago, Deep-Sea Res. Pt. II, 54, 2174–2190, doi:10.1016/j.dsr2.2007.06.009, 2007.

Bailleul, F. D. R., Charrassin, J.-B. T., Monestiez, P., Roquet, F., Biuw, M., and Guinet, C.: Successful foraging zones of southern elephant seals from the Kerguelen Islands in relation to oceanographic conditions, Philos. T. R. Soc. A., 362, 2169-2181, doi: 10.1098/rstb.2007.2109, 2007.

Beckmann, A., and Haidvogel, D. B.: Numerical Simulation of Flow around a Tall Isolated Seamount. Part I: Problem Formulation and Model Accuracy, J. Phys. Oceanogr., 23, 1736-1753, doi: 10.1175/1520-0485(1993)023<1736:NSOFAA>2.0.CO;2, 1993.

Benitez-Nelson, C. R., Vink, S. M., Carrillo, J. H., and Huebert, B. J.: Volcanically influenced iron and aluminum cloud water deposition to hawaii, Atmos. Environ, 535–544, 2003.

Blain, S., Queguiner, B., Armand, L., Belviso, S., Bombled, B., Bopp, L., Bowie, A., Brunet, C., Brussaard, C., Carlotti, F., Christaki, U., Corbiere, A., Durand, I., Ebersbach, F., Fuda, J.-L., Garcia, N., Gerringa, L., Griffiths, B., Guigue, C., Guillerm, C., Jacquet, S., Jeandel, C., Laan, P., Lefevre, D., Lo Monaco, C., Malits, A., Mosseri, J., Obernosterer, I., Park, Y.-H., Picheral, M., Pondaven, P., Remenyi, T., Sandroni, V., Sarthou, G., Savoye, N., Scouarnec, L., Souhaut, M., Thuiller, D., Timmermans, K., Trull, T., Uitz, J., van Beek, P., Veldhuis, M., Vincent, D., Viollier, E., Vong, L., and Wagener, T.: Effect of natural iron fertilization on carbon sequestration in the southern ocean, Nature, 446, 1070-1074, 10.1038/nature05700, 2007.

Blain, S., Sarthou, G., and Laan, P.: Distribution of dissolved iron during the natural iron-fertilization experiment KEOPS (Kerguelen Plateau, Southern Ocean), Deep-Sea Res. Pt. II, 55, 594–605, doi:10.1016/j.dsr2.2007.12.028, 2008.

Blain, S., Treguer, P., Belviso, S., Bucciarelli, E., Denis, M., Desabre, S., Fiala, M., Jézéque, V. M., Fevre, J. L., Mayzaud, P., Marty, J.-C., and Razouls, S.: A biogeochemical study of the island mass effect in the context of the iron hypothesis: Kerguelen Islands, Southern Ocean, Deep-Sea Res. Pt. I, 48, 163-187, 2001.

Boehlert, G. W., Watson, W., and Sun, L. C.: Horizontal and vertical distributions of larval fishes around an isolated oceanic island in the tropical pacific, Deep-Sea Res. A, 39, 439-466, doi: 10.1016/0198-0149(92)90082-5, 1992.

Boehme, L., Meredith, M. P., Thorpe, S. E., Biuw, M., and Fedak, M.: Antarctic Circumpolar Current frontal system in the South Atlantic: Monitoring using merged Argo and animal-borne sensor data, J. Geophys. Res., 113, C09012, doi:10.1029/2007jc004647, 2008.

Boning, C. W., Dispert, A., Visbeck, M., Rintoul, S. R., and Schwarzkopf, F. U.: The response of the Antarctic Circumpolar Current to recent climate change, Nature Geosci, 1, 864-869, 2008.

Borrione I., Aumont O., Nielsdóttir M. and Schlitzer R.: Sedimentary and atmospheric sources of iron around South Georgia, Southern Ocean: a modeling perspective, Biogeosciences Discuss., 10, 10811-10858, doi:10.5194/bgd-10-10811-2013, 2013.

Borrione, I., and Schlitzer, R.: Distribution and recurrence of phytoplankton blooms around South Georgia, Southern Ocean, Biogeosciences, 10, 217-231, doi: 10.5194/bg-10-217-2013, 2013.

Boutin, J. and Merlivat, L.: New in situ estimates of carbon biological production rates in the Southern Ocean from CARIOCA drifter measurements, Geophys. Res. Lett., 36, L13608, doi:10.1029/2009gl038307, 2009.

Bowie, A. R., Achterberg, E. P., Croot, P. L., de Baar, H. J. W., Laan, P., Moffett, J. W., Ussher, S., and Worsfold, P. J.: A community-wide intercomparison exercise for the determination of dissolved iron in seawater, Mar. Chem., 98, 81-99, doi: 10.1016/j.marchem.2005.07.002, 2006.

Boyd, P. W., Jickells, T., Law, C. S., Blain, S., Boyle, E. A., Buesseler, K. O., Coale, K. H., Cullen, J. J., de Baar, H. J. W., Follows, M., Harvey, M., Lancelot, C., Levasseur, M., Owens, N. P. J., Pollard, R., Rivkin, R. B., Sarmiento, J., Schoemann, V., Smetacek, V., Takeda, S., Tsuda, A., Turner, S., and Watson, A. J.: Mesoscale Iron Enrichment Experiments 1993– 2005: Synthesis and Future Directions, Science, 315, 612–617, doi:10.1126/science.1131669, 2007.

Boyd, P. W., Law, C. S., Wong, C. S., Nojiri, Y., Tsuda, A., Levasseur, M., Takeda, S., Rivkin, R., Harrison, P. J., Strzepek, R., Gower, J., McKay, R. M., Abraham, E., Arychuk, M., Barwell-Clarke, J., Crawford, W., Crawford, D., Hale, M., Harada, K., Johnson, K., Kiyosawa, H., Kudo, I., Marchetti, A., Miller, W., Needoba, J., Nishioka, J., Ogawa, H., Page, J., Robert, M., Saito, H., Sastri, A., Sherry, N., Soutar, T., Sutherland, N., Taira, Y., Whitney, F., Wong, S.-K. E., and Yoshimura, T.: The decline and fate of an iron-induced subarctic phytoplankton bloom, Nature, 428, 549-553, 2004.

Boyer, T. P., Antonov, J. I., Baranova, O. K., Garcia, H. E., Johnso, D. R., Locarnini, R. A., Mishonov, A. V., O'Brien, T. D., Seidov, D., Smolyar, I. V., and M. M. Zweng, DVDs.: World Ocean Database 2009, edited by: Levitus, S., NOAA Atlas NESDIS 66, US Gov. Printing Office,Washington, DC, 216 pp., DVDs, 2009.

Brand, L. E., Sunda, W. G., and Guillard, R. R. L.: Limitation of marine-phytoplankton reproductive rates by zinc, manganese, and iron, Limnol. Oceanogr., 28, 1182–1198, 1983.

Breitbarth, E., Achterberg, E. P., Ardelan, M. V., Baker, A. R., Bucciarelli, E., Chever, F., Croot, P. L., Duggen, S., Gledhill, M., Hassellöv, M., Hassler, C., Hoffmann, L. J., Hunter, K. A., Hutchins, D. A., Ingri, J., Jickells, T., Lohan, M. C., Nielsdóttir, M. C., Sarthou, G., Schoemann, V., Trapp, J. M., Turner, D. R., and Ye, Y.: Iron biogeochemistry across marine systems - progress from the past decade, Biogeosciences, 7, 1075-1097, doi: 10.5194/bg-7-1075-2010, 2010.

Bucciarelli, E., Blain, S., and Tréguer, P.: Iron and manganese in the wake of the Kerguelen Islands (Southern Ocean), Mar. Chem., 73, 21-36, doi: 10.1016/S0304-4203(00)00070-0, 2001.

Buesseler, K. O., Andrews, J. E., Pike, S. M., and Charette, M. A.: The effects of iron fertilization on carbon sequestration in the southern ocean, Science, 304, 414-417, doi: 10.1126/science.1086895, 2004.

Buesseler, K. O., Doney, S. C., Karl, D. M., Boyd, P. W., Caldeira, K., Chai, F., Coale, K. H., de Baar, H. J. W., Falkowski, P. G., Johnson, K. S., Lampitt, R. S., Michaels, A. F., Naqvi, S. W. A., Smetacek, V., Takeda, S., and Watson, A. J.: Ocean Iron Fertilization--Moving Forward in a Sea of Uncertainty, Science, 319, 162-, doi: 10.1126/science.1154305, 2008.

Carton, J. A., and Giese, B. S.: A Reanalysis of Ocean Climate Using Simple Ocean Data Assimilation (SODA), Monthly Weather Review, 136, 2999-3017, doi: 10.1175/2007mwr1978.1, 2008.

Casey, K. S., and Cornillon, P.: A Comparison of Satellite and In Situ-Based Sea Surface Temperature Climatologies, J. Climate, 12, 1848-1863, doi: 10.1175/1520-0442(1999)012<1848:acosai>2.0.co;2, 1999.

Cassar, N., Bender, M. L., Barnett, B. A., Fan, S., Moxim, W. J., Levy, H., II, and Tilbrook, B.: The southern ocean biological response to aeolian iron deposition, Science, 317, 1067-1070, 10.1126/science.1144602, 2007.

Charette, M. A., Gille, S. T., Sanders, R. J., and Zhou, M.: Southern ocean natural iron fertilization, Deep Sea Research Part II: Topical Studies in Oceanography, 90, 1-3, doi: 10.1016/j.dsr2.2013.04.014, 2013.

Chelton, D. B., deSzoeke, R. A., Schlax, M. G., El Naggar, K., and Siwertz, N.: Geographical variability of the first baroclinic rossby radius of deformation, J. Phys. Oceanogr., 28, 433-460, doi: 10.1175/1520-0485(1998)028<0433:gvotfb>2.0.co;2, 1998.

Chever, F., Sarthou, G., Bucciarelli, E., Blain, S., and Bowie, A. R.: An iron budget during the natural iron fertilisation experiment KEOPS (Kerguelen Islands, Southern Ocean), Biogeosciences, 7, 455–468, doi:10.5194/bg-7-455-2010, 2010.

Clarke, A., Meredith, M. P., Wallace, M. I., Brandon, M. A., and Thomas, D. N.: Seasonal and interannual variability in temperature, chlorophyll and macronutrients in northern Marguerite Bay, Antarctica, Deep Sea Res. Pt. II, 55, 1988-2006, doi: 10.1016/j.dsr2.2008.04.035, 2008.

Coale, K. H., Johnson, K. S., Fitzwater, S. E., Gordon, R. M., Tanner, S., Chavez, F. P., Ferioli, L., Sakamoto, C., Rogers, P., Millero, F., Steinberg, P., Nightingale, P., Cooper, D., Cochlan, W. P., Landry, M. R., Constantinou, J., Rollwagen, G., Trasvina, A., and Kudela, R.: A massive phytoplankton bloom induced by an ecosystem-scale iron fertilization experiment in the equatorial Pacific Ocean, Nature, 383, 495-501, 1996.

Comiso, J. C., McClain, C. R., Sullivan, C. W., Ryan, J. P., and Leonard, C. L.: Coastal Zone Color Scanner Pigment Concentrations in the Southern Ocean and Relationships to Geophysical Surface Features, J. Geophys. Res., 98, 2419–2451, doi:10.1029/92jc02505, 1993.

Conkright, M. E., Locarnini, R. A., Garcia, H. E., O'Brien, T. D., Boyer, T. P., Stephens, C., and Antonov, J. I.: World Ocean Atlas 2001: Objective Analyses, Data Statistics, and Figures, CD-ROM Documentation National Oceanographic Data Center, Silver Spring, MD, 17 pp., 2002.

Da Silva, A.M., Young, C.C., Levitus, S.: Atlas of surface marine data 1994, Vol. 1, algorithms and procedures, NOAA Atlas NESDIS 6, U. S. Department of Commerce, NOAA, NESDIS, USA, 74 pp., 1994.

Deacon, G.E.R., 1933. A general account of the hydrology of the South Atlantic Ocean. Discovery Reports 7, 171–238.

Deacon, G.E.R., 1937. The hydrology of the Southern Ocean. Discovery Reports 15, 1–124.

de Baar, H. J. W., and de Jong, J. T. M.: Distributions, sources and sinks of iron in seawater, in: Biogeochemistry of iron in seawater, edited by: Turner, D. a. H., K. A., 7, IUPAC Book Series on Analytical and Physical Chemistry of Environmental Systems, 123–253, 2001.

de Baar, H. J. W., de Jong, J. T. M., Bakker, D. C. E., Loscher, B. M., Veth, C., Bathmann, U., and Smetacek, V.: Importance of iron for plankton blooms and carbon dioxide drawdown in the southern ocean, Nature, 373, 412-415, doi: 10.1038/373412a0, 1995.

Debreu, L., and Blayo, E.: Two-way embedding algorithms: a review, Ocean Dynam., 58, 415-428, doi: 10.1007/s10236-008-0150-9, 2008.

de Jong, J., Schoemann, V., Lannuzel, D., Croot, P., de Baar, H., and Tison, J.-L.: Natural iron fertilization of the Atlantic sector of the Southern Ocean by continental shelf sources of the Antarctic Peninsula, J. Geophys. Res., 117, G01029, doi:10.1029/2011jg001679, 2012.

Dong, S., Sprintall, J., Gille, S. T., and Talley, L.: Southern Ocean mixed-layer depth from Argo float profiles, J. Geophys. Res., 113, C06013, doi:10.1029/2006JC004051, 2008.

Doty, M. S., and Oguri, M.: The island mass effect, J. Cons. Int. Explor. Mer, 22, 33-37, 1956.

Dulaiova, H., Ardelan, M. V., Henderson, P. B., and Charette, M. A.: Shelf-derived iron inputs drive biological productivity in the southern Drake Passage, Global Biogeochem. Cy., 23, GB4014, doi:10.1029/2008gb003406, 2009.

Dunn, J. R., and Ridgway, K. R.: Mapping ocean properties in regions of complex topography, Deep-Sea Res. Pt. I, 49, 591-604, doi: 10.1016/S0967-0637(01)00069-3, 2002.

Elrod, V. A., Berelson, W. M., Coale, K. H., and Johnson, K. S.: The flux of iron from continental shelf sediments: A missing source for global budgets, Geophys. Res. Lett., 31, L12307, doi: 10.1029/2004gl020216, 2004.

Falkowski, P. G., Barber, R. T., and Smetacek, V.: Biogeochemical Controls and Feedbacks on Ocean Primary Production, Science, 281, 200–206, doi:10.1126/science.281.5374.200, 1998.

Fitch, D. T. and Moore, J. K.: Wind speed influence on phytoplankton bloom dynamics in the Southern Ocean Marginal Ice Zone, J. Geophys. Res., 112, C08006, doi:10.1029/2006jc004061, 2007.

Fretwell, P. T., Tate, A. J., Deen, T. J., and Belchier, M.: Compilation of a new bathymetric dataset of South Georgia, Antarct. Sci., 21, 171-174, doi:10.1017/S0954102008001703, 2009.

Garcia, C. A. E., Garcia, V. M. T., and McClain, C. R.: Evaluation of SeaWiFS chlorophyll algorithms in the Southwestern Atlantic and Southern Oceans, Remote Sens. Environ., 95, 125– 137, doi:10.1016/j.rse.2004.12.006, 2005.

Garcia, H. E., Locarnini R. A., Boyer T. P., Antonov J. I., Baranova O. K. , Zweng M. M., and Johnson D. R. World Ocean Atlas 2009, Volume 3: Dissolved Oxygen, Apparent Oxygen Utilization, and Oxygen Saturation. S. Levitus, Ed. NOAA Atlas NESDIS 70, U.S. Government Printing Office, Washington, D.C., 344 pp, 2010a.

Garcia, H. E., Locarnini R. A., Boyer T. P. , Antonov J. I. ,Zweng M. M., Baranova O. K., and Johnson D. R.. World Ocean Atlas 2009, Volume 4: Nutrients (phosphate, nitrate, silicate). S. Levitus, Ed. NOAA Atlas NESDIS 71, U.S. Government Printing Office, Washington, D.C., 398 pp., 2010b.

Gargett, A., Wells, J., Tejada-Martínez, A. E., and Grosch, C. E.: Langmuir Supercells: A Mechanism for Sediment Resuspension and Transport in Shallow Seas, Science, 306, 1925-1928, doi: 10.1126/science.1100849, 2004.

Gassó, S. and Stein, A. F.: Does dust from Patagonia reach the sub-Antarctic Atlantic Ocean?, Geophys. Res. Lett., 34, L01801, doi:10.1029/2006gl027693, 2007.

Gassó, S., Stein, A., Marino, F., Castellano, E., Udisti, R., and Ceratto, J.: A combined observational and modeling approach to study modern dust transport from the Patagonia desert to East Antarctica, Atmos. Chem. Phys., 10, 8287–8303, doi:10.5194/acp-10-8287-2010, 2010.

Gerringa, L. J. A., Blain, S., Laan, P., Sarthou, G., Veldhuis, M. J. W., Brussaard, C. P. D., Viollier, E., and Timmermans, K. R.: Fe-binding dissolved organic ligands near the kerguelen archipelago in

the southern ocean (indian sector), Deep Sea Res. Pt. II, 55, 606-621, doi: 10.1016/j.dsr2.2007.12.007, 2008.

Ginoux, P., Chin, M., Tegen, I., Prospero, J. M., Holben, B., Dubovik, O., and Lin, S.-J.: Sources and distributions of dust aerosols simulated with the GOCART model, J. Geophys. Res.-Atmos., 106, 20255-20273, doi: 10.1029/2000jd000053, 2001.

Gordon, J. E., Haynes, V. M., and Hubbard, A.: Recent glacier changes and climate trends on South Georgia, Global Planet. Change, 60, 72-84, doi: 10.1016/j.gloplacha.2006.07.037, 2008.

Griffies, S. M., Biastoch, A., Böning, C., Bryan, F., Danabasoglu, G., Chassignet, E. P., England, M. H., Gerdes, R., Haak, H., Hallberg, R. W., Hazeleger, W., Jungclaus, J., Large, W. G., Madec, G., Pirani, A., Samuels, B. L., Scheinert, M., Gupta, A. S., Severijns, C. A., Simmons, H. L., Treguier, A. M., Winton, M., Yeager, S., and Yin, J.: Coordinated Ocean-ice Reference Experiments (COREs), Ocean Modelling, 26, 1-46, doi: 10.1016/j.ocemod.2008.08.007, 2009.

Hart T.J.: On the Phytoplankton of the South-West Atlantic and the Bellingshausen Sea, 1929– 1931 Discovery Reports 8, 1-268, 1934

Hasegawa, D., Yamazaki, H., Lueck, R. G., and Seuront, L.: How islands stir and fertilize the upper ocean, Geophys. Res. Lett., 31, L16303, doi: 10.1029/2004gl020143, 2004.

Henson, S. A., Sarmiento, J. L., Dunne, J. P., Bopp, L., Lima, I., Doney, S. C., John, J., and Beaulieu, C.: Detection of anthropogenic climate change in satellite records of ocean chlorophyll and productivity, Biogeosciences, 7, 621-640, doi:10.5194/bg-7-621-2010, 2010.

Heywood, K. J., Barton, E. D., and Simpson, J. H.: The effects of flow disturbance by an oceanic island, J. Mar. Res., 48, 55-73, 1990.

Hewes, C. D., Reiss, C. S., Kahru, M., Mitchell, B. G., and Holm- Hansen, O.: Control of phytoplankton biomass by dilution and mixed layer depth in the western Weddell-Scotia Confluence, Mar. Ecol.-Prog. Ser., 366, 15–19, doi:10.3354/meps07515, 2008.

Hinz, D. J., Nielsd´ottir, M. C., Korb, R. E., Whitehouse, M. J., Poulton, A. J., Moore, C. M., Achterberg, E. P., and Bibby, T. S.: Responses of microplankton community structure to iron addition in the Scotia Sea, Deep-Sea Res. Pt. II, 59–60, 36– 6, doi:10.1016/j.dsr2.2011.08.006, 2012.

Hogg, O. T., Barnes, D. K. A., and Griffiths, H. J.: Highly Diverse, Poorly Studied and Uniquely Threatened by Climate Change: An Assessment of Marine Biodiversity on South Georgia's Continental Shelf, PLoS ONE, 6, e19795, doi:10.1371/journal.pone.0019795, 2011.

Holeton, C., N´ed´elec, F., Sanders, R., Brown, L., Moore, C., Stevens, D., Heywood, K., Statham, P., and Lucas, C.: Physiological state of phytoplankton communities in the Southwest Atlantic sector of the Southern Ocean, as measured by fast repetition rate fluorometry, Polar Biol., 29, 44–52, doi:10.1007/s00300-005-0028-y, 2005.

Holm-Hansen, O., Kahru, M., Hewes, C. D., Kawaguchi, S., Kameda, T., Sushin, V. A., Krasovski, I., Priddle, J., Korb, R., Hewitt, R. P., and Mitchell, B. G.: Temporal and spatial distribution of chlorophyll-a in surface waters of the Scotia Sea as determined by both shipboard measurements and satellite data, Deep- Sea Res. Pt. II, 51, 1323–1331, doi:10.1016/j.dsr2.2004.06.004, 2004.

Hopkinson, B. M., Mitchell, B. G., Reynolds, R. A., Wang, H., Selph, K. E., Measures, C. I., Hewes, C. D., Holm-Hansen, O., and Barbeau, K. A.: Iron Limitation across Chlorophyll Gradients in the

Southern Drake Passage: Phytoplankton Responses to Iron Addition and Photosynthetic Indicators of Iron Stress, Limnol. Oceanogr., 52, 2540–2554, 2007.

Hunter, K.A., Boyd, P.W.: Iron-binding ligands and their role in the ocean biogeochemistry of iron, Environ. Chem. 4, 221-232, doi:10.1071/EN07012, 2007.

Jiang, M., Barbeau, K. A., Selph, K. E., Measures, C. I., Buck, K. N., Azam, F., Mitchell, B. G., and Zhou, M.: The role of organic ligands in iron cycling and primary productivity in the Antarctic Peninsula: A modeling study, Deep-Sea Res. Pt. II, doi: 10.1016/j.dsr2.2013.01.029, 2013.

Jickells, T. D., An, Z. S., Andersen, K. K., Baker, A. R., Bergametti, G., Brooks, N., Cao, J. J., Boyd, P. W., Duce, R. A., Hunter, K. A., Kawahata, H., Kubilay, N., laRoche, J., Liss, P. S., Mahowald, N., Prospero, J. M., Ridgwell, A. J., Tegen, I., and Torres, R.: Global iron connections between desert dust, ocean biogeochemistry, and climate, Science, 308, 67-71, doi: 10.1126/science.1105959, 2005.

Johnson, K. S., Gordon, R. M., and Coale, K. H.: What controls dissolved iron concentrations in the world ocean?, Mar. Chem., 57, 137-161, doi: 10.1016/S0304-4203(97)00043-1, 1997.

Johnson, M. S., Meskhidze, N., Solmon, F., Gassó, S., Chuang, P. Y., Gaiero, D. M., Yantosca, R. M., Wu, S., Wang, Y., and Carouge, C.: Modeling dust and soluble iron deposition to the South Atlantic Ocean, J. Geophys. Res., 115, D15202, doi: 10.1029/2009jd013311, 2010.

Jones, E. M., Bakker, D. C. E., Venables, H. J., and Watson, A. J.: Dynamic seasonal cycling of inorganic carbon downstream of South Georgia, Southern Ocean, Deep-Sea Res. Pt. II, 59-60, 25-35, doi: 10.1016/j.dsr2.2011.08.001, 2012.

Jouandet, M. P., Blain, S., Metzl, N., Brunet, C., Trull, T. W., and Obernosterer, I.: A seasonal carbon budget for a naturally iron-fertilized bloom over the Kerguelen Plateau in the Southern Ocean, Deep-Sea Res. Pt. II, 55, 856–867, doi:10.1016/j.dsr2.2007.12.037, 2008.

Jouandet, M. P., Blain, S., Metzl, N., and Mongin, M.: Interannual variability of net community production and air-sea CO2 flux in a naturally iron fertilized region of the Southern Ocean (Kerguelen Plateau), Antarct. Sci., 23, 589–596, doi:10.1017/S0954102011000411, 2011.

Kahru, M., Mitchell, B. G., Gille, S. T., Hewes, C. D., and Holm-Hansen, O.: Eddies enhance biological production in the Weddell-Scotia Confluence of the Southern Ocean, Geophys. Res. Lett., 34, L14603, doi:10.1029/2007gl030430, 2007.

Karakas, G., Nowald, N., Blaas, M., Marchesiello, P., Frickenhaus, S., Schlitzer, R.: High-resolution modeling of sediment erosion and particle transport across the northwest African shelf, J. Geophys. Res., 111, C06025, doi: 10.1029/2005jc003296, 2006.

Kistler, R., Kalnay E., Collins W., Saha S., White G., Woollen J., Chelliah M., Ebisuzaki W., Kanamitsu M., Kousky V., van den Dool H., Jenne R., andFiorino M.: The NCEP-NCAR 50-Year Reanalysis: Monthly Means CD-ROM and Documentation. Bull. Amer. Meteor. Soc., 82, 247-268, 2001

Klunder, M. B., Laan, P., Middag, R., De Baar, H. J. W., and van Ooijen, J. C.: Dissolved iron in the Southern Ocean (Atlantic sector), Deep-Sea Res. Pt. II, 58, 2678-2694, doi: 10.1016/j.dsr2.2010.10.042, 2011.

Korb, R. E., and Whitehouse, M.: Contrasting primary production regimes around South Georgia, Southern Ocean: large blooms versus high nutrient, low chlorophyll waters, Deep-Sea Res. Pt. I, 51, 721-738, doi: 10.1016/j.dsr.2004.02.006, 2004.

Korb, R. E., Whitehouse, M. J., Atkinson, A., and Thorpe, S. E.: Magnitude and maintenance of the phytoplankton bloom at South Georgia: a naturally iron-replete environment, Mar. Ecol.-Prog. Ser., 368, 75-91, doi: 10.3354/meps07525, 2008.

Korb, R. E., Whitehouse, M. J., and Ward, P.: SeaWiFS in the southern ocean: spatial and temporal variability in phytoplankton biomass around South Georgia, Deep-Sea Res. Pt. II, 51, 99-116, doi: 10.1016/j.dsr2.2003.04.002, 2004.

Korb, R. E., Whitehouse, M. J., Gordon, M., Ward, P., and Poulton, A. J.: Summer microplankton community structure across the Scotia Sea: implications for biological carbon export, Biogeosciences, 7, 343–356, doi:10.5194/bg-7-343-2010, 2010.

Korb, R. E., Whitehouse, M. J., Ward, P., Gordon, M., Venables, H. J., and Poulton, A. J.: Regional and seasonal differences in microplankton biomass, productivity, and structure across the Scotia Sea: Implications for the export of biogenic carbon, Deep-Sea Res. Pt. II, 59–60, 67–77, doi:10.1016/j.dsr2.2011.06.006, 2012.

Lam, P. J., Bishop, J. K. B., Henning, C. C., Marcus, M. A., Waychunas, G. A., and Fung, I. Y.: Wintertime phytoplankton bloom in the subarctic Pacific supported by continental margin iron, Global Biogeochem. Cy., 20, GB1006, doi: 10.1029/2005gb002557, 2006.

Lannuzel, D., Schoemann, V., de Jong, J., Tison, J.-L., and Chou, L.: Distribution and biogeochemical behaviour of iron in the East Antarctic sea ice, Mar. Chem., 106, 18–32, doi:10.1016/j.marchem.2006.06.010, 2007.

Le Quéré, C., Harrison, S. P., Colin Prentice, I., Buitenhuis, E. T., Aumont, O., Bopp, L., Claustre, H., Cotrim Da Cunha, L., Geider, R., Giraud, X., Klaas, C., Kohfeld, K. E., Legendre, L., Manizza, M., Platt, T., Rivkin, R. B., Sathyendranath, S., Uitz, J., Watson, A. J., and Wolf-Gladrow, D.: Ecosystem dynamics based on plankton functional types for global ocean biogeochemistry models, Global Change Biol., 11, 2016-2040, 10.1111/j.1365-2486.2005.1004.x, 2005.

Li, F., Ginoux, P., and Ramaswamy, V.: Distribution, transport, and deposition of mineral dust in the southern ocean and antarctica: Contribution of major sources, J. Geophys. Res., 113, D10207, doi: 10.1029/2007jd009190, 2008.

Lin, H., Rauschenberg, S., Hexel, C. R., Shaw, T. J., and Twining, B. S.: Free-drifting icebergs as sources of iron to the Weddell Sea, Deep-Sea Res. Pt. II, 58, 1392–1406, doi:10.1016/j.dsr2.2010.11.020, 2011.

Locarnini, R. A., Mishonov A. V. , Antonov J. I. , Boyer T. P., Garcia H. E. , Baranova O. K., Zweng M. M., and Johnson D. R. World Ocean Atlas 2009, Volume 1: Temperature. S. Levitus, Ed. NOAA Atlas NESDIS 68, U.S. Government Printing Office, Washington, D.C., 184 pp. 2010.

Loeb, V., Hofmann, E. E., Klinck, J. M., and Holm-Hansen, O.: Hydrographic control of the marine ecosystem in the South Shetland-Elephant Island and Bransfield Strait region, Deep-Sea Res. II, 57, 519-542, 2010.

Lourantou, A. and Metzl, N.: Decadal evolution of carbon sink within a strong bloom area in the subantarctic zone, Geophys. Res. Lett., 38, L23608, doi:10.1029/2011gl049614, 2011.

Lutz, V. A., Segura, V., Dogliotti, A. I., Gagliardini, D. A., Bianchi, A. A., and Balestrini, C. F.: Primary production in the Argentine Sea during spring estimated by field and satellite models, J. Plankton Res., 32, 181–195, doi:10.1093/plankt/fbp117, 2010.

Marinov, I., Gnanadesikan, A., Toggweiler, J. R., and Sarmiento, J. L.: The Southern Ocean biogeochemical divide, Nature, 441, 964-967, doi: 10.1038/nature04883, 2006.

Mahowald, N. M., Baker, A. R., Bergametti, G., Brooks, N., Duce, R. A., Jickells, T. D., Kubilay, N., Prospero, J. M., and Tegen, I.: Atmospheric global dust cycle and iron inputs to the ocean, Global Biogeochem. Cy., 19, GB4025, doi: 10.1029/2004gb002402, 2005.

Mahowald, N. M., and Luo, C.: A less dusty future?, Geophys. Res. Lett., 30, 1903, doi: 10.1029/2003gl017880, 2003.

Martin, J. H.: Glacial-interglacial CO2 change: the iron hypothesis, Paleoceanography, 5, 1-13, 1990a.

Martin, J. H., Fitzwater, S. E., and Gordon, R. M.: Iron deficiency limits phytoplankton growth in antarctic waters, Global Biogeochem. Cy., 4, 5–12, doi:10.1029/GB004i001p00005, 1990b.

Martinez, E., Antoine, D., D'Ortenzio, F., and de Boyer Montégut, C.: Phytoplankton spring and fall blooms in the North Atlantic in the 1980s and 2000s, J. Geophys. Res., 116, C11029, doi:10.1029/2010jc006836, 2011.

Mazzocchi, M. G., Gonzalez, H. E. , Vandromme, P. , Borrione, I. , Ribera d'Alcalà, M. , Gauns, M. , Assmy, P. , Fuchs, B. , Klaas, C. , Martin, P. , Montresor, M. , Ramaiah, N. , Naqvi, W. Smetacek, V.: A non-diatom plankton bloom controlled by copepod grazing and amphipod predation: Preliminary results from the lohafex iron-fertilisation experiment, GLOBEC International Newsletter, 15, 3-6, 2009.

McClain, C. R., Cleave, M. L., Feldman, G. C., Gregg, W. W., Hooker, S. B., and Kuring, N.: Science quality SeaWiFS data for global biosphere research, Sea Technol., 39, 10–16, 1998.

Meredith, M. P., Brandon, M. A., Murphy, E. J., Trathan, P. N., Thorpe, S. E., Bone, D. G., Chernyshkov, P. P., and Sushin, V. A.: Variability in hydrographic conditions to the east and northwest of South Georgia, 1996-2001, J. Marine Syst., 53, 143-167, doi: 10.1016/j.jmarsys.2004.05.005, 2005.

Meredith, M. P., Watkins, J. L., Murphy, E. J., Cunningham, N.J., Wood, A. G., Korb, R., Whitehouse, M. J., Thorpe, S. E., and Vivier, F.: An anticyclonic circulation above the Northwest Georgia Rise, Southern Ocean, Geophys. Res. Lett., 30, 2061, doi:10.1029/2003gl018039, 2003.

Meskhidze, N., Nenes, A., Chameides, W. L., Luo, C., and Mahowald, N.: Atlantic Southern Ocean productivity: Fertilization from above or below?, Global Biogeochem. Cy, 21, GB2006, doi: 10.1029/2006gb002711, 2007.

Middelburg, J. J., Soetaert, K., Herman, P. M. J., and Heip, C. H. R.: Denitrification in marine sediments: A model study, Global Biogeochem. Cy., 10, 661-673, doi: 10.1029/96gb02562, 1996.

Mongin, M., Molina, E., and Trull, T. W.: Seasonality and scale of the Kerguelen plateau phytoplankton bloom: A remote sensing and modeling analysis of the influence of natural iron fertilization in the Southern Ocean, Deep-Sea Res. Pt. II, 55, 880–892, doi:10.1016/j.dsr2.2007.12.039, 2008.

Monterey, G. and Levitus, S.: Seasonal Variability of Mixed Layer Depth for the World Ocean, NOAA Atlas NESDIS 14, US Gov. Printing Office, Washington, DC, 1997.

Moore, J. K. and Abbott, M. R.: Phytoplankton chlorophyll distributions and primary production in the Southern Ocean, J. Geophys. Res., 105, 28709–28722, doi:10.1029/1999jc000043, 2000.

Moore, J. K., Abbott, M. R., and Richman, J. G.: Location and dynamics of the Antarctic Polar Front from satellite sea surface temperature data, J. Geophys. Res., 104, 3059–3073, doi:10.1029/1998jc900032, 1999.

Moore, J. K., and Braucher, O.: Sedimentary and mineral dust sources of dissolved iron to the World Ocean, Biogeosciences, 5, 631-656, doi: 10.5194/bg-5-631-2008, 2008.

Morris, P. J., and Charette, M. A.: A synthesis of upper ocean carbon and dissolved iron budgets for Southern Ocean natural iron fertilisation studies, Deep-Sea Res. Pt. II, 90, doi: 10.1016/j.dsr2.2013.02.001, 2013.

Naveira Garabato, A. C., Strass, V. H., and Kattner, G.: Fluxes of nutrients in a three-dimensional meander structure of the Antarctic Polar Front, Deep-Sea Res. Pt. II, 49, 3771-3792, doi: 10.1016/S0967-0645(02)00110-8, 2002.

Nielsdóttir, M. C., Bibby, T. S., Moore, C. M., Hinz, D. J., Sanders, R., Whitehouse, M., Korb, R., and Achterberg, E. P.: Seasonal and spatial dynamics of iron availability in the Scotia Sea, Mar. Chem., 130-131, 62-72, doi: 10.1016/j.marchem.2011.12.004, 2012.

Nishioka, J., Ono, T., Saito, H., Sakaoka, K., and Yoshimura, T.: Oceanic iron supply mechanisms which support the spring diatom bloom in the Oyashio region, western subarctic Pacific, J. Geophys. Res., 116, C02021, doi:10.1029/2010jc006321, 2011.

Olbers, D., Borowski, D., Vöker, C., and Wölff, J.-O.: The dynamical balance, transport and circulation of the antarctic circumpolar current, Antarctic Science, 16, 439-470, doi:10.1017/S0954102004002251, 2004.

Orsi, A. H., Whitworth, T., and Nowlin, W. D.: On the meridional extent and fronts of the Antarctic Circumpolar Current, Deep-Sea Res. Pt. I, 42, 641-673, doi: 10.1016/0967-0637(95)00021-W, 1995.

Parekh, P., Follows, M. J., and Boyle, E.: Modeling the global ocean iron cycle, Global Biogeochem. Cy., 18, GB1002, doi: 10.1029/2003GB002061, 2004.

Park, J., Oh, I.-S., Kim, H.-C., and Yoo, S.: Variability of SeaWiFS chlorophyll-a in the southwest Atlantic sector of the Southern Ocean: Strong topographic effects and weak seasonality, Deep- Sea Res. Pt. I, 57, 604–620, doi:10.1016/j.dsr.2010.01.004, 2010.

Penven, P., Debreu, L., Marchesiello, P., and McWilliams, J. C.: Evaluation and application of the ROMS 1-way embedding procedure to the central california upwelling system, Ocean Model., 12, 157-187, doi: 10.1016/j.ocemod.2005.05.002, 2006.

Penven, P., Marchesiello, P., Debreu, L., and Lefèvre, J.: Software tools for pre- and post-processing of oceanic regional simulations, Environ. Modell. Softw., 23, 660-662, doi: 10.1016/j.envsoft.2007.07.004, 2008.

Planquette, H., Statham, P. J., Fones, G. R., Charette, M. A., Moore, C. M., Salter, I., Nédélec, F. H., Taylor, S. L., French, M., Baker, A. R., Mahowald, N., and Jickells, T. D.: Dissolved iron in the vicinity of the Crozet Islands, Southern Ocean, Deep-Sea Res. Pt. II, 54, 1999-2019, doi: 10.1016/j.dsr2.2007.06.019, 2007.

Pollard, R. T., Salter, I., Sanders, R. J., Lucas, M. I., Moore, C. M., Mills, R. A., Statham, P. J., Allen, J. T., Baker, A. R., Bakker, D. C. E., Charette, M. A., Fielding, S., Fones, G. R., French, M., Hickman,

A. E., Holland, R. J., Hughes, J. A., Jickells, T. D., Lampitt, R. S., Morris, P. J., Nedelec, F. H., Nielsdottir, M., Planquette, H., Popova, E. E., Poulton, A. J., Read, J. F., Seeyave, S., Smith, T., Stinchcombe, M., Taylor, S., Thomalla, S., Venables, H. J., Williamson, R., and Zubkov, M. V.: Southern Ocean deep-water carbon export enhanced by natural iron fertilization, Nature, 457, 577–580, doi:10.1038/nature07716, 2009.

Poulton, A. J., Mark Moore, C., Seeyave, S., Lucas, M. I., Fielding, S., and Ward, P.: Phytoplankton community composition around the Crozet Plateau, with emphasis on diatoms and Phaeocystis, Deep-Sea Res. Pt. II, 54, 2085–2105, doi:10.1016/j.dsr2.2007.06.005, 2007.

Quéguiner, B.: Iron fertilization and the structure of planktonic communities in high nutrient regions of the Southern Ocean, Deep Sea Res. Pt. II, 90, 43-54, doi: 10.1016/j.dsr2.2012.07.024, 2013.

Raiswell, R., Benning, L.G., Davidson, L., Tranter, M.: Nanoparticulate bioavailable iron minerals in icebergs and glaciers, Mineral. Mag. 72, 345-348, doi: 10.1180/minmag.2008.072.1.345, 2008.

Ridgway, K. R., Dunn, J. R., and Wilkin, J. L.: Ocean interpolation by four-dimensional least squares -Application to the waters around Australia, J. Atmos. Ocean. Tech., 19, 1357-1375, 2002.

Rintoul, S. R., C. W. Hughes, and Olbers, D.: The antarctic circumpolar current system, in: Ocean circulation and climate: Observing and modelling the global ocean, edited by: G. Siedler, Church, J., and J. Gould, Elsevier, New York, 271– 302, 2001.

Robinson, C., Steinberg, D. K., Anderson, T. R., Arístegui, J., Carlson, C. A., Frost, J. R., Ghiglione, J. F., Hernandez-Leon, S., Jackson, G. A., Koppelmann, R., Quéguiner, B., Ragueneau, O., Rassoulzadegan, F., Robison, B. H., Tamburini, C., Tanaka, T., Wishner, K. F., and Zhang, J.: Mesopelagic zone ecology and biogeochemistry - a synthesis, Deep-Sea Res. Pt. II, 57, 1504-1518, doi: 10.1016/j.dsr2.2010.02.018, 2010.

Sachs, O., Sauter, E. J., Schlüter, M., Rutgers van der Loeff, M. M., Jerosch, K., and Holby, O.: Benthic organic carbon flux and oxygen penetration reflect different plankton provinces in the southern ocean, Deep Sea Res. Pt. I, 56, 1319-1335, doi: 10.1016/j.dsr.2009.02.003, 2009.

Sarmiento, J.L. Gruber, N.: Ocean Biogeochemical Dynamics. Princeton University Press, (2006)

Schlitzer, R.: Carbon export fluxes in the Southern Ocean: results from inverse modeling and comparison with satellite-based estimates, Deep-Sea Res. Pt. II, 49, 1623-1644, doi:10.1016/S0967-0645(02)00004-8, 2002.

Schlitzer, R.: Ocean Data View, http://odv.awi.de, 2012.

Shchepetkin, A. F., and McWilliams, J. C.: The regional oceanic modeling system (ROMS): a split-explicit, free-surface, topography-following-coordinate oceanic model, Ocean Model., 9, 347-404, doi: 10.1016/j.ocemod.2004.08.002, 2005.

Schmidt, K., Atkinson, A., Steigenberger, S., Fielding, S., Lindsay, M. C. M., Pond, D. W., Tarling, G. A., Klevjer, T. A., Allen, C. S., Nicol, S., and Achterberg, E. P.: Seabed foraging by antarctic krill: Implications for stock assessment, bentho-pelagic coupling, and the vertical transfer of iron, Limnol. Oceanogr., 56, 1411-1428, doi: 10.4319/lo.2011.56.4.1411, 2011.

Smetacek, V., Klaas, C., Strass, V. H., Assmy, P., Montresor, M., Cisewski, B., Savoye, N., Webb, A., d'Ovidio, F., Arrieta, J. M., Bathmann, U., Bellerby, R., Berg, G. M., Croot, P., Gonzalez, S., Henjes, J., Herndl, G. J., Hoffmann, L. J., Leach, H., Losch, M., Mills, M. M., Neill, C., Peeken, I., Rottgers, R., Sachs, O., Sauter, E., Schmidt, M. M., Schwarz, J., Terbruggen, A., and Wolf-Gladrow, D.: Deep

carbon export from a southern ocean iron-fertilized diatom bloom, Nature, 487, 313-319, doi: 10.1038/nature11229, 2012.

Sievers, H. A., and Nowlin, W. D.: The stratification and water masses at Drake Passage, J. Geophys. Res., 89, 10489-10514, doi: 10.1029/JC089iC06p10489, 1984.

Slemons, L., Gorgues, T., Aumont, O., Menkes, C., and Murray, J. W.: Biogeochemical impact of a model western iron source in the Pacific Equatorial Undercurrent, Deep-Sea Res. Pt. I, 56, 2115-2128, doi: 10.1016/j.dsr.2009.08.005, 2009.

Smetacek, V., Assmy, P., and Henjes, J.: The role of grazing in structuring Southern Ocean pelagic ecosystems and biogeochemical cycles, Antarct. Sci., 16, 541–558, doi:10.1017/S0954102004002317, 2004.

Smetacek, V. and Naqvi, S. W. A.: The next generation of iron fertilization experiments in the Southern Ocean, Philos. T. R. Soc. A., 366, 3947–3967, doi:10.1098/rsta.2008.0144, 2008.

Smith, R. C., Martinson, D. G., Stammerjohn, S. E., Iannuzzi, R. A., and Ireson, K.: Bellingshausen and western Antarctic Peninsula region: Pigment biomass and sea-ice spatial/temporal distributions and interannual variability, Deep-Sea Res. Pt. II, 55, 1949–1963, doi:10.1016/j.dsr2.2008.04.027, 2008.

Smith, W. H. F., and Sandwell, D. T.: Global Sea Floor Topography from Satellite Altimetry and Ship Depth Soundings, Science, 277, 1956-1962, doi: 10.1126/science.277.5334.1956, 1997.

Sokolov, S., and Rintoul, S. R.: On the relationship between fronts of the antarctic circumpolar current and surface chlorophyll concentrations in the Southern Ocean, J. Geophys. Res., 112, C07030, doi: 10.1029/2006jc004072, 2007.

Sokolov, S., and Rintoul, S. R.: Circumpolar structure and distribution of the antarctic circumpolar current fronts: 1. Mean circumpolar paths, J. Geophys. Res., 114, C11018, doi: 10.1029/2008jc005108, 2009.

Stammer, D., Wunsch, C., Giering, R., Eckert, C., Heimbach, P., Marotzke, J., Adcroft, A., Hill, C. N., and Marshall, J.: Global ocean circulation during 1992–1997, estimated from ocean observations and a general circulation model, J. Geophys. Res., 107, 3118, doi: 10.1029/2001jc000888, 2002.

Sunda, W. G., and Huntsman, S. A.: Iron uptake and growth limitation in oceanic and coastal phytoplankton, Mar. Chem., 50, 189-206, doi: 10.1016/0304-4203(95)00035-P, 1995.

Szeto, M., Werdell, P. J., Moore, T. S., and Campbell, J. W.: Are the world's oceans optically different?, J. Geophys. Res., 116, C00H04, doi:10.1029/2011jc007230, 2011.

Tagliabue, A., Bopp, L., and Aumont, O.: Ocean biogeochemistry exhibits contrasting responses to a large scale reduction in dust deposition, Biogeosciences, 5, 11-24, doi: 10.5194/bg-5-11-2008, 2008.

Tagliabue, A., Bopp, L., and Aumont, O.: Evaluating the importance of atmospheric and sedimentary iron sources to Southern Ocean biogeochemistry, Geophys. Res. Lett., 36, L13601, doi: 10.1029/2009gl038914, 2009a.

Tagliabue, A., Bopp, L., Aumont, O., and Arrigo, K. R.: Influence of light and temperature on the marine iron cycle: From theoretical to global modeling, Global Biogeochem. Cy., 23, GB2017, doi: 10.1029/2008gb003214, 2009b.

Tagliabue, A., Bopp, L., Dutay, J.-C., Bowie, A. R., Chever, F., Jean-Baptiste, P., Bucciarelli, E., Lannuzel, D., Remenyi, T., Sarthou, G., Aumont, O., Gehlen, M., and Jeandel, C.: Hydrothermal

contribution to the oceanic dissolved iron inventory, Nat. Geosci., 3, 252-256, doi: 10.1038/ngeo818, 2010.

Tarling, G. A., Ward, P., Atkinson, A., Collins, M. A., and Murphy, E. J.: Discovery 2010: Spatial and temporal variability in a dynamic polar ecosystem, Deep-Sea Res Pt II, 59-60, 1-13, doi: 10.1016/j.dsr2.2011.10.001, 2012.

Tegen, I., and Fung, I.: Contribution to the atmospheric mineral aerosol load from land surface modification, J. Geophys. Res.-Atmos., 100, 18707-18726, doi: 10.1029/95jd02051, 1995.

Tegen, I., Werner, M., Harrison, S. P., and Kohfeld, K. E.: Relative importance of climate and land use in determining present and future global soil dust emission, Geophys. Res. Lett., 31, L05105, doi: 10.1029/2003gl019216, 2004.

Thomalla, S. J., Fauchereau, N., Swart, S., and Monteiro, P. M. S.: Regional scale characteristics of the seasonal cycle of chlorophyll in the Southern Ocean, Biogeosciences, 8, 2849–2866, doi:10.5194/bg-8-2849-2011, 2011.

Thorpe, S. E., Heywood, K. J., Brandon, M. A., and Stevens, D. P.: Variability of the southern Antarctic Circumpolar Current front north of South Georgia, J. Mar. Syst., 37, 87–105, doi:10.1016/S0924-7963(02)00197-5, 2002.

Tovar-Sanchez, A., Duarte, C. M., Hernández-León, S., and Sañudo-Wilhelmy, S. A.: Krill as a central node for iron cycling in the southern ocean, Geophys. Res. Lett., 34, L11601, doi: 10.1029/2006gl029096, 2007.

Tovar-Sanchez A., S.-W., S. A., Kustka, A. B., Agusti S. , and Dachs, J., Hutchins, D. A., Capone, D. G., Duarte, C. M.: Effects of dust deposition and river discharges on trace metal composition of trichodesmium spp. In the tropical and subtropical north Atlantic ocean, Limnol. Oceanogr., 51, 1755–1761, 2006.

Thuróczy, C. E., Gerringa, L. J. A., Klunder, M. B., Laan, P., and de Baar, H. J. W.: Observation of consistent trends in the organic complexation of dissolved iron in the atlantic sector of the southern ocean, Deep Sea Res. Pt. II, 58, 2695-2706, doi: 10.1016/j.dsr2.2011.01.002, 2012.

Trathan, P., Bishop, C., Maclean, G., Brown, P., Fleming, A., and Collins, M. A.: Linear tracks and restricted temperature ranges characterise penguin foraging pathways, Mar Ecol-Prog Ser, 370, 285-294, doi: 10.3354/meps07638, 2008.

Tréguer, P., and Jacques, G.: Dynamics of nutrients and phytoplankton, and fluxes of carbon, nitrogen and silicon in the antarctic ocean, Polar Biology, 12, 149-162, doi: 10.1007/BF00238255, 1992.

Trull, T. W., Bray, S. G., Manganini, S. J., Honjo, S., and Franc¸ois, R.: Moored sediment trap measurements of carbon export in the Subantarctic and Polar Frontal Zones of the Southern Ocean, south of Australia, J. Geophys. Res., 106, 31489– 1509, doi:10.1029/2000jc000308, 2001.

Venables, H., Meredith, M. P., Atkinson, A., and Ward, P.: Fronts and habitat zones in the Scotia Sea, Deep-Sea Res. Pt. II, 59–60, 14–24, doi:10.1016/j.dsr2.2011.08.012, 2012.

Venables, H. and Moore, C. M.: Phytoplankton and light limitation in the Southern Ocean: Learning from high-nutrient, high-chlorophyll areas, J. Geophys. Res., 115, C02015, doi:10.1029/2009jc005361, 2010.

Ward, P., Shreeve, R., Whitehouse, M., Korb, B., Atkinson, A., Meredith, M., Pond, D., Watkins, J., Goss, C., and Cunningham, N.: Phyto- and zooplankton community structure and production around South Georgia (Southern Ocean) during Summer 2001/02, Deep-Sea Res. Pt. I, 52, 421–441, doi:10.1016/j.dsr.2004.10.003, 2005.

Westberry, T. K., Behrenfeld, M. J., Milligan, A. J., and Doney, S. C.: Retrospective satellite ocean color analysis of purposeful and natural ocean iron fertilization, Deep-Sea Res. Pt. I, 73, 1-16, doi: 10.1016/j.dsr.2012.11.010, 2013.

Whitehouse, M. J., Atkinson, A., Korb, R. E., Venables, H. J., Pond, D. W., and Gordon, M.: Substantial primary production in the land-remote region of the central and northern Scotia Sea, Deep-Sea Res. Pt. II, 59–60, 47–56, doi:10.1016/j.dsr2.2011.05.010, 2012.

Whitehouse, M. J., Atkinson, A., Ward, P., Korb, R. E., Rothery, P., and Fielding, S.: Role of krill versus bottom-up factors in controlling phytoplankton biomass in the northern Antarctic waters of South Georgia, Mar. Ecol.-Prog. Ser., 393, 69–82, doi:10.3354/meps08288, 2009.

Whitehouse, M. J., Korb, R. E., Atkinson, A., Thorpe, S. E., and Gordon, M.: Formation, transport and decay of an intense phytoplankton bloom within the High-Nutrient Low- Chlorophyll belt of the Southern Ocean, J. Mar. Syst., 70, 150– 167, doi:10.1016/j.jmarsys.2007.05.003, 2008a.

Whitehouse, M. J., Meredith, M. P., Rothery, P., Atkinson, A.,Ward, P., and Korb, R. E.: Rapid warming of the ocean around South Georgia, Southern Ocean, during the 20th century: Forcings, characteristics and implications for lower trophic levels, Deep- Sea Res. Pt. I, 55, 1218–1228, doi:10.1016/j.dsr.2008.06.002, 2008b.

Whitehouse, M. J., Priddle, J., and Symon, C.: Seasonal and annual change in seawater temperature, salinity, nutrient and chlorophyll a distributions around South Georgia, South Atlantic, Deep-Sea Res. Pt. I, 43, 425-443, doi: 10.1016/0967-0637(96)00020-9, 1996.

Whitworth, T., Nowlin, W. D., and Worley, S. J.: The net transport of the antarctic circumpolar current through drake passage, J. Phys. Oceanogr., 12, 960-971, 1982.

Young, E. F., Meredith, M. P., Murphy, E. J., and Carvalho, G. R.: High-resolution modelling of the shelf and open ocean adjacent to South Georgia, Southern Ocean, Deep-Sea Res. Pt. II, 58, 1540-1552, doi: 10.1016/j.dsr2.2009.11.003, 2011.

Zhang, B., and Klinck, J. M.: The effect of antarctic circumpolar current transport on the frontal variability in drake passage, Dynamics of Atmospheres and Oceans, 45, 208-228, doi: 10.1016/j.dynatmoce.2008.05.002, 2008.

## Acknowledgements

This PhD thesis is the fruitful outcome of 5 years of intense and productive research. Now I see very well that obstacles encountered along the way were open doors to new opportunities that have improved and strengthened the scientific (and personal) side of me.

I want to sincerely thank my supervisor, Prof. Dr. Reiner Schlitzer for his guidance and support since the very first moment. I acknowledge the late Dr. Gökay Karakas who picked me up the first day in Bremerhaven and walked me through ROMS during the first years of this PhD. Much of the work presented in this thesis started with him at my side.

Dr. Olivier Aumont, who hosted me at IRD in Plouzané several times during the past years is also particularly acknowledged. Every stay in France was a great success. I learned so much about modelling and "my" models. How they work, and why often they don't work or don't *want* to work. I learned how to think with a model, use it and also enjoy using it. Every model simulation is an expression of curiosity and creativity.

I thank very much Prof. Dr. Michal Kucera for his willingness to review and comment this PhD thesis, as well as all the PhD committee members that will attend my defence.

The Earth System Science Research School (ESSReS), an initiative of the Helmholtz Association of German research centres (HGF) at the Alfred Wegener Institute for Polar and Marine Research, is the starting point of this journey as a PhD student: it has given me THE opportunity to pursue a PhD, and start a scientific career of my own. I thank Dr. Klaus Grosfeld, Prof. Dr. Gerrit Lohmann and all the ESSReS team for this. As an ESSReS student I could attend several lectures and soft-skill trainings. I think that all PhD students should live, at some point of their career, the same open-minded approach to science I could experience in these years.

One very special and unique experience changed many aspects of me and my PhD: a 70 day long oceanographic expedition to the Southern Ocean on board the super-cool icebreaker R.V. Polarstern. I would like to thank very much Prof. Dr. Victor Smetacek for taking me along during the Indo-German ocean fertilization experiment LOHAFEX, and Prof. Maria Grazia Mazzocchi for welcoming me in the zooplankton group and for teaching me so much about those little creatures living in the ocean. *Calanus simillimus* is still my favorite one. On board I also met Dr. Christine Klaas and Prof. Dr. Dieter Wolf-Gladrow to whom I often turned for help, discussions, ideas during the following months and years.

I would like to further thank Prof. Dr. Victor Smetacek for sharing his knowledge on (marine polar) biology and ecology, and for his great help in shaping (reading, discussing, re-reading sooooo many times) my very first published paper.

Thanks to all the special international friends I made during these years, starting from Conny and David who welcomed me in the PhD world; Franzi, Chris and Jacqui my first PhD colleagues and companions. Marie and Jenia for the many things we shared in Bremerhaven and outside Germany. Maddalena, Verena, Xiaoping and Ling, Thomas and Johannes, my office friends! Xiaoping and Xiaotong thank you very much for sharing with me your culture, traditions and food!

A special thank you to my family members' *Forza e coraggio!* Romina, zia Elsa, zia Nada, Giorgio, Dunia, Farouk.

The most difficultly written thank yous are those that go to my parents: words are just not enough. This PhD would have been so much tougher without the love and support of my parents who always encouraged and supported me throughout all these years. Becoming a scientist is hard. It is less hard when your beloved ones surround you and believe in you; this thesis is dedicated to my Mother and Father, the sparkles of it all. I share with you the happiness and immense joy of submitting and (hopefully very soon) defending my PhD thesis.

Finally, I want to thank the person who followed me in several parts of Europe, and with whom I explored large parts of the cities I visited, making traveling-for-work closer to traveling-for-fun. Two inhabitants from small towns somewhere in northern Italy can be a really good team out there! Thank you for your encouragements, for listening - very patiently - to those incredibly long skype calls about satellites, strange data formats, ROMS, PISCES, the nightmare MATLAB scripts, the fun MATLAB scripts. Luca, thank you for being there all this time.

***

Financial support for this PhD was provided by the Earth System Science Research School, the Geosciences division at the Alfred-Wegener-Institut Helmholtz-Zentrum für Polar- u. Meeresforschung in Bremerhaven and the EU FP7 project CARBOCHANGE under grant agreement no. 264879.

# E r k l ä r u n g

Hiermit erkläre ich, dass ich:

- die Arbeit ohne unerlaubte fremde Hilfe angefertig habe;
- keine anderen als die hier angegebenen Quellen und Hilfsmittel benuzt habe;
- die den benutzten Werken wörtlich oder inhaltlich entnommen Stellen als solche kenntlich gemacht habe.

Inès Borrione